

NASA Contractor Report 4221

Feasibility of Generating an 'Artificial' Burst in a Turbulent Boundary Layer

Phase II SBIR

Mohamed Gad-el-Hak
Flow Industries, Inc.
Kent, Washington

Prepared for
Langley Research Center
under Contract NAS1-18292



National Aeronautics and
Space Administration
Office of Management
Scientific and Technical
Information Division

1989

1

NATIONAL AERONAUTICS AND SPACE ADMINISTRATION

PHASE II SBIR - FINAL REPORT

PROJECT SUMMARY

PROJECT TITLE	: Feasibility of Generating an 'Artificial' Burst in a Turbulent Boundary Layer - Phase II SBIR
CONTRACT NUMBER	: NAS1-18292
ISSUED BY	: NASA-Langley Research Center
TECHNICAL MONITOR	: Stephen P. Wilkinson
CONTRACTOR	: Flow Industries, Inc.
PRINCIPAL INVESTIGATOR	: Mohamed Gad-el-Hak
DURATION	: 12 May 1986 - 30 October 1988

Viscous aerodynamic drag accounts for about half of the total drag on commercial aircraft at subsonic cruise conditions. Two avenues are available to achieve drag reduction: either laminar flow control or turbulence manipulation. The present research deals with the latter approach.

It is generally agreed that the bursting phenomenon is the most significant dynamic event in a turbulent boundary layer. About 80 percent of the momentum transport occurs during these bursts. Previous attempts to understand the physics and structure of these events were frustrated by the fact that bursts occur randomly in space and time and that successive bursts are not necessarily identical. During Phase I of this investigation, 'artificial' bursts were generated in laminar and turbulent boundary layers. The burst-like events were produced by withdrawing near-wall fluid from two minute holes separated in the spanwise direction or by pitching a miniature delta wing that was flush-mounted to the wall. Either of these actions generated streamwise vorticity and a low-speed streak that resembled a naturally occurring one. The resulting sequence of events occurred at a given location and at controlled times, allowing detailed examination and

comparison with natural, random bursts by means of flow visualization and fast-response probe measurement techniques.

The primary objective of Phase II research was to investigate experimentally the feasibility of substantially reducing the skin friction drag in a turbulent boundary layer using a novel technique. The method combines the beneficial effects of suction and a longitudinally ribbed surface. At a sufficiently large spanwise separation, the streamwise grooves act as a nucleation site causing a focusing of low-speed streaks over the peaks. Suction is then applied intermittently through longitudinal slots located at selected locations along those peaks to obliterate the low-speed regions and to prevent bursting. The selective suction technique requires minuscule energy expenditure and alleviates the need for using porous materials. The successful application of the present innovation on commercial aircraft will result in annual fuel savings of several billion dollars.

Phase II research was divided into two tasks. In the first, selective suction from a single streamwise slot was used to eliminate either a single burst-like event or a periodic train of artificially generated bursts in laminar and turbulent boundary layers that develop on a flat plate towed in a water channel. Flow visualization and hot-film probe measurements were used together with pattern recognition algorithms to demonstrate the feasibility of the turbulence-modification technique. Our results indicated that equivalent values of the suction coefficient as low as 0.0006 were sufficient to eliminate the artificially generated bursts in a laminar boundary layer. This rate is 5 times smaller than that reported in other experiments employing uniform transpiration as the rate necessary to yield zero growth of the boundary layer's momentum thickness.

In the second task, the selective suction technique was applied to eliminate natural bursts occurring on a grooved surface. This task of the experiment was conducted in a subsonic, low-turbulence, closed-return wind tunnel. Velocity profiles and bursting statistics were measured in the presence of longitudinal roughness elements (LREs). The LREs seem simply to impose a no-slip boundary condition at an elevation equivalent to their diameter.

TABLE OF CONTENTS

	<u>Page</u>
Project Summary.	1
Table of Contents	3
1. Introduction	4
1.1 Background	4
1.2 Methods to Reduce Drag	5
1.3 Phase I Research	8
1.4 Phase II Research	11
1.5 Present Report.	12
2. Governing Equations.	13
3. Suction/Injection Effects on Drag	21
4. Previous Research Using Suction/Injection.	24
5. Selective Suction Concept.	31
6. Experimental Approach	34
6.1 Towing Tank.	34
6.2 Wind Tunnel	34
6.3 Flat Plates	36
6.4 Burst Generator.	38
6.5 Streamwise Suction Slot.	38
6.6 Visualization Methods.	40
6.7 Velocity Measurements	41
6.8 Pattern-Recognition Algorithms	43
7. Results of Phase I Research	44
7.1 Bursts in Laminar Flow	44
7.2 Bursts in a Turbulent Boundary Layer	53
7.3 Pattern Recognition of Bursts and Streaks.	57
8. Selective Suction in Laminar Flows.	63
8.1 Visualization Results.	63
8.2 Fast-Response Probe Results.	76
9. Selective Suction in Turbulent Flows	84
10. Wind-Tunnel Result.	88
10.1 Longitudinal Roughness Elements	88
10.2 Suction in a Turbulent Boundary Layer	105
11. Summary	118
References.	122
Appendix: Publications Resulting from Present Research	127
Report Documentation Page.	130

1. INTRODUCTION

Viscous or skin-friction drag accounts for about half of the total drag on modern aircraft at subsonic cruise conditions. The annual fuel cost for all commercial airlines in the United States is presently in excess of \$10 billion. Hence, a reduction in skin friction of 20% translates into an annual fuel saving of \$1 billion. Two avenues are available to achieve drag reduction: either laminar flow control or turbulence manipulation. The present research concerns the latter approach. According to Bushnell (1983), the leverage in this area of research is quite substantial and justifies the study of unusual or high-risk approaches on an exploratory basis.

A new technique to substantially reduce skin-friction drag in a turbulent boundary layer is considered in the present investigation. The method combines the beneficial effects of two presently known techniques: suction and longitudinally ribbed surfaces. At a sufficiently large spanwise separation, the streamwise grooves act as a nucleation site causing a focusing of low-speed streaks over their peaks. Suction is then applied intermittently through longitudinal slots located at selected locations along those peaks to obliterate the low-speed regions and to prevent bursting.

During the first phase of the present research, 'artificial' bursts were generated in laminar and turbulent boundary layers. The primary objective of Phase II research was to investigate experimentally the feasibility of the selective suction technique. This phase was divided into two tasks. In the first, suction from a single streamwise slot was used to eliminate either a single burst-like event or a periodic train of artificially generated bursts in laminar and turbulent boundary layers that develop on a flat plate towed in a water channel. In the second task, conducted in a subsonic, low-turbulence, closed-return wind tunnel, the selective suction method was applied to eliminate natural bursts occurring on a grooved surface.

1.1 BACKGROUND

Recent turbulent boundary layer research has clearly shown that the wall region is dominated by a sequence of eddy motions that are collectively called the bursting phenomenon.

This process was reviewed by Willmarth (1975) and summarized by Blackwelder (1978). Qualitatively, the process begins with a pair of elongated, streamwise, counter-rotating vortices having diameters of approximately $40\nu/u_\tau$, where ν/u_τ is the viscous scale, ν is the kinematic viscosity and u_τ is the friction velocity. The vortices exist in a strong shear and induce low- and high-speed regions between them as shown in Section BB of Figure 1. The vortices and the accompanying eddy structures occur randomly in space and time. However, their appearance is regular enough that an average spanwise wavelength of approximately 80 to $100\nu/u_\tau$ has been identified by Kline et al. (1967) and others. Kline et al. also observed that the low-speed regions grow downstream and develop inflectional $U(y)$ profiles, as sketched in Figure 1. At approximately the same time, the interface between the low- and high-speed fluid begins to oscillate. The low-speed region lifts up away from the wall as the oscillation amplitude increases, and then the flow rapidly breaks down into a completely random pattern. Since this latter process occurs on a very short time scale, Kline et al. called it a "burst." Corino & Brodkey (1969) showed that the low-speed regions are quite narrow, i.e., $20\nu/u_\tau$, and may also have significant shear in the spanwise direction.

Considerably more has been learned about the bursting process during the last decade. For example, Falco (1980) has shown that the wall region is continuously bombarded by "pockets" of high-speed fluid originating in the logarithmic and possibly the outer layers of the flow. These pockets tend to promote and/or enhance the inflectional velocity profiles by increasing the instantaneous shear leading to a more rapidly growing instability. Blackwelder & Haritonidis (1983) have shown that the frequency of occurrence of these events scales with the viscous parameters consistent with the usual boundary-layer scaling arguments.

1.2 METHODS TO REDUCE DRAG

In spite of the rapid accumulation of knowledge about the eddy structures within the wall region, there have been few successful efforts to favorably alter or control them. The most successful method by far has been the introduction of minute concentrations of long-chain

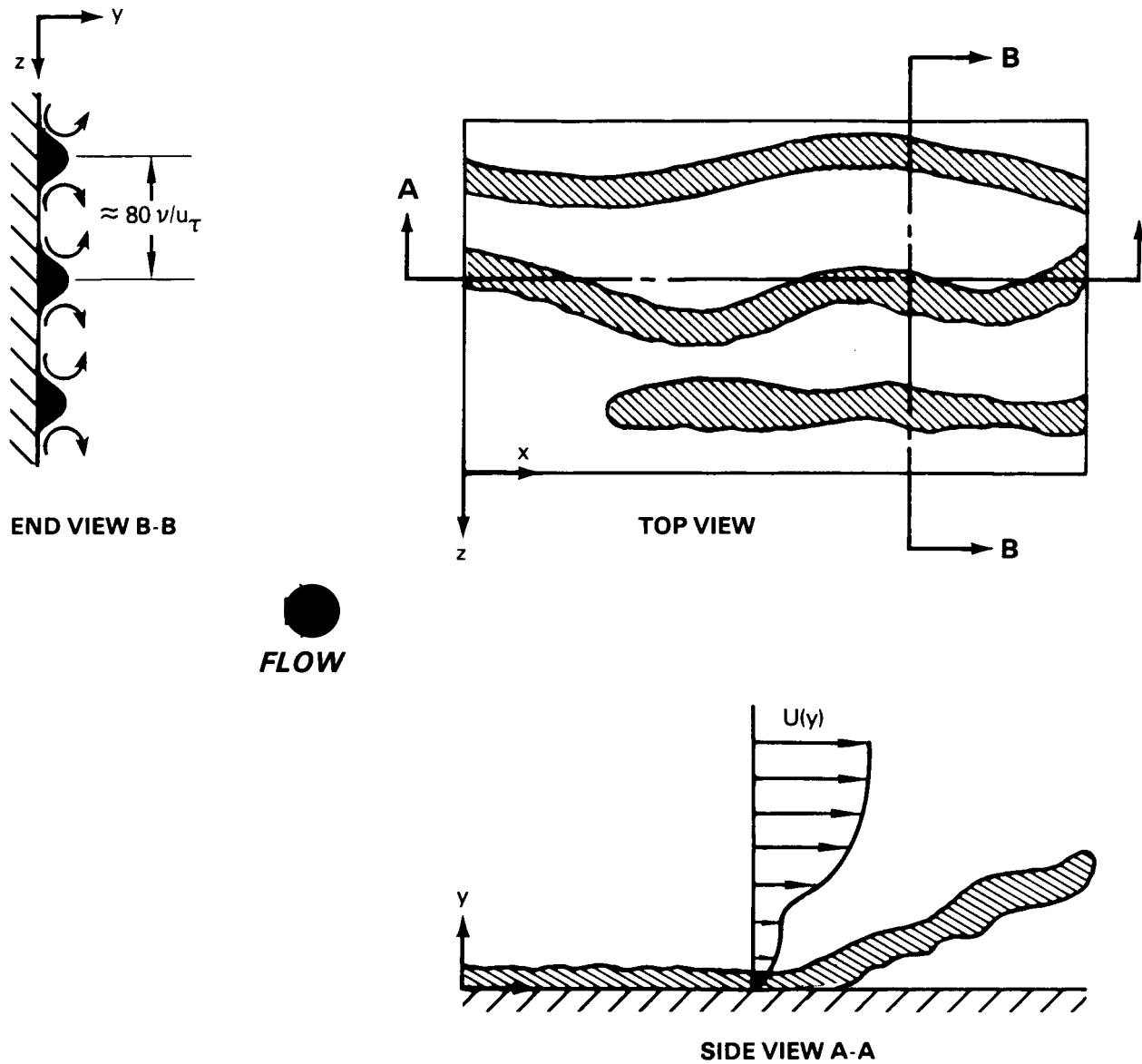


Figure 1. Sketch of the Low-Speed Streaks in the Wall Region. The Counter-Rotating Eddies between the Streaks are Indicated in Section B-B.

polymers into liquid flow fields (Berman, 1978). Several authors have observed that the polymer can reduce the drag by 50 to 80 percent, depending upon the polymer type, concentration, etc. Further research has shown that the polymers accomplish this by increasing the length scale in the wall region without significantly altering the eddy structure. That is, the distance between the streamwise vortices is increased, the buffer layer thickness is increased, etc. Hence, the eddies in the polymer case appear to be approximately the same as those seen without the polymer but at a much lower Reynolds number. Since the polymers only slightly alter the kinematic viscosity, it is not clear if they increase the length scale directly by decreasing the wall shear or if they accomplish it indirectly by changing the scales of the eddies. If the latter is true, this single success suggests that there may be other techniques for changing the wall structure and also reducing the drag. The present research suggests exploring another avenue toward this goal.

A novel method to reduce skin-friction drag is sought in the present investigation. The innovation is designed to exploit the present day knowledge of the bursting process to achieve substantial drag reduction. It is realized that in a two-dimensional mean shear flow the tangential Reynolds stress is responsible for transferring energy from the mean flow into the turbulence. The studies of Lu & Willmarth (1973) and Blackwelder & Kaplan (1976) have shown that most of the tangential Reynolds stress carried by the turbulent flow is associated with the bursting process. Kline et al. (1967) indicated that the Reynolds stress was primarily produced by the ejection of the low-speed streak from the wall region. Lu & Willmarth (1973) and Brodkey, Wallace & Eckelmann (1974) showed that the pockets of high-speed fluid bombarding the wall also contribute to the Reynolds stress below $y^+ \simeq 15$. Thus, if these events could be inhibited, the Reynolds stress could be decreased and the turbulence production interrupted.

One possible means of decreasing the Reynolds stress is to remove selectively some or all of the low-speed streaks from the flow field. This would inhibit the ejection process and thus decrease the Reynolds stress. Previous research on turbulent bursts indicates that the Reynolds stress is a random function of space and time; that is, the ejection and production of turbulence occur randomly. Consequently, it seems logical that the control of this process would also be

optimized by applying the inhibiting mechanism randomly in space and time. Obviously, this cannot be easily achieved. However, the recent experiments by Johansen & Smith (1986) indicate the feasibility of greatly reducing the spatial randomness of the low-speed streaks by using a longitudinally ribbed surface. At sufficiently large spanwise spacing, the ribbed surface seems to act as a nucleation site, causing focusing of the streaks over the peaks of the longitudinal grooves. Moreover, modest drag reduction can be achieved by using such a surface, albeit with a different spanwise spacing (Walsh, 1980; 1982; 1983; Walsh & Lindemann, 1984). The present innovation is aimed at using longitudinal roughness elements (LREs), thus "fixing" the spatial position of the low-speed streaks, together with selective suction to achieve a more tangible reduction in the skin-friction drag than that achieved by either of the two techniques separately. The suction is applied intermittently through longitudinal slots located at selected locations along the peaks of the LREs. This arrangement is quite different from that used by Wilkinson et al. (1980), who applied continuous suction along the troughs of their longitudinally ribbed surface.

1.3 **PHASE I RESEARCH**

To prove and optimize the selective suction concept, the first set of experiments conducted in the present investigation included determining the effects of suction from a single streamwise slot on a single or a periodic train of artificially generated bursting events. In this section, we briefly review the methods available for simulating bursting events in laminar and turbulent boundary layers. More complete details are available in the paper by Gad-el-Hak & Hussain (1986).

The complexity of the bursting phenomenon should be apparent from the fact that extensive investigations have failed to provide an explanation for the origin of bursting (Offen & Kline, 1975; Praturi & Brodkey, 1978; Falco, 1979; 1980; Smith, 1983) or the topological characteristics of the bursting coherent structure, as well as its evolution and dynamics (Hussain, 1983a). Sophisticated experiments have been conducted to capture the bursting signature (Blackwelder & Kaplan, 1976; Nishioka et al, 1981; Antonia, 1981), but it is clear that the deduced signature is

dependent on the detection scheme as well as on the threshold level of a given detection scheme (Kunen et al., 1983; Sato, 1983).

Hussain (1983b) reiterated that a single-point detection of an inherently three-dimensional random structure must produce significant smearing. That is, eduction of the bursting coherent structure should not only involve a three-dimensional detection scheme but also require first the identification of the mode (i.e., spatial configuration) of the structure and then the probability density distribution as a function of the characteristic structure parameters, like shape, size, strength, orientation, convection velocity, etc. Furthermore, a stationary sensor may intersect successive three-dimensional structures (say, hairpin vortices) at different relative spanwise locations, and a structure may advect past a sensor at different transverse displacements so that a stronger structure farther away could not be necessarily differentiated from a weaker structure nearby.

It should thus be clear that an array of probes in a transverse rake must be used for measurement. Furthermore, the measuring rake should be located in between two detection rakes so that the relative spanwise location of the measuring rake within the three-dimensional advecting structure can be determined instantaneously.

Since the coherent vorticity Ω is the principal property of a coherent structure, event detection must be based on Ω and not on the correlation of velocity, pressure and/or intermittency signals (Hussain 1980). Only large-scale vorticity is involved, however, so a transverse rake of X-wires is adequate to measure the instantaneous map of the spanwise vorticity $\langle \Omega \rangle$ in the (y, t) plane. From the smoothed maps $\langle \Omega(y, t) \rangle$, one should decide which structures should be accepted. That is, eduction involves accepting only those structures of a given mode with the peak value (denoting strength) of $\langle \Omega \rangle$ above a certain level and the peak location at an optimally selected transverse location and accepting structures of a given shape and size. The accepted structures should then be ensemble averaged after proper phase alignment. One way to align is appropriate time shifting of realizations via the method of iterative cross-correlation of each realization with the ensemble average (Zilberman et al., 1977). Whatever survives the phase

averaging (i.e., ensemble averaging at a fixed phase) of the appropriately aligned realizations is the coherent structure, and the departure of each realization from the phase averaging is the corresponding incoherent turbulence. The phase-averaged contours of coherent vorticity, coherent and incoherent Reynolds stress, coherent production, etc., provide the necessary structure properties. The phase-averaged velocity vector pattern in the frame of the structure superimposed on the contours of $\langle \Omega \rangle$ will denote the spatial variations of entrainment (Hussain & Zaman, 1980).

It is necessary to emphasize that these elaborate efforts are justified if the flow is characterized by "preferred modes", as the coherent structure approach to turbulence is not very helpful if the flow has a large variety of coherent structures. Furthermore, capturing an individual structure via spatial smoothing is not helpful, as there is no test for convergence of the smoothing that removes sharp fronts otherwise retained by ensemble averaging. Also, one must assure that the educed structure is not "freak" and does indeed represent a "preferred mode". A classical example of such a freak structure is the single, large horseshoe vortex detected by Wygant et al. (1976) and Cantwell et al. (1978) by ensemble averaging an artificial turbulent spot. The results of Gad-el-Hak et al. (1981) clearly indicate the dynamic insignificance of such a structure.

Returning to the bursting coherent structure, it should be clear that the variations in their characteristic parameters as well as the random occurrence in time and the random transverse and spanwise displacements of natural bursting structures must have produced unacceptable smearing, thus frustrating prior eduction schemes in the boundary layer. Furthermore, we are unaware of any attempt to determine if all structures included in the educed bursting signature (which differed from a phase average) are of the same mode. In an attempt to remove significantly the inherent smearing in the eduction of natural bursting structures, a new approach has been attempted by Gad-el-Hak & Hussain (1986): eduction of artificially induced bursting. The structure details can then be educed via measurements phase-locked to the excitation (Hussain & Reynolds, 1972), much the same as was done in the case of the artificial turbulent spot (Gad-el-Hak et al., 1981; Riley & Gad-el-Hak, 1985). Gad-el-Hak & Hussain (1986) were able to generate an artificial

burst in both laminar and turbulent boundary layers. The sequence of events induced artificially was compared to that of a natural burst in a turbulent boundary layer using flow visualization and hot-film probe measurements. In all the comparisons that have been made thus far by Gad-el-Hak & Hussain (1986), the artificial event was kinematically and dynamically identical to the bursts occurring randomly in space and time in a turbulent boundary layer. Samples of their results are presented in Section 7 of this report.

1.4 **PHASE II RESEARCH**

The ability to generate an artificial burst and control its occurrence in space and time offers a great opportunity to prove and optimize the selective suction concept. Phase II research was divided into two tasks. In the first, conducted in a water channel, a single artificial burst or a train of periodic bursts were generated in either a laminar or a turbulent boundary layer. A streamwise suction slot centered around and located downstream of the burst generator, and synchronized with respect to it, withdrew the resulting (unstable) low-speed streaks. The effect of the intermittent suction was then determined using several unique visualization techniques developed by the present author, including the use of fluorescent dyes and hydrogen bubbles illuminated by sheets of laser light (Gad-el-Hak et al., 1983; Gad-el-Hak, 1986; 1988a; 1988b). The minimal amount of suction required to obliterate a low-speed streak and to prevent bursting was determined. Attempts were also made to impede bursting by injecting fluid in the high-speed region, which relieved the strong spanwise velocity gradient, $\partial U/\partial z$, and eliminated the breakdown. Comparison between suction and injection as a means of preventing a burst were made.

In the second task, conducted in a wind tunnel, the selective suction technique was employed in the more practical environment of a turbulent boundary layer. Johansen & Smith (1986) have shown that the low-speed streaks can be organized to a large extent by placing small longitudinal strips on the surface. Their strips were of the order of $4\nu/u_\tau$ in diameter and were spaced approximately $100\nu/u_\tau$ apart. Their visual results using hydrogen bubbles indicate that the low-speed streaks tend to align themselves with the streamwise strips, thus almost eliminating

the meandering in the spanwise direction. A similar surface roughness was used to form a "holder" for the naturally occurring low-speed regions in a turbulent boundary layer. At the end of the strips, streamwise slots were used to apply suction/injection selectively to either the low- or high-speed regions.

1.5 PRESENT REPORT

The equations needed in the present article are recalled in Section 2. Sections 3, 4 and 5 introduce the selective suction concept and review previous research using suction/injection. In Section 6, the experimental facility and equipment are described. Results of Phase I research are summarized in Section 7. Results of the first task of Phase II are given in Sections 8 and 9. The wind-tunnel results, constituting the second task of Phase II, are detailed in Section 10. Section 11 summarizes the entire project including recommendations for future research. The last section is a bibliography followed by an appendix listing the publications resulting from the present research.

2. GOVERNING EQUATIONS

The principles of conservation of mass, momentum and energy govern all fluid motions. In general, a set of partial, nonlinear differential equations expresses these principles, and together with appropriate boundary and initial conditions constitute a well-posed problem. It is of course beyond the scope of this report to derive these equations and the reader is referred to any advanced textbook in Fluid Dynamics (Landau and Lifshitz, 1963; Batchelor, 1967; Hinze, 1975; Kays and Crawford, 1980; Panton, 1984). The equations will be first recalled in as general a form as possible.

In Cartesian tensor notation, the equation of conservation of mass reads:

$$\frac{\partial \rho}{\partial t} + \frac{\partial}{\partial x_i} (\rho U_i) = 0, \quad (2.1)$$

and Newton's second law is:

$$\rho \left(\frac{\partial U_i}{\partial t} + U_j \frac{\partial U_i}{\partial x_j} \right) = \frac{\partial}{\partial x_j} \tau_{ji} + F_i, \quad (2.2)$$

where U_i is an instantaneous velocity component, ρ is the density, F_i is the body force and τ_{ji} is the second-order stress tensor which must be related to the deformation tensor in order to reduce the number of unknowns to be equal to the number of equations. The independent variables are time t and the three spatial coordinates x_1 , x_2 , and x_3 (or x , y , and z). For a Newtonian fluid a linear relation between the stress and the rate of strain is assumed:

$$\tau_{ji} = -P \delta_{ji} + \mu \left(\frac{\partial U_i}{\partial x_j} + \frac{\partial U_j}{\partial x_i} - \frac{2}{3} \frac{\partial U_k}{\partial x_k} \delta_{ji} \right), \quad (2.3)$$

where P is the hydrostatic pressure, μ is the dynamic viscosity, and δ_{ji} is the unit second-order tensor (Kronecker delta). While (2.3) is valid for air and water under most

practical conditions, different constitutive relations must be sought for non-Newtonian fluids such as dilute solutions of drag-reducing polymers.

For a Newtonian fluid, (2.3) is substituted in (2.2) to yield the momentum equation:

$$\rho \left(\frac{\partial U_i}{\partial t} + U_j \frac{\partial U_i}{\partial x_j} \right) = - \frac{\partial P}{\partial x_i} + \frac{\partial}{\partial x_j} \left[\mu \left(\frac{\partial U_i}{\partial x_j} + \frac{\partial U_j}{\partial x_i} \right) \right] - \frac{2}{3} \frac{\partial}{\partial x_i} \left(\mu \frac{\partial U_k}{\partial x_k} \right) + F_i . \quad (2.4)$$

For a compressible, Newtonian fluid, (2.1) and (2.4) must be complemented by an equation of state and the energy equation to form six equations for the six unknowns U_i , ρ , P and T , where $T(x_i, t)$ is the temperature field.

If the flow is incompressible, then $\frac{\partial U_k}{\partial x_k} = 0$, density is assumed given, and (2.4)

reads:

$$\rho \left(\frac{\partial U_i}{\partial t} + U_j \frac{\partial U_i}{\partial x_j} \right) = - \frac{\partial P}{\partial x_i} + \frac{\partial}{\partial x_j} \left[\mu \left(\frac{\partial U_i}{\partial x_j} + \frac{\partial U_j}{\partial x_i} \right) \right] + F_i . \quad (2.5)$$

Note that in (2.5), μ has not been assumed constant, a useful generalization when surface heating/cooling is used.

The familiar Navier-Stokes equation is obtained from (2.2) by assuming a Newtonian, incompressible, constant-viscosity fluid:

$$\rho \left(\frac{\partial U_i}{\partial t} + U_j \frac{\partial U_i}{\partial x_j} \right) = - \frac{\partial P}{\partial x_i} + \mu \frac{\partial^2 U_i}{\partial x_j \partial x_j} + F_i . \quad (2.6)$$

In this case, the momentum and continuity equations form four equations for the four unknowns U_i and P .

All the above equations are valid for nonturbulent as well as turbulent flows. However, in the latter case all the dependent variables are in general random functions of space and time. No straightforward method exists for solving stochastic, nonlinear partial differential equations. The recent attempts to use dynamical systems theory to study turbulent flows has not yet reached fruition especially at Reynolds numbers far above transition. The brute-force numerical integration of the equations using the supercomputer is prohibitively expensive at practical Reynolds numbers. For the present at least, a statistical approach, where a temporal, spatial or ensemble mean is defined and the equations of motion are written for the various moments of the fluctuations about this mean, is the only route available to get meaningful engineering results. Unfortunately, the nonlinearity of the Navier-Stokes equations guarantees that the process of averaging to obtain moments results in an open system of equations, where the number of unknowns is always more than the number of equations, and more or less heuristic modeling is used to close the equations.

In (2.6), let $U_i = \overline{U_i} + u_i$ and $P = \overline{P} + p'$, where $\overline{U_i}$ and \overline{P} are temporal averages for the velocity and pressure, respectively, and u_i and p' are the velocity and pressure fluctuations about the respective averages. The equation governing the mean velocity for a Newtonian, incompressible, constant-viscosity, turbulent flow becomes:

$$\rho \left(\frac{\partial \overline{U_i}}{\partial t} + \overline{U_j} \frac{\partial \overline{U_i}}{\partial x_j} \right) = - \frac{\partial \overline{P}}{\partial x_i} + \frac{\partial}{\partial x_j} \left(\mu \frac{\partial \overline{U_i}}{\partial x_j} - \rho \overline{u_i u_j} \right) + F_i. \quad (2.7)$$

This equation is written in a form that facilitates the physical interpretation of the turbulent stress tensor (Reynolds stresses), $-\rho \overline{u_i u_j}$, as additional stresses on a fluid element to be considered along with the conventional viscous stresses and pressure. An equation for the components of this

tensor may be derived but it will contain third-order moments such as $\overline{u_i u_j u_k}$, and so on. The equations are closed by expressing the second- or third-order quantities in terms of the first- or second-moments, respectively. For a review of these first- and second-order closure schemes see Lumley (1983; 1987).

For external flows at high Reynolds number, viscous forces are confined to a relatively thin layer along the surface of a body, although this layer's thickness increases in the downstream direction. Outside the boundary layer, the flow could be computed using the potential flow theory. Within the viscous region, the classical boundary-layer approximations apply (Rosenhead, 1963; Schlichting, 1979). Ignoring body forces, the continuity and streamwise-momentum equations along a two-dimensional (or axisymmetric) surface of small curvature are obtained from (2.1) and (2.4), respectively:

$$\frac{\partial \rho}{\partial t} + \frac{\partial}{\partial x_1} (\rho U_1) + \frac{\partial}{\partial x_2} (\rho U_2) = 0, \quad (2.8)$$

$$\rho \left(\frac{\partial U_1}{\partial t} + U_1 \frac{\partial U_1}{\partial x_1} + U_2 \frac{\partial U_1}{\partial x_2} \right) = - \frac{dP}{dx_1} + \frac{\partial}{\partial x_2} \left(\mu \frac{\partial U_1}{\partial x_2} \right). \quad (2.9)$$

These equations are valid for variable properties ρ and μ . In (2.8) and (2.9), x_1 is in the main-flow direction along the body and x_2 is normal to the surface. Within the boundary-layer approximation, the pressure is constant in the normal direction and its value is determined by the inviscid flow at the outer edge of the boundary layer.

For steady flow, the above equations can be integrated in the x_2 direction, subject to the usual boundary conditions and including the possibility of wall mass transfer, resulting in the

momentum integral equation:

$$\frac{C_f}{2} = \frac{d \delta_\theta}{d x_1} + \delta_\theta \left[\left(2 + \frac{\delta^*}{\delta_\theta} \right) \frac{1}{U_\infty} \frac{d U_\infty}{d x_1} + \frac{1}{\rho_\infty} \frac{d \rho_\infty}{d x_1} + \frac{1}{R} \frac{d R}{d x_1} \right] - \frac{\rho_0 v_0}{\rho_\infty U_\infty} . \quad (2.10)$$

$$\text{In (2.10), } C_f = \text{local skin-friction coefficient} \equiv \frac{\tau_0}{1/2 \rho_\infty U_\infty^2} , \quad (2.11)$$

$$\delta^* = \text{displacement thickness} \equiv \int_0^\infty \left(1 - \frac{\rho U_1}{\rho_\infty U_\infty} \right) d x_2 , \quad (2.12)$$

$$\delta_\theta = \text{momentum thickness} \equiv \int_0^\infty \frac{\rho U_1}{\rho_\infty U_\infty} \left(1 - \frac{U_1}{U_\infty} \right) d x_2 , \quad (2.13)$$

R is the radius of curvature of the two-dimensional surface or the radius of revolution of the axisymmetric body, ρ_∞ and U_∞ are the density and velocity of the freestream, respectively, ρ_0 and v_0 are the density and normal velocity of fluid injected through the surface, and τ_0 is the shear stress at the wall.

Since the skin-friction coefficient in the momentum integral equation is defined in terms of the shear stress and not in terms of the velocity gradient at the wall, (2.10) is, in fact, valid for both laminar and turbulent flows as well as for both Newtonian and non-Newtonian fluids; the only assumptions being that the boundary-layer flow is steady and two-dimensional in the mean. For an incompressible fluid, $\rho = \rho_\infty = \text{constant}$. In case of a turbulent flow, the mean streamwise velocity, $\overline{U_1}(x_1, x_2)$, is used in the definition of δ^* and δ_θ . For a Newtonian fluid,

$$\tau_0 = \mu \left. \frac{\partial U_1}{\partial x_2} \right|_{\text{wall}} \quad (2.14)$$

In the following, we develop the turbulent boundary-layer equations. Applying the boundary-layer approximations to the time-averaged continuity, streamwise-momentum, and normal-momentum equations for a steady, two-dimensional turbulent flow of a Newtonian, incompressible fluid, the resulting equations read:

$$\frac{\partial \overline{U_1}}{\partial x_1} + \frac{\partial \overline{U_2}}{\partial x_2} = 0 \quad , \quad (2.15)$$

$$\rho \left(\overline{U_1} \frac{\partial \overline{U_1}}{\partial x_1} + \overline{U_2} \frac{\partial \overline{U_1}}{\partial x_2} \right) = - \frac{\partial \overline{P}}{\partial x_1} + \frac{\partial}{\partial x_2} \left(\mu \frac{\partial \overline{U_1}}{\partial x_2} - \rho \overline{u_1 u_2} \right) \quad , \quad (2.16)$$

$$0 = - \frac{\partial \overline{P}}{\partial x_2} + \frac{\partial}{\partial x_2} \left(\rho \overline{u_2^2} \right) \quad , \quad (2.17)$$

where $\overline{U_1}$ and $\overline{U_2}$ are the time-averaged velocity in the streamwise and normal directions, respectively, \overline{P} is the mean pressure, ρ is the constant density, μ is the variable viscosity, $-\rho \overline{u_1 u_2}$ is the tangential Reynolds stress, and $-\rho \overline{u_2^2}$ is the normal Reynolds stress.

Equation (2.17) can be integrated to yield:

$$\overline{P} = P_0 - \rho \overline{u_2^2} \quad , \quad (2.18)$$

where P_0 is the pressure just outside the turbulent region, determined from the potential flow solution. Within the same order of approximation,

$$\frac{\partial \overline{P}}{\partial x_1} = \frac{d P_0}{d x_1} \quad , \quad (2.19)$$

leaving (2.15) and (2.16) as two equations for the three unknowns $\overline{U_1}$, $\overline{U_2}$ and $\overline{u_1 u_2}$.

Obviously, no solution can be obtained from first principles, and we must rely on more or less

heuristic models to close the equations. Nevertheless, both equations can be integrated in the normal direction to yield the Von Karman integral momentum-balance equation:

$$\begin{aligned}
 C_f &\equiv \frac{2 \tau_0}{\rho U_\infty^2} = \frac{2\nu}{U_\infty^2} \left[\frac{\partial \overline{U_1}}{\partial x_2} \right]_0 = 2 \left(\frac{u_\tau}{U_\infty} \right)^2 \\
 &= 2 \frac{d \delta_\theta}{d x_1} + 2 \delta_\theta \left[\left(2 + \frac{\delta^*}{\delta_\theta} \right) \frac{1}{U_\infty} \frac{d U_\infty}{d x_1} + \frac{1}{R} \frac{d R}{d x_1} \right] - 2 \frac{v_0}{U_\infty} ,
 \end{aligned}
 \tag{2.20}$$

where, C_f is the local skin-friction coefficient, δ^* and δ_θ are the displacement and momentum thicknesses, respectively, U_∞ is the freestream velocity, R is the radius of curvature of the wall, and v_0 is the normal velocity of fluid injected through the surface (positive for injection and negative for suction).

A second useful equation is obtained from (2.16) by taking the limit $x_2 \rightarrow 0$. At a fixed wall, the equation becomes after some rearranging:

$$\begin{aligned}
 \rho v_0 \left[\frac{\partial \overline{U_1}}{\partial x_2} \right]_0 + \frac{d P_0}{d x_1} - \frac{d \mu}{d \overline{T}} \left[\frac{\partial \overline{T}}{\partial x_2} \frac{\partial \overline{U_1}}{\partial x_2} \right]_0 + \rho \left[\frac{\partial \overline{u_1 u_2}}{\partial x_2} \right]_0 \\
 = \left[\mu \frac{\partial^2 \overline{U_1}}{\partial x_2^2} \right]_0 ,
 \end{aligned}
 \tag{2.21}$$

where \overline{T} is the mean temperature field, and the subscript $[]_0$ indicates flow quantities computed at the wall. For a two-dimensional boundary layer, mean vorticity is only in the spanwise direction and is equal to $-\partial \overline{U_1} / \partial x_2$. The right-hand side of (2.21) therefore represents the vorticity flux at the surface. In the absence of suction/injection, pressure gradient,

heating/cooling, the first three terms on the left-hand side of (2.21) vanish. The sign of the curvature of the mean velocity profile (or the vorticity flux) at the wall is then determined by the sign of the normal derivative of the tangential Reynolds stress. Information regarding $\overline{u_1 u_2}$ has to come from experiment. The Reynolds stress must be zero at the wall and at the outer edge of the boundary layer. In between, $\overline{u_1 u_2}$ is negative reaching a minimum at a height above the wall of typically $x_2 = 0.05\delta$ or less, where δ is the boundary layer thickness. Even though the slope of the tangential Reynolds stress profile is very large near the wall, at the wall itself this slope must be zero. It follows, then, that the canonical turbulent boundary layer* has a streamwise mean velocity profile with zero curvature at the wall, much the same as the corresponding laminar boundary layer. Notwithstanding this common characteristic with the Blasius boundary layer, the turbulent boundary layer is quite different from the laminar one. The turbulent mixing concentrates most of the mean vorticity much closer to the wall than in the laminar case, resulting in higher skin friction.

In the turbulent case, transpiration through the wall, shaping, and heat transfer affect the mean velocity profile qualitatively in the same direction as in the laminar case. The effects are complicated, however, because these modulations also influence the Reynolds stress term.

* Steady, incompressible, isothermal, two dimensional, fixed wall, zero pressure gradient, and no transpiration.

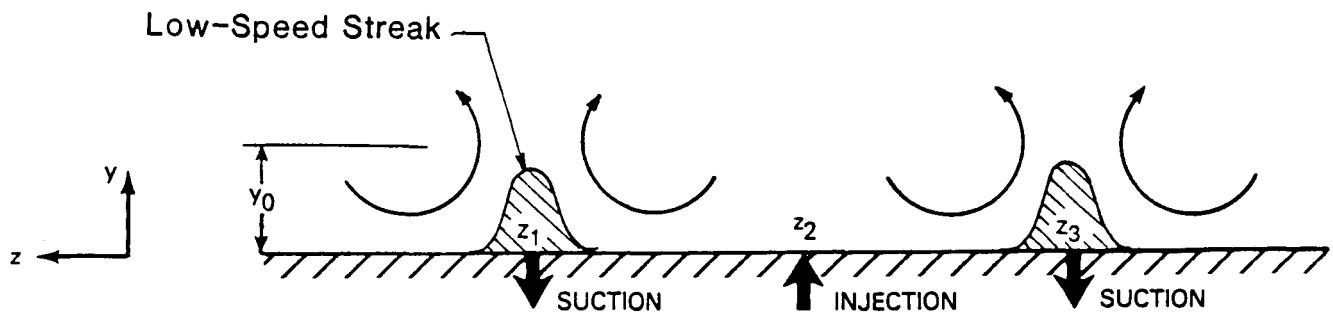
3. SUCTION/INJECTION EFFECTS ON DRAG

It is suggested that selective suction and/or injection of a like fluid be used to examine its effects upon the eddy structure within the wall region. Simpson et al. (1969), Simpson (1970), Antonia et al. (1988) and others have shown that uniform suction increases the streamwise length scales in the wall region, and injection has the opposite effect. However the effect of suction/injection on the eddy structure and upon the Reynolds stress has not been studied in detail and hence is not clear. In principle, one would like to be able to identify where a low-speed streak is presently located and apply a small amount of suction under it. Assuming that the oscillations and Reynolds stress are due to the instability of an inflectional $U(y)$ velocity profile, one needs to remove only enough fluid so that the inflectional nature of the profile is alleviated. The amount and spatial distribution of the suction would depend on the growth stage of the low-speed streak, i.e., on the magnitude of the shear associated with the inflectional profile. Thus, if the low-speed region is rather weak (possibly because it has a large spanwise scale or is relatively young), it may require very little suction to prevent the profile from becoming inflectional. On the other hand, a robust streak may have already produced a strong inflectional profile and would require a much larger amount of suction to eliminate the inflectional character. In either case, the total amount of fluid removed from the boundary layer would conceivably be much less than in the case of uniform suction over the entire wall area.

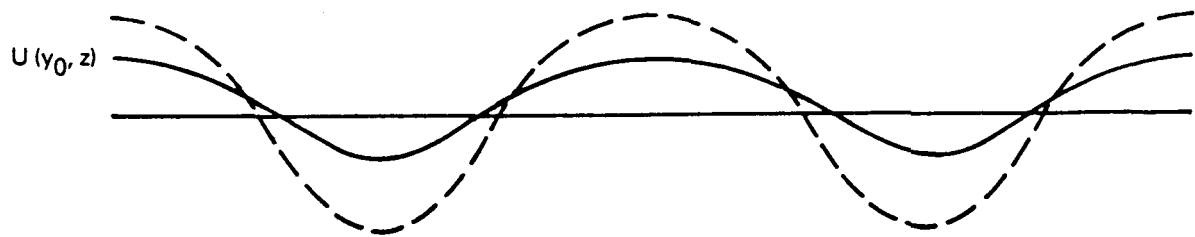
Although suction may reduce the Reynolds stress, it is not clear that the drag will also be reduced. In parallel bounded shear flows, the total stress is the sum of the Reynolds tangential stress and the viscous stress. Whereas the tangential Reynolds stress, $-\overline{uv}$, is responsible for the turbulent production, which peaks at $y^+ \approx 12$ to 15 , the viscous stress at the wall determines the drag. Hence, reducing the Reynolds stress does not necessarily guarantee that the drag on the solid boundary will be decreased. In low-concentration polymer flows, both the Reynolds and the viscous stresses are reduced, possibly because the viscous scale is increased. This example suggests that selective suction to reduce the Reynolds stress might also reduce the drag.

An alternative technique that could conceivably reduce the Reynolds stress and reduce the drag is to inject fluid selectively under the high-speed regions. The immediate effect would be to decrease the viscous shear at the wall resulting in less drag. In addition, the velocity profiles in the spanwise direction, $U(z)$, would have a smaller shear, $\partial U/\partial z$, because the injection would create a more uniform flow. Since Swearingen & Blackwelder (1984) have found that inflectional $U(z)$ profiles occur as often as inflection points are observed in $U(y)$ profiles, injection under the high-speed regions would decrease this shear and hence the resulting instability.

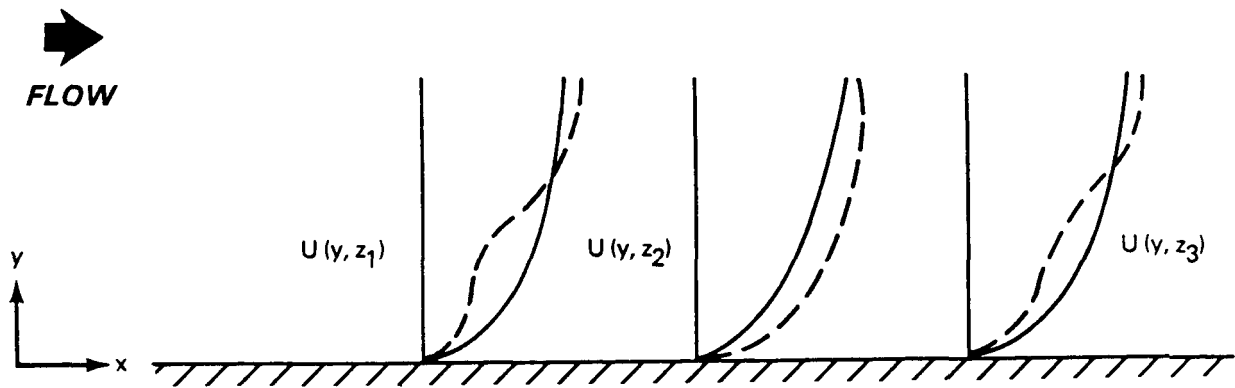
The combination of selective suction and injection is sketched in Figure 2. In Figure 2a, the vortices are sketched idealized by a periodic distribution in the spanwise direction. The instantaneous velocity profiles without suction and injection at constant y and z locations are shown by the dashed lines in Figures 2b and 2c. Clearly, the $U(y_0, z)$ profile is inflectional, having two inflection points per wavelength. At z_1 and z_3 and inflectional $U(y)$ profile is also evident. The same profiles with suction at z_1 z_3 and injection at z_2 are shown by the solid lines. In all cases, the shear associated with the inflection points has been reduced. Since the inflectional profiles are all inviscidly unstable with growth rates proportional to the shear, the resulting instabilities would be weakened by the suction/injection process. Since the turbulent shear stress, $-\overline{uv}$, is believed to result from the inflectional instability, it also should be reduced.



a. Streamwise Vortices in the y - z Plane. Suction/Injection Applied at z_1 , z_2 and z_3



b. Resulting Spanwise Velocity Distribution at $y = y_0$



c. Velocity Profiles Normal to the Plate

Figure 2. Effects of Suction/Injection on Velocity Profiles. Dashed Lines are Reference Profiles and Solid Lines are Profiles with Suction/Injection Applied

4. PREVIOUS RESEARCH USING SUCTION/INJECTION

Most of the previous research on suction and injection has been concerned with either delaying transition by maintaining a more stable laminar boundary layer (Reshotko, 1980; Gad-el-Hak, 1989a; 1989b) or increasing the lift and decreasing the drag on an airfoil, usually by preventing separation. Consequently, very little is known about the effects of suction on the turbulent eddies within the boundary layer, especially those near the wall. The only research on the wall region in the presence of suction seems to be that of Eléna (1975) and more recently Antonia et al. (1988). Eléna made detailed measurements of u' and θ' in the heated wall region of a large-diameter turbulent pipe flow with and without suction. He used suction coefficients of $0 \leq C_q \equiv v_0/U_\infty \leq 0.003$, where v_0 is the average normal velocity at the wall and U_∞ is the mean bulk velocity in the pipe. Eléna found that the maximum u' turbulence level at $y^+ \approx 13$ dropped from 15 to 12 percent as C_q varied from 0 to 0.003 as shown in Figure 3. More dramatically, the tangential Reynolds stress dropped by a factor of 2 for the same variation of C_q as shown in Figure 4. The dissipation length scale near the wall increased by 40 percent and the integral length scale by 25 percent with the suction.

Eléna (1975) reported some measurements of the instantaneous velocity and temperature signals with and without suction. He found that suction decreased the magnitude of both the temperature and velocity fluctuations and increased the time interval between large-amplitude fluctuations. The suction especially decreased the negative velocity excursions at $y^+ < 30$. These results are consistent with the idea that the suction primarily affects the low-speed streaks by reducing their magnitude and thus inhibiting their ability to participate in the formation of inflectional velocity profiles.

In a conventional boundary layer, the skewness of the mean velocity fluctuations is known to be positive near the wall and negative in the logarithmic region, with a zero value at approximately $y^+ = 20$. The ejections of low-speed fluid from the wall produce a Reynolds stress with fluctuations $u < 0, v > 0$. As the ejected fluid moves into higher speed fluid, it contributes to a negative skewness factor. Conversely, the pockets of high-speed fluid

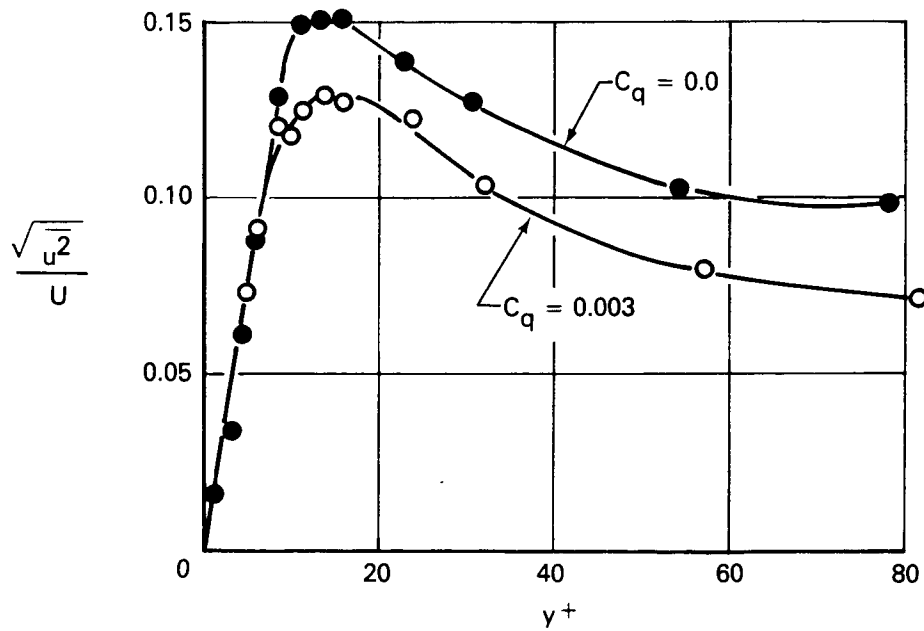


Figure 3. Streamwise Velocity Fluctuations in a Pipe Flow with and without Suction (from Elena, 1975)

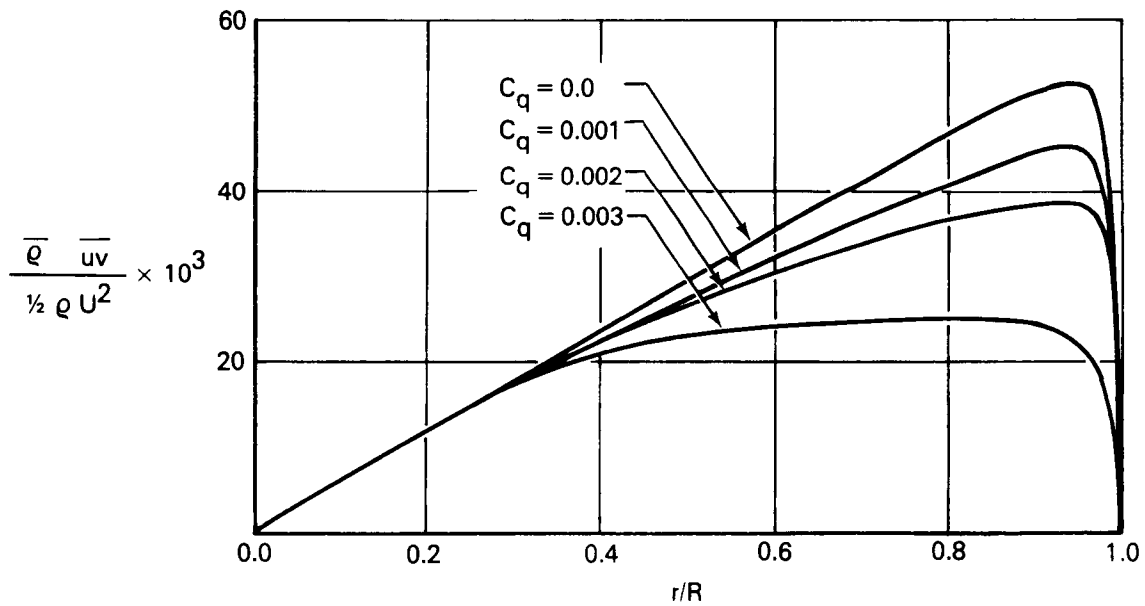


Figure 4. Reynolds Stress in a Pipe Flow with and without Suction (from Elena, 1975)

bombarding the wall region produce a Reynolds stress with $u > 0$ and $v < 0$. As they move nearer the wall, the pockets produce a positive skewness factor. Consequently, the position of zero skewness is an indicator of where these two types of eddies have established a relative balance of equal importance. Since suction would preferentially remove more of the low-speed regions than pockets, the pockets will penetrate further to the wall and the location of the zero skewness should also move toward the wall. Eléna's (1975) results, reproduced in Figure 5, show that the skewness crossing does indeed move from $y^+ \approx 20$ at zero suction to $y^+ \approx 12$ with $C_q = 0.003$.

In a study to measure the total drag, Wilkinson, Ash & Weinstein (1980) tailored a suction surface to combine the favorable aspects of uniform suction on the surface with streamwise riblets and slots. The surface consisted of streamwise grooves spaced 5 to $20\nu / u_\tau$ apart modeled after the riblets of Walsh (1980). The surface was constructed by wrapping the test model with string; hence, the suction occurred between the strings (at the troughs of the ribbed surface) but was otherwise spatially uniform and was continuous in time. Zero boundary layer growth, $d\delta_0/dx \approx 0$, was achieved with suction coefficients of $C_q \approx 0.003$, in agreement with the results of Rotta (1970) and Verollet et al. (1972). Wilkinson et al. measured the drag with a direct drag balance and compared it with that of a flat plate. The total drag, consisting of the integrated skin friction and the momentum loss due to suction, increased with C_q , in agreement with the results of Favre et al. (1966) and Simpson et al. (1969). Wilkinson et al. concluded that the longitudinal slots did not have any advantage over other porous surfaces. In our opinion, based on the results of Johansen & Smith (1986), Wilkinson et al. applied the suction at the wrong place. The ribbed surface causes the low-speed streaks to focus over the peaks of the longitudinal grooves and the high-speed regions to concentrate at the troughs. Wilkinson et al.'s suction slots removed the high-speed fluid, thus causing an increase in the $U(z)$ profile's shear, which is destabilizing. In the present innovation, the suction slots are located over the peaks of the longitudinal grooves. Low-speed regions are intermittently removed, yielding lower shear in the $U(z)$ profile and a bursting rate and requiring minuscule energy expenditure.

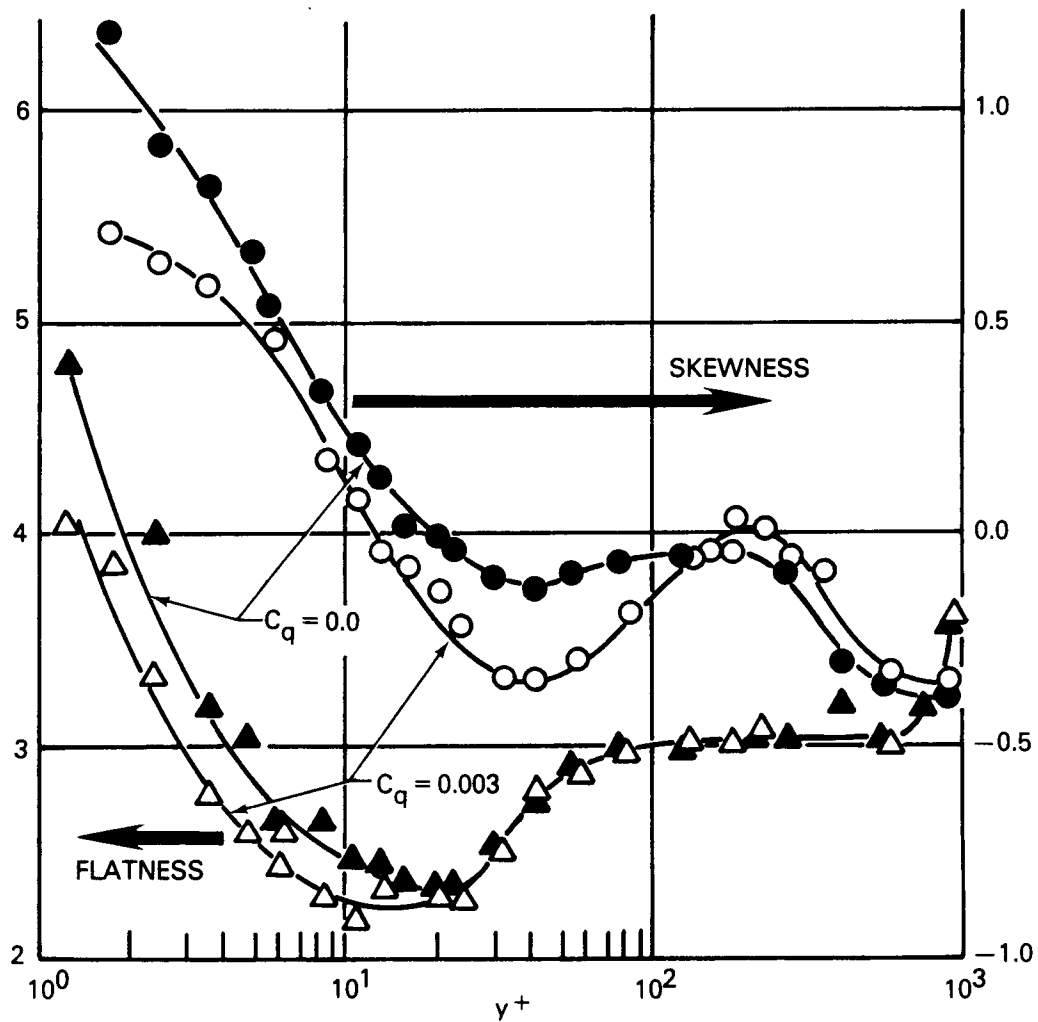


Figure 5. Skewness and Flatness Factors of the Steamwise Velocity Component in a Pipe Flow with and without Suction (from Elena, 1975)

The only published research on intermittent or pulsed suction from a turbulent boundary layer appears to be that by Arakeri & Narasimha (1983). They used a single slit with a width of $0.58\delta^*$ ($40\nu/u_\tau$) aligned perpendicular to the freestream flow with continuous and periodic suction at frequencies up to the estimated bursting frequency. No attempt was made to synchronize the pulsed suction to the naturally occurring bursts. In addition, the authors used an extremely large suction flow rate with average suction coefficients exceeding unity i.e., $v_0 > U_\infty$. Since the suction was only through a single slot, this must have produced almost a discontinuity in the boundary layer, although the authors do not document or comment upon this. They do measure the mean velocity profile, the fluctuating velocity intensity and the wall shear stress at a single location at 2.5δ downstream of the slot. At these large suction coefficients, they find that the pulsating suction has no apparent advantage over continuous suction.

In another unique piece of research possibly related to the present innovation, Bechert et al. (1985) have speculated that the scales found on sharks use tangential injection to reduce the turbulent shear stress. They conclude that the low-speed streaks occur in regions of low instantaneous local pressure on the surface. The shark's scales are aligned so that the low pressure induces a tangential injection of flow into the wall region. Simultaneously, suction may be occurring elsewhere, for example, beneath the higher speed fluid. This hypothesis is supported by their examination of shark's scales from several species. They find rounded leading edges and sharp trailing ones and underlying cavities capable of maintaining a suction/injection mechanism.

This selective suction/injection model for sharks is qualitatively supported by the pressure-velocity gradient correlations of Moin & Kin (1982) shown in Figure 6. From the streamwise vortex model of Figure 2, it is easily seen that symmetry imposes $w = 0$ on the centerline of the low-speed region, i.e., $z = z_1$. Also, near the wall, i.e., $y^+ < 15$, $\partial w / \partial z$ must be negative on the centerline (based on the sign convention established in Figure 2). The correlation data of Figure 6 imply that the average pressure must be negative there also. A similar argument indicates that $\partial v / \partial y > 0$ would be consistent with a low pressure. The low values of p $\partial u / \partial x$ indicate

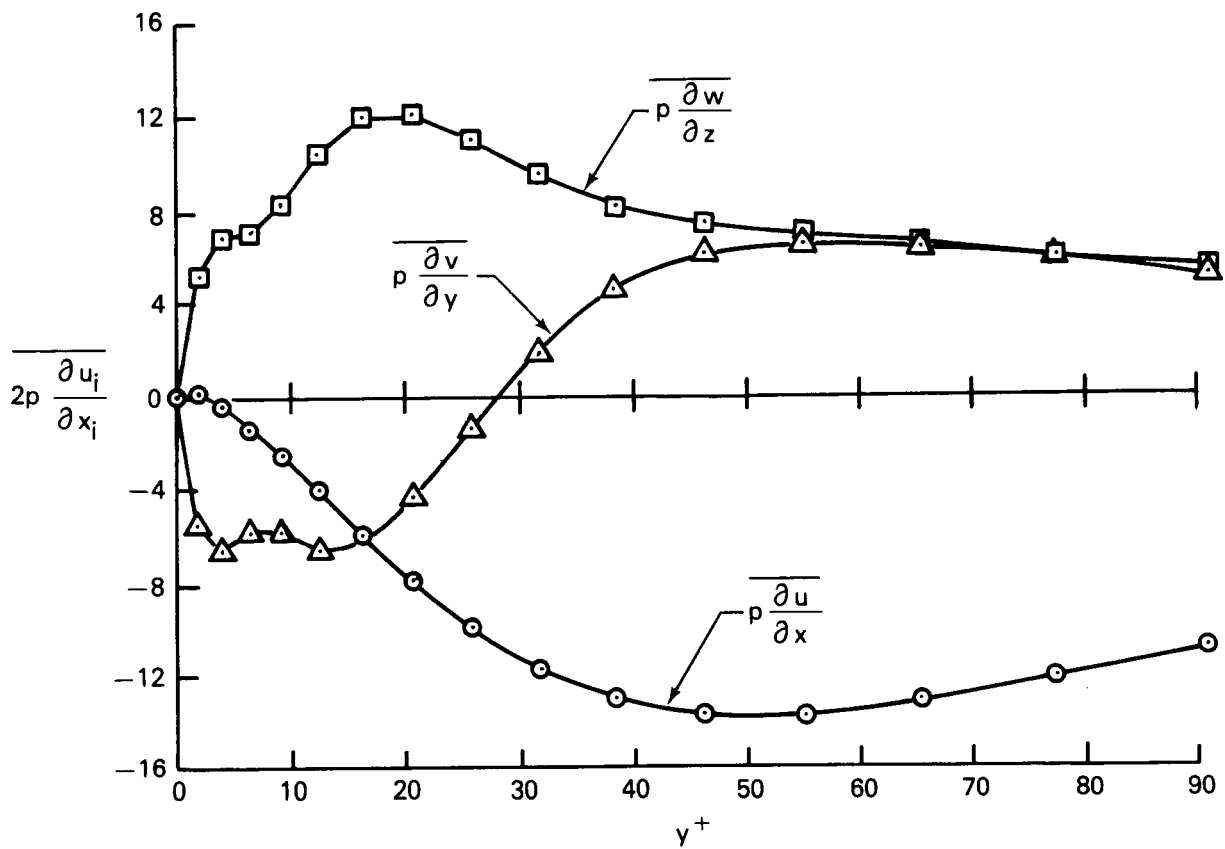


Figure 6. Pressure-Velocity Shear Correlations in the Wall Region of a Turbulent Channel Flow (from Moin & Kim, 1982)

that the pressure is not correlated with the same scale as u in the streamwise direction, a fact that is supported by the instantaneous pressure and velocity contours of Moin & Kim (see their Figures 19 and 21).

5. SELECTIVE SUCTION CONCEPT

It is easy to see the basic problem of using uniform suction to achieve a net drag reduction. A commercial aircraft travelling at a speed of 300 m/s would have a unit Reynolds number of $2 \times 10^7/\text{m}$ at sea level and $1 \times 10^7/\text{m}$ at an altitude of 10 km. Due to the much smaller kinematic viscosity of water, a ship or an underwater vehicle moving at the modest speed of 10 m/s (≈ 20 knots) would have the same unit Reynolds number of $1 \times 10^7/\text{m}$. Near the front of a wide-body aircraft the Reynolds number is then $O[10^7]$ and near its tail Re is $O[5 \times 10^8]$. At Reynolds number of 10^7 , the coefficient of skin friction for a turbulent boundary layer over a flat plate is about 0.003. When suction is applied uniformly, Figure 4 indicates that the slope of the Reynolds stress profile in the near-wall region does not change, although the peak Reynolds stress decreases as the suction rate increases. The first term in the left-hand-side of equation (2.21) becomes negative when suction is applied, which means that the curvature of the velocity profile at the wall becomes more negative (more full). This is stabilizing. Sufficient suction from the wall can yield zero growth of the momentum thickness, as shown in Section 4. Let us inspect equation (2.20). At $C_q = 0.003$, $d\delta_\theta/dx_1 = 0$ according to the experiments reviewed in the last section. However, $C_f = 2 d\delta_\theta/dx_1 + 2 C_q$, which means that at this suction rate, the coefficient of skin friction is $C_f = 0.006$, twice what it was without suction. At this particular Reynolds number, the breakeven point is achieved if we succeed in achieving a zero growth of the momentum thickness with a suction coefficient of 0.0015. If this asymptotic C_q becomes as low as 0.0008, a 50% drag reduction is attained. We maintain that the only way to achieve this goal is to use suction only where and when it is needed rather than uniformly in space and continuously in time. This is the essence of the selective suction innovation.

It is suggested that selective suction and/or injection be explored to ascertain if it can be used to control the turbulence production mechanism in the wall region of turbulent shear flows. Previous research has shown that the eddy structure in the wall region is random in space and time. Thus, in a naturally occurring turbulent flow, it is presently not feasible to use selective suction or injection in phase with a particular aspect of the eddy structure without employing a sophisticated

detection criterion. However, the recent experiment by Johansen & Smith (1986) indicates the feasibility of greatly reducing the spatial randomness of the low-speed streaks by using longitudinal roughness elements (LREs) with a spanwise spacing that matches the average streak spacing. The present investigation is aimed toward using such a surface together with longitudinal suction slots located at selected locations along the peaks of the longitudinal grooves. The low-speed streaks are removed intermittently through the suction slots.

To prove and optimize the proposed concept, two sets of experiments are conducted. First, the idea of selective suction is tested in a water facility using a single or a periodic train of artificially generated bursting events. Second, a more practical version of the innovation is studied in a wind tunnel using a ribbed surface and selective suction.

The selective suction technique was studied in the present investigation using flow visualization and fast-response probe measurement techniques. Fluorescent dyes and hydrogen bubbles were illuminated using sheets of laser light projected in the desired plane. The effects of the selective suction on the generation and evolution of artificially generated bursts were determined visually. For quantitative data, hot-film probes were placed inside the boundary layer to measure the instantaneous velocity. The velocity fluctuation records were analyzed using pattern recognition techniques that detect the occurrence and evolution of low-speed streaks and bursting events (Gad-el-Hak et al., 1984a).

In the wind tunnel experiments, important statistical turbulence quantities were computed to assess the performance of the proposed selective suction device. The mean streamwise velocity variations in the vertical and spanwise directions, $U(y)$ and $U(z)$, were determined by using vertical and horizontal rakes of single-element hot-film probes.

The present experiment is designed to see if the suction/injection can be used under naturally occurring conditions. Although the strips used to hold the streaks in position can easily be installed on many practical surfaces exposed to a turbulent flow, the suction/injection poses a larger deterrent for practical installation. However, if the earlier results are successful, it is felt

that practical solutions can be found to circumvent the plumbing details of the suction mechanism.

A simple mechanism similar to a shark's scales may suffice (see Bechert et al., 1985).

6. EXPERIMENTAL APPROACH

6.1 TOWING TANK

Turbulent and laminar boundary layers were generated by towing a flat plate in a water channel that is 18 meters long, 1.2 meters wide and 0.9 meter deep. The towing tank, shown in Figure 7, has been described by Gad-el-Hak (1987). The flat plate was rigidly mounted under a carriage that rides on two tracks mounted on top of the tank. During towing, the carriage was supported by an oil film to ensure a vibrationless tow, having an equivalent freestream turbulence of about 0.1 percent. The carriage was towed by two cables driven through a reduction gear by a 1.5-hp Boston Ratiotrol motor. The towing speed was regulated within an accuracy of 0.1 percent. The system was able to achieve towing speeds between 5 and 140 cm/s for the present study. However, most of the runs reported here were conducted at a speed of 20 cm/s.

6.2 WIND TUNNEL

The flow field in the closed-return wind tunnel is established by a 107 cm diameter nine-blade axial fan powered by a 25 horsepower variable-speed d.c. motor. Downstream of the fan, the flow expands through a $5\frac{1}{2}^\circ$ diffuser until the cross-sectional flow area is 2.5 x 2.5 m. After two 90° turns, the flow passes through a 10 cm long honeycomb having 0.48 cm cells. The screen section consists of four individual damping screens; the first three are 20 x 20 mesh screens having an open area of 53% followed by a 24 x 24 mesh screen having an open area of 72%. The settling chamber downstream of the screens is 1.8 m long before the flow enters a two-dimensional contraction into the test section. The test section has a cross-sectional area of 60 x 90 cm and is 6.0 m long. After exiting from the test section the flow encounters two 90° turns before the fan. All of the 90° turns within the tunnel are equipped with turning vanes. The turbulence level within the test section is less than 0.05% at all freestream velocities. The maximum velocity in the test sections is 20 m/s in its present configuration.

ORIGINAL PAGE IS
OF POOR QUALITY

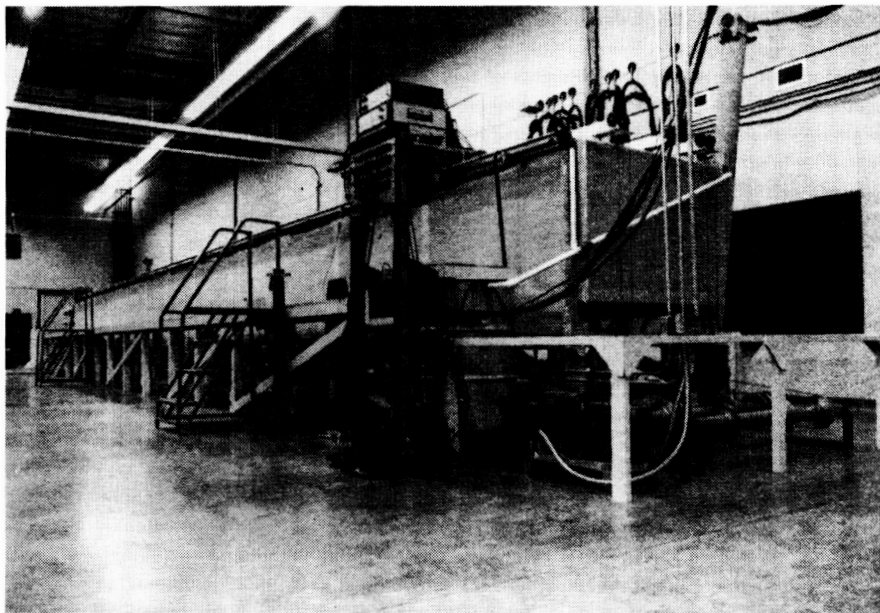


Figure 7. Flow Research 18-Meter Towing Tank

6.3 FLAT PLATES

A unique, zero-pressure-gradient flat plate was constructed for the present investigation. The 1-meter by 2-meter structure, shown in Figure 8, is made of glass-reinforced polycarbonate plate 6 mm thick, glued to a stainless steel frame designed for minimum obstruction to the flow. The plate has an elliptic nose at the leading edge and an adjustable lifting flap at the trailing edge. To avoid leading-edge separation and premature transition, the flap is adjusted so that the stagnation line near the leading edge is located on the working surface of the plate. The plate's smooth surface and flatness to within a few microns* make it one of the most controlled test beds available for boundary layer research. A laminar boundary layer can be obtained over the entire working surface for towing speeds in the range of 5 to 80 cm/s. Trips are used to generate a fully developed turbulent boundary layer. The trips are brass cylinders 0.32 cm in diameter and 0.25 cm high placed 5 cm downstream of the leading edge and having their axes perpendicular to the flat plate.

For the wind-tunnel experiments, a 90 x 600 cm flat plate was installed in the test section. The first 360 cm is a 0.6 cm thick aluminum plate reinforced on the backside so that it is flat within 0.01 mm.* The remaining 240 cm of the flat plate is Plexiglas. The junction between the aluminum and Plexiglas plates is aerodynamically smooth such that the surface discontinuities are less than 0.01 mm everywhere. The leading edge of the aluminum plate is round. At the trailing edge of the Plexiglas plate, a flap is installed to control the stagnation point at the leading edge.

A fully developed turbulent boundary layer is generated using a row of conventional three-dimensional trips located 45 cm downstream of the plate's leading edge. In order to lock in the low-speed streaks in the boundary layer, nylon strings having diameter of 0.4 mm (5 wall units) and length of 1300 mm (17,000 wall units) are placed in the streamwise direction 3800 mm from the leading edge with a spanwise spacing of 6.4 mm (80 wall units).**

* As measured when the plate is placed on a machinist's table. During actual operations, the plate may have some sagging and this tight tolerance is probably not attained.

** All the length scales are chosen based upon running the tunnel at a velocity of 500 cm/s, which results in a nominal value for the friction velocity of 21 cm/s.

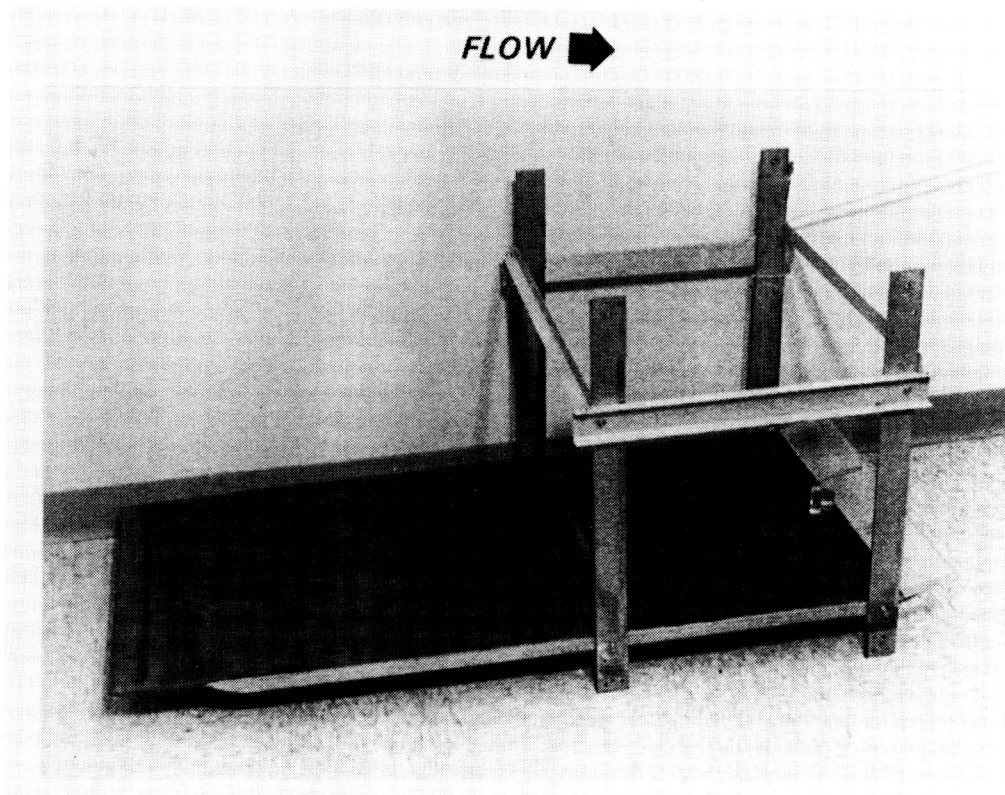


Figure 8. Photograph of the Zero-Pressure-Gradient Flat Plate

6.4 BURST GENERATOR

To generate an artificial burst, several excitation techniques were tried. Suction was applied suddenly through one, two, three or four holes separated in the spanwise direction by a distance of 10 mm ($\Delta Z^+ \approx 100$). The minute holes were 0.4 mm ($\approx 4\nu/u_\tau$) in diameter and were connected to a vacuum chamber controlled with a solenoid valve that is driven by a signal generator. This allowed the sudden withdrawal of a given amount of fluid and the generation of a horseshoe vortex that evolved into a burst.

The second excitation technique tried was the sudden pitching of a miniature delta wing having a span of 8 mm (80 wall units). The wing, with its apex facing the flow, was normally flush-mounted to the surface of the plate. At the desired instant, a pin centered around the trailing edge of the wing was driven upward using a solenoid to pitch the delta wing to a negative angle of attack of 30° . This produced two strong, longitudinal, counter-rotating vortices that lifted away from the wall and evolved into a burst. The burst generators were located 79 cm downstream of the plate's leading edge. Figure 9 is a close-up photograph of the surface of the flat plate, showing the flush-mounted delta wing and the four suction holes (located to the left of the white marks in the picture).

6.5 STREAMWISE SUCTION SLOT

A single streamwise slot flush-mounted with the flat plate was used to withdraw selectively the near wall fluid in the water boundary layer. The slot was located just behind the artificial burst generator at $x = 79.4$ cm, had a width of 0.1 mm (≈ 1 wall unit) and a maximum length of 150 mm ($\approx 1500 \nu/u_\tau$). The lateral position of the slot was chosen to correspond to the location of the artificially-generated low-speed streaks. The usable slot length was adjusted by covering the unused portion with an electric tape. In the present investigation, most of the runs were conducted using the upstream portion of the slot having a length of 50 mm ($\approx 500 \nu/u_\tau$). An internal reservoir directly underneath the streamwise slot ensured that the flow rate was uniform to within 2 percent along the entire length of the slot. A small conduit connected the reservoir to a vacuum chamber controlled with a solenoid valve that is driven by a signal generator.

ORIGINAL PAGE IS
OF POOR QUALITY

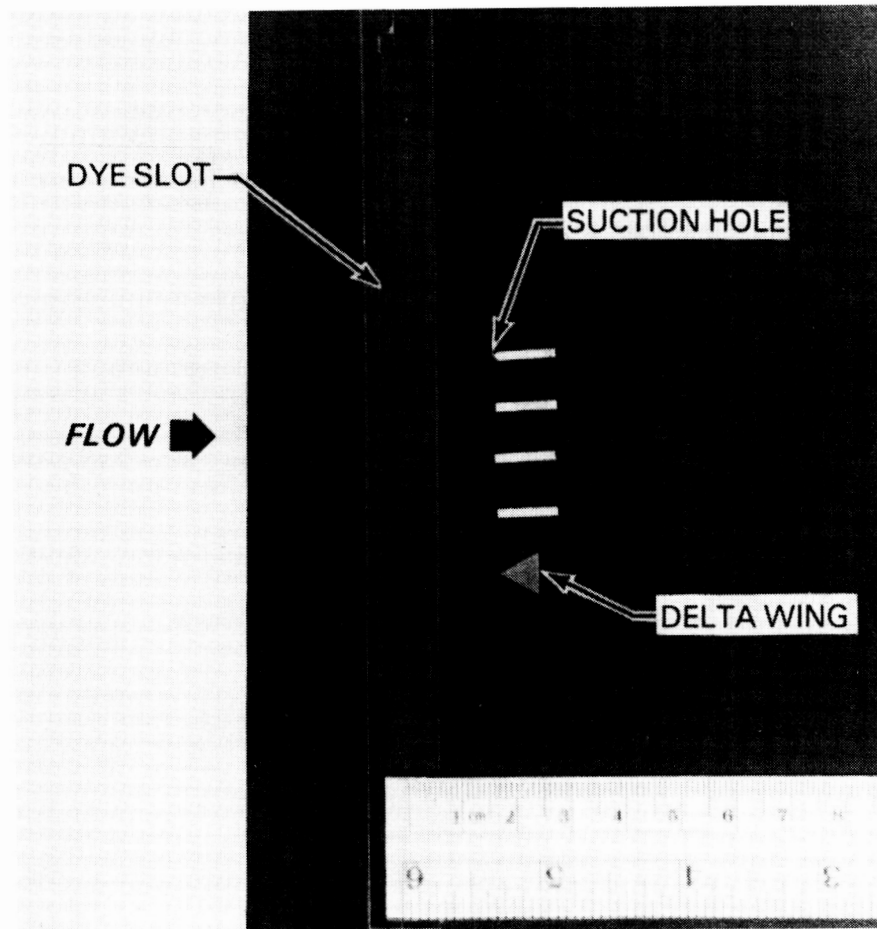


Figure 9. Close Up of the Flush-Mounted Delta Wing and the Suction Holes

This allowed the sudden withdrawal of a given amount of fluid from the slot. The phase between the artificial generation of a burst and the withdrawal of near wall fluid was controlled within the limitations of the experimental apparatus.

The amount of fluid withdrawn from the streamwise slot was controlled by changing the suction duration and the pressure inside the low-pressure chamber. In the continuous mode, the flow rate varied between 1 and 10 cm³/s. Since suction is never applied uniformly over the surface, the average normal velocity is used to define the suction coefficient. The average normal velocity is the flow rate divided by an appropriate reference area. The width of the slot was 0.1 mm and its cross-section area was 5 mm². Only one slot is necessary for each low-speed streak and the average spanwise distance between low-speed streaks in the flow was 10 mm ($100\nu/u_\tau$). Thus, the effective area over which the suction was applied was 500 mm², which yields an equivalent average normal velocity of 0.2 to 2 cm/s; i.e., this velocity applied uniformly over the plate would remove the same amount of fluid. The corresponding values of the suction coefficient, $C_q = 0.01 - 0.1$, are large compared with previous suction results, however further reductions should be possible by optimizing the geometry of the suction slot. For example, increasing the width of the slot to more closely correspond to the width of the low-speed streaks, i.e. $20\nu/u_\tau$, would reduce the normal velocities and apply more of a perturbation to the streak. Moreover, the above calculations assume that the streamwise slots continue along the entire length of the plate and are periodic in the spanwise direction. Further savings are feasible by using slots with finite length and periodically repeating the pattern in the streamwise direction. Additionally, as seen in Section 8.2, intermittent suction reduces the equivalent average normal velocity considerably.

6.6. VISUALIZATION METHODS

To visualize the near-wall events in the natural and perturbed turbulent boundary layers in the towing tank, both fluorescent dye and hydrogen-bubble techniques were used (Gad-el-Hak, 1986; 1988a; 1988b). The dyes were seeped into the boundary layer through a spanwise slot 0.15 mm wide and 15 cm long and located 77 cm downstream of the leading edge of the flat plate. The

dye slot was milled at a 45° angle inclined toward the plate's trailing edge to minimize the flow disturbance. The hydrogen bubbles were generated using either a platinum or a stainless-steel wire having a diameter of 50 microns and a length of 10 cm. The wire was placed at different locations either parallel to or perpendicular to the flat plate to obtain top views or side views, respectively, of the flow field. To create time lines, a standard circuit was employed to supply intermittently 100 volts to the wire, which acted as a cathode.

Both the fluorescent dyes and the hydrogen bubbles were illuminated using sheets of laser light projected in the desired plane. This provided an extra degree of freedom in observing the large-eddy structures and the bursting events, because both the tracer and light location could be controlled within the limitations of the experimental apparatus. In order to generate a sheet of light, a 5-watt argon-ion laser (Spectra Physics Model 164) was used with a mirror mounted on an optical scanner having a natural frequency of 720 Hz (General Scanning, Inc.) and driven by a sine-wave signal generator of the desired frequency. The frequency of the sine wave was usually set equal to the inverse of the shutter speed of the camera. The light sheets were approximately 1 mm thick, which was sufficient to resolve the large structure within the turbulent regions. A vertical sheet of laser light parallel to the flow was used to visualize side views of the wall events and the large-eddy structures, and a horizontal sheet near the surface of the plate was used to obtain top views of the flow field in the vicinity of the wall.

6.7 VELOCITY MEASUREMENTS

Miniature boundary-layer hot-film probes (TSI Model 1260) were used in the water experiments to measure the longitudinal mean and fluctuating velocities. The probe diameters were 0.025 mm, and their sensing lengths were 0.25 mm. A probe traverse powered by a stepping motor was controlled through an APPLE II Microcomputer was used for surveying the boundary layers. Conventional statistical quantities, such as the mean, the root mean square, the spectral distribution, the autocorrelation coefficient, and the probability density function, were computed from the velocity signals.

For the wind-tunnel experiments, both individual hot-wire probes and a hot-wire rake were used. In both cases, the hot-wire sensors are attached to jewellers' broaches extending upstream from the probe support approximately 1.5 cm. The jewellers broaches are tapered to a diameter of 0.05 mm at the tip. In the individual probes, the broaches are spaced at various distances so that a variety of hot wires having different lengths could be used. The sensing elements of the hot-wire probes are soft-soldered directly onto the broaches. Platinum-10% rhodium wires having diameters ranging from 1.2 to 5.0 μm are used. Constant-temperature hot-wire anemometers are used with a nominal overheat ratio of 33%. By using higher and lower values, the effect of the overheat ratio was found to be nil. Depending upon the diameter of the hot-wire sensor, the frequency response of the anemometers varies from 5 to 12 kHz. The output signals from the anemometers enter a bucking amplifier, which subtracts a fixed voltage and amplifies the remaining signal by a factor of 10. These signals are connected to analog-to-digital converters, which are controlled by a PDP 11/55 computer and are capable of digitizing data at the rate of 350 000 samples/s. However, to acquire digital data continuously in time without inter-record gaps, the acquisition speed is limited by the transfer rate to the disk pack. By using double buffering, a maximum aggregate digitizing rate of 240 kwords/s is possible, giving data which are continuous in time from one block to the next. The digitized velocities are stored on an 80 Mbyte Winchester disk for further processing. During calibration, the hot-wire sensors are placed in the freestream near a Pitot-static tube. The resulting pressure difference at each velocity is measured by an MKS Baratron pressure transducer. The pressure signal is also digitized during calibration, and the Bernoulli's equation is used to obtain the freestream velocity. The acquired data set for each run is typically linearized and written onto a magnetic tape for permanent storage. All of the remaining digital processing is accomplished on the PDP 11/55 computer using FORTRAN programs. A 4010 Tektronix terminal is used to communicate with the computer as well as to display the graphical output of the data.

6.8 PATTERN-RECOGNITION ALGORITHMS

Two pattern-recognition algorithms were used to more objectively detect low-speed streaks and bursts. A novel technique that utilizes the streamwise velocity signal from three hot-film probes was developed to detect low-speed streaks (Gad-el-Hak et al., 1984a). The probes were located at $y^+ = 10$ at the same streamwise position with a spanwise separation of approximately $20 \nu/u_\tau$. Thus, the total array spanned $40 \nu/u_\tau$, which is approximately half the average low-speed streak spacing. A pattern recognition algorithm identified a low-speed region whenever all three signals were less than the local mean velocity by one-half the root-mean-square (rms) value, and the velocity measured by the middle probe was less than the velocity on either side. The beginning and end of each low-speed region could thus be identified, and the streaks' average length and frequency computed.

To test this algorithm, experiments were first carried out using a rake of twelve velocity probes located at $y^+ = 10$ but having a significantly broader spanwise extent. Low-speed streaks were readily identified using the iso-velocity contours computed from the rake's output, and their spacing was in reasonable agreement with results obtained from visualization experiments conducted under similar conditions. The results of the algorithm were compared with the low-speed streaks obtained from the rake. The comparison showed that the detected algorithm picked out the streaks exceedingly well, and that the streaks meander in the spanwise direction so that often a single streak crosses the probes two or more times, resulting in multiple detections.

The second pattern-recognition algorithm employed in the present investigation was a burst detection scheme using the variable-interval time-averaging (VITA) technique developed by Blackwelder & Kaplan (1976). A single hot-film probe located at $y^+ = 20$ was used for burst detection. The program counted the number of bursts that occur near the wall and recorded their intensities.

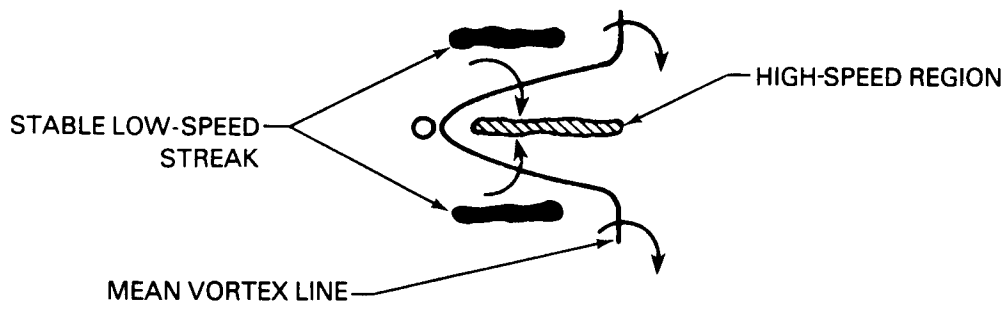
7. RESULTS OF PHASE I RESEARCH

A single bursting event or a periodic train of bursts was generated in the present investigation to demonstrate the feasibility of the selective suction concept. In this section, we briefly review our previous results concerning artificial burst generation. For more complete details, the reader is referred to the paper by Gad-el-Hak & Hussain (1986).

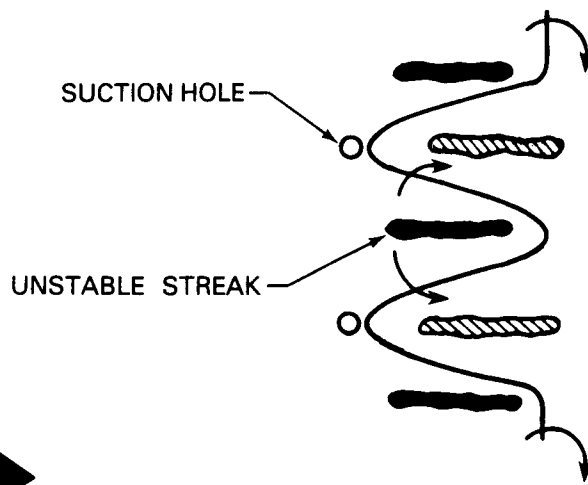
7.1 BURSTS IN LAMINAR FLOW

To understand how the artificial burst generator works, the initial experiments were conducted in a laminar boundary layer environment. This allowed relatively easy visualization of the artificial events, free from the random background that exists in a turbulent boundary layer. Of course, the artificial event evolves differently in the laminar and the turbulent cases. However, the resulting patterns are qualitatively the same.

In a two-dimensional laminar boundary layer, the vorticity vector is in the spanwise direction. Consider the boundary layer to consist of a row of rectilinear vortices aligned in the spanwise direction. Consider further the result of suddenly withdrawing near-wall fluid from one, two or three suction holes separated in the spanwise direction. As shown in the schematic in Figure 10, a near-wall vortex line will then be "pinned down" at the location of the suction holes, thus forming one or more horseshoe-type hoops. In the case of two holes, one horseshoe vortex with its head pointing downstream forms. For three suction holes, two such vortices are generated. The longitudinal vortices exist in a strong shear and induce low- and high-speed regions between them, as shown in Figure 10. For the single-hole case, two low-speed streaks and one high-speed region form. In the case of two holes, three low-speed streaks and two high-speed regions form. Because of the particular direction of rotation of the counter-rotating vortices, only the middle low-speed streak will lift up, causing an unstable, inflectional velocity profile and bursting. Similarly, for three holes, two unstable streaks form, leading to two bursts. These arguments can be extended to an arbitrary number of spanwise suction holes.

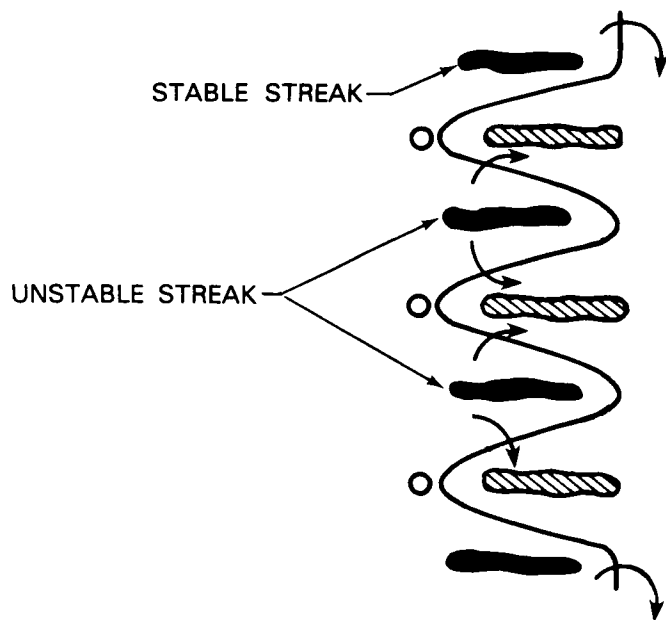


a. Single Hole



b. Two Holes

➔
FLOW



c. Three holes

Figure 10. Artificial Burst Generation. Suction Hole Effects on Spanwise Vortex Lines in a Boundary Layer

The artificial events resulting from withdrawing near-wall fluid in a laminar boundary layer through one, two, three or four suction holes were visualized using fluorescent dye seeping from the spanwise slot and a horizontal sheet of laser light at the surface of the plate. The results for a freestream speed of 20 cm/s are shown in individual movie frames in Figures 11, 12, 13 and 14. The flow relative to the flat plate is from left to right, and the time from the onset of suction is indicated on each movie frame. As expected, for a single suction hole, two stable streaks form and no bursting events are observed. Three low-speed streaks are marked by the bright dye accumulation in Figure 12 for the case of two suction holes, but only the middle one breaks into a burst. In Figures 13 and 14, two and three unstable streaks are observed, respectively, for the case of three and four suction holes.

The hydrogen-bubble technique was also used to visualize the bursting events in a laminar boundary layer. Figure 15 shows a top view of the events resulting from withdrawing near-wall fluid through two suction holes separated in the spanwise direction. The hydrogen-bubble wire is perpendicular to the flow and parallel to the flat plate at a distance of 2 mm above the surface and 1 cm downstream of the suction holes. A horizontal sheet of laser light illuminates the bubbles. The low-speed regions are manifested as upstream kinks of the time lines, and longitudinal vorticity is indicated by the wrapping of these lines. The unstable region grows as it convects downstream and eventually breaks into a burst-like event.

A side view of the events depicted in Figure 15 is visualized using a vertical hydrogen-bubble wire and a vertical sheet of laser light. The fluid is withdrawn from the laminar boundary layer through the two suction holes located 1 cm upstream of the hydrogen-bubble wire. The resulting events are shown in Figure 16 for six time intervals after the onset of the artificial event. The undisturbed Blasius profile can be reconstructed from the time lines shed from the hydrogen-bubble wire. The formation, lifting and stretching of the hairpin vortex that results from distorting the originally spanwise vortex lines is clearly indicated in the pictures shown in Figure 16. The vortex head reaches the outer region of the laminar boundary layer about 1 s after the suction has been initiated. The breakup of the vortex head is also indicated in the figure.

ORIGINAL PAGE IS
OF POOR QUALITY

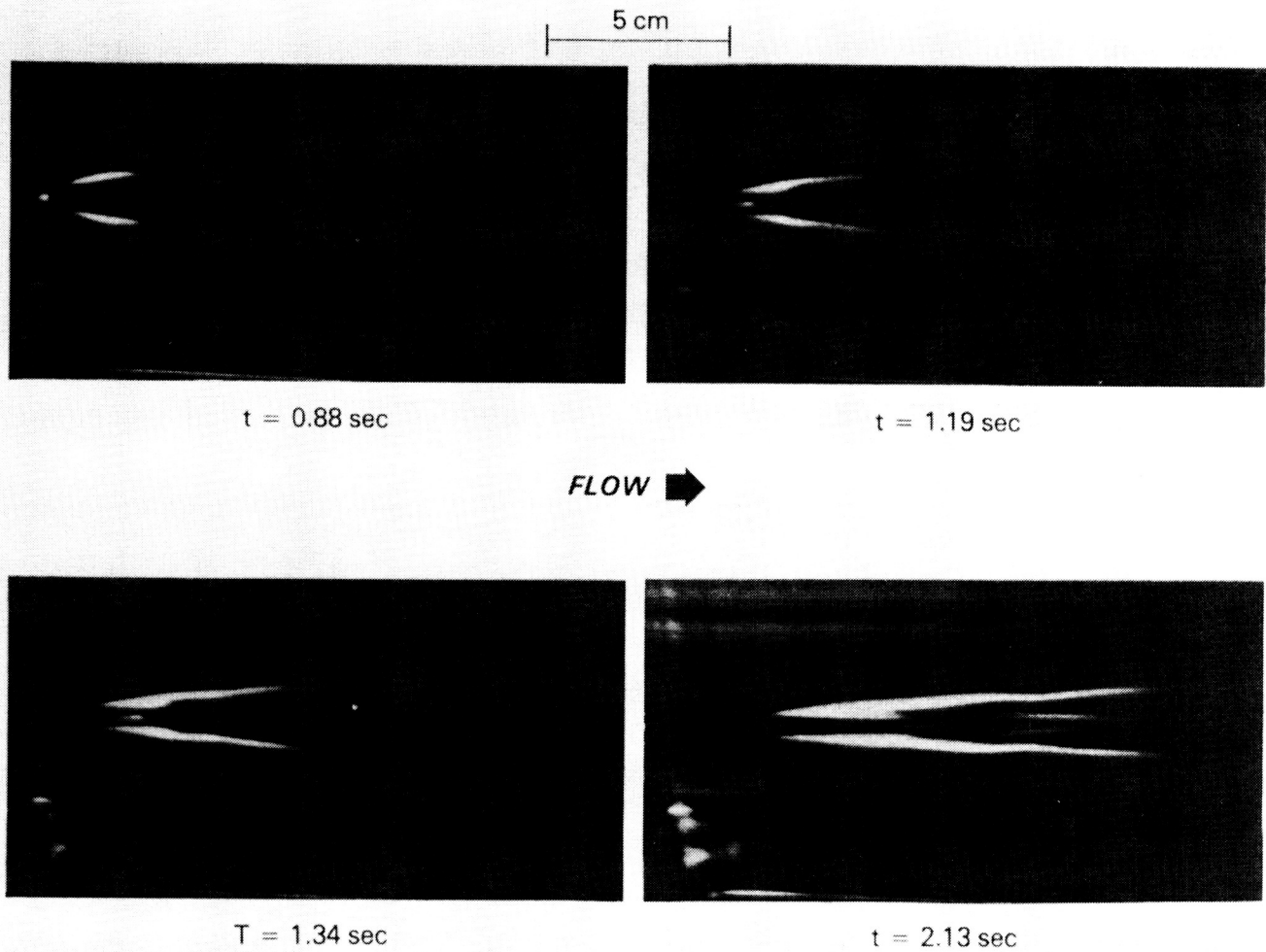


Figure 11. Sequence of Events when Fluid is Withdrawn from a Single Suction Hole. Laminar Boundary Layer is Visualized from the Top Using Fluorescent Dye and Sheet of Laser Light

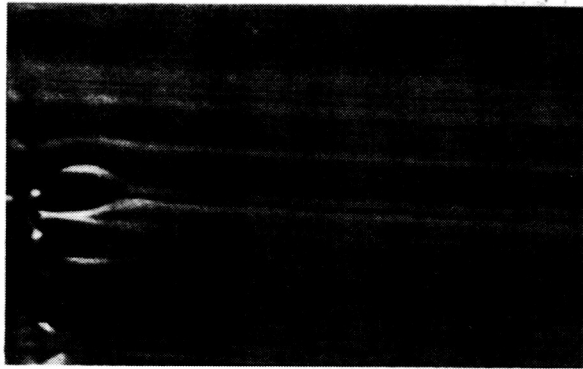
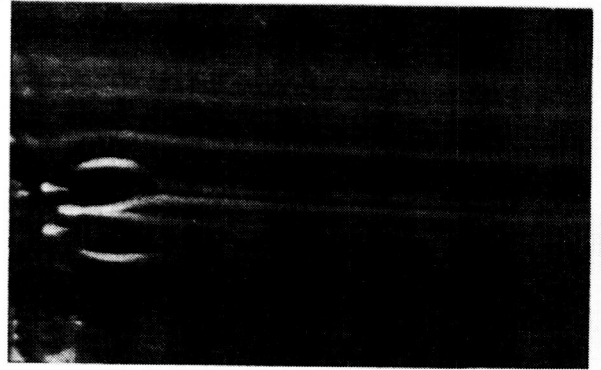
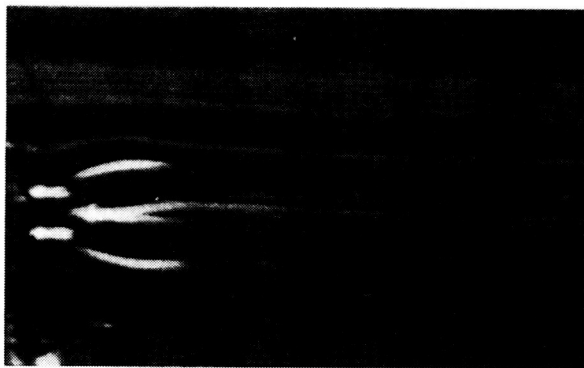
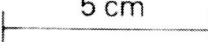
 $t = 0.39 \text{ sec}$  $t = 0.47 \text{ sec}$ FLOW  $t = 0.63 \text{ sec}$  $t = 0.78 \text{ sec}$ 5 cm $t = 0.94 \text{ sec}$  $t = 1.25 \text{ sec}$

Figure 12. Sequence of Events when Fluid is Withdrawn from Two Holes to Generate a Single Artificial Burst

ORIGINAL PAGE IS
OF POOR QUALITY

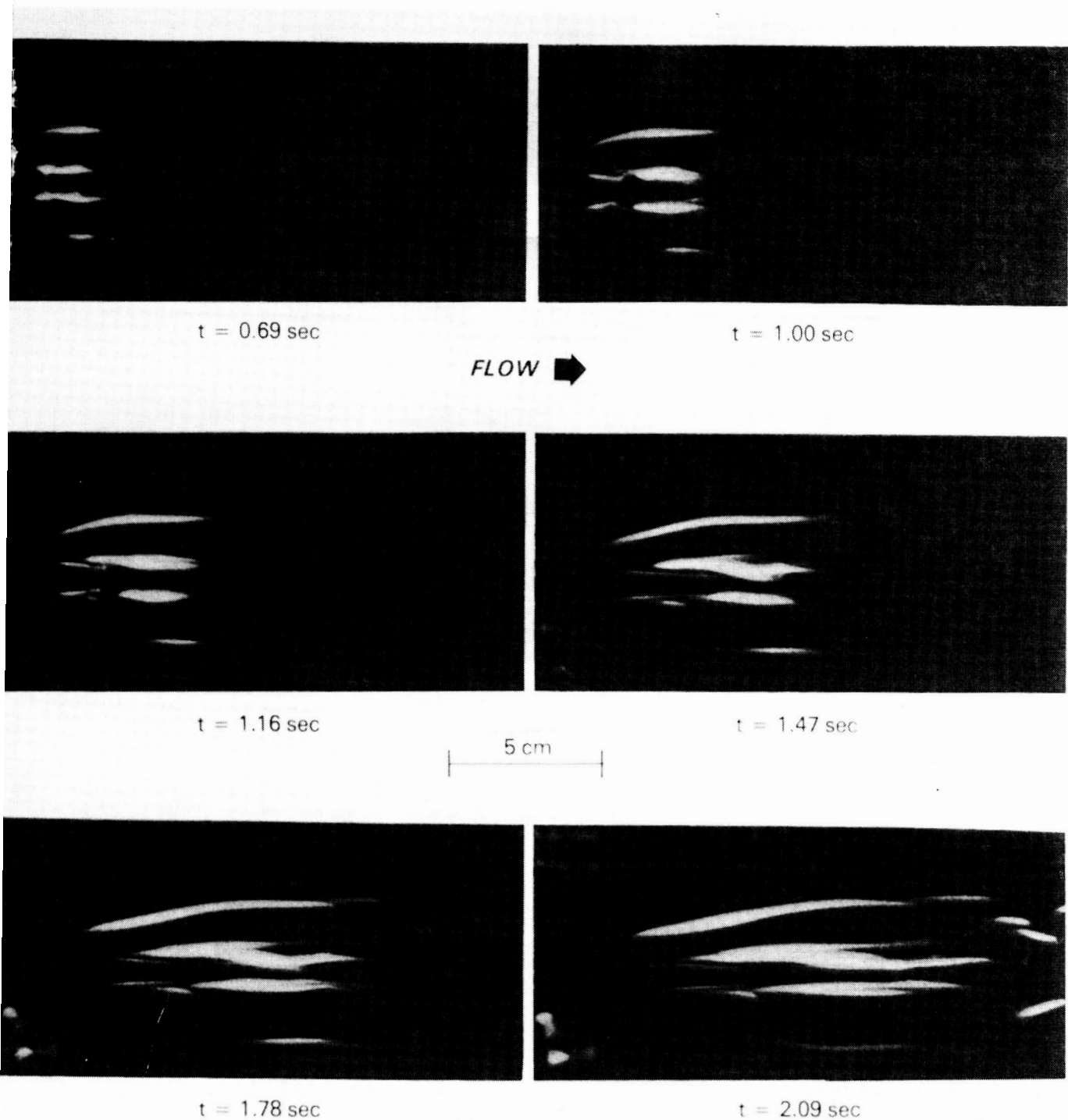


Figure 13. Four Streaks are Generated when Fluid is Withdrawn from Three Suction Holes. Only Two Low-Speed Streaks are Unstable, and Two Bursts are Generated

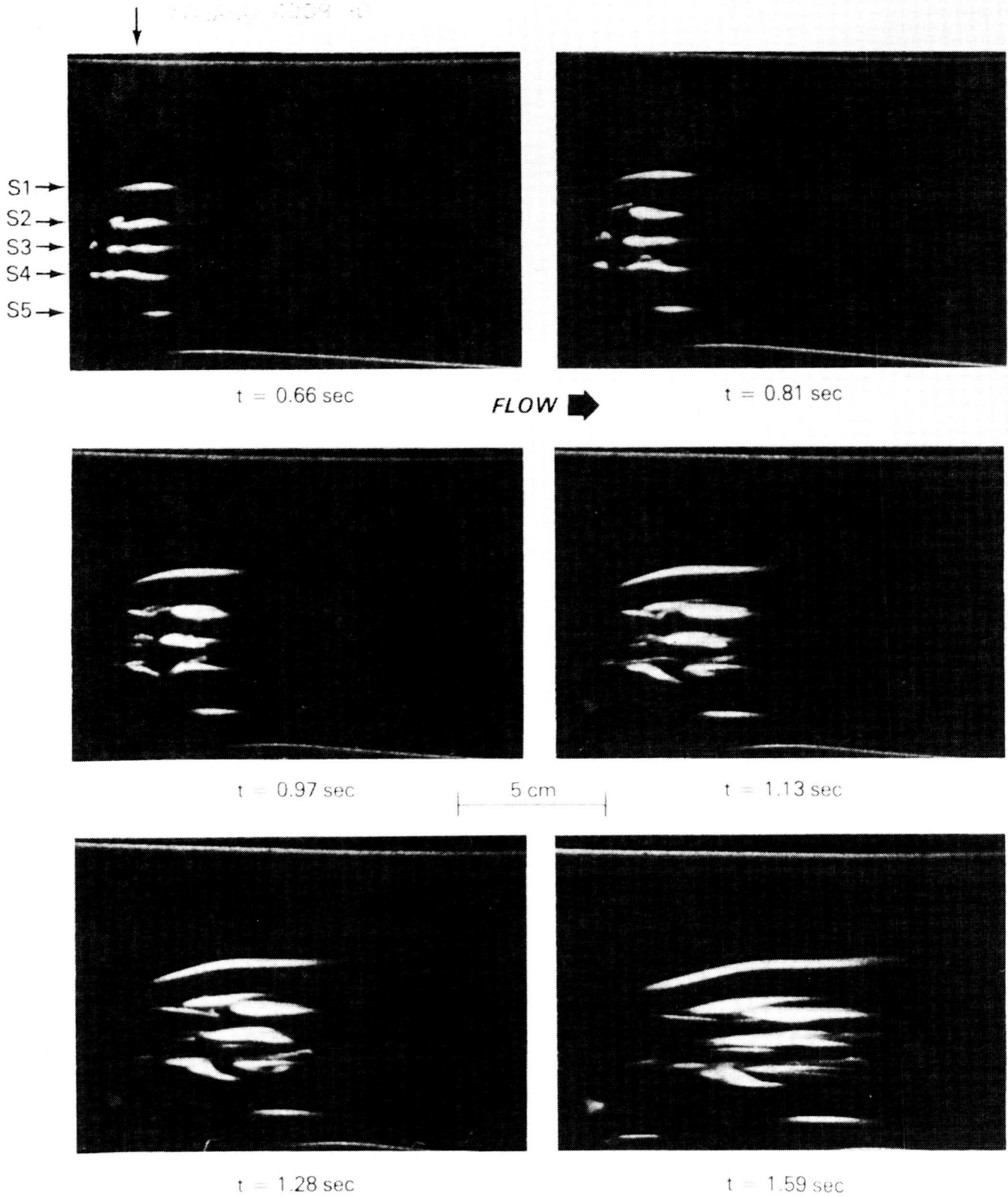
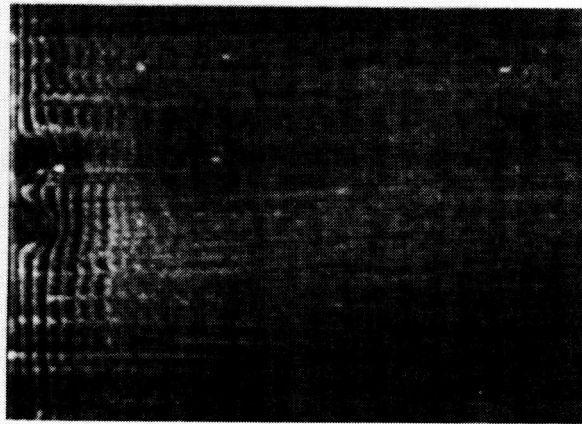
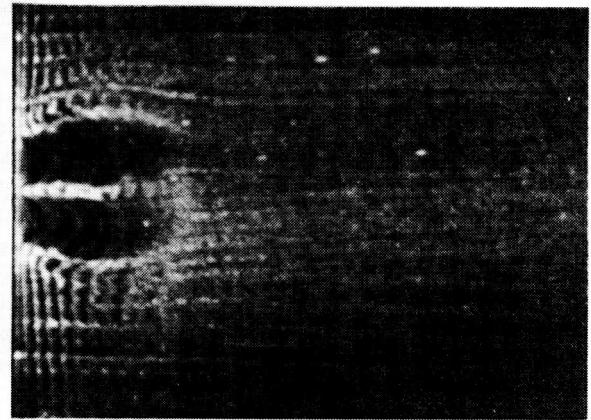
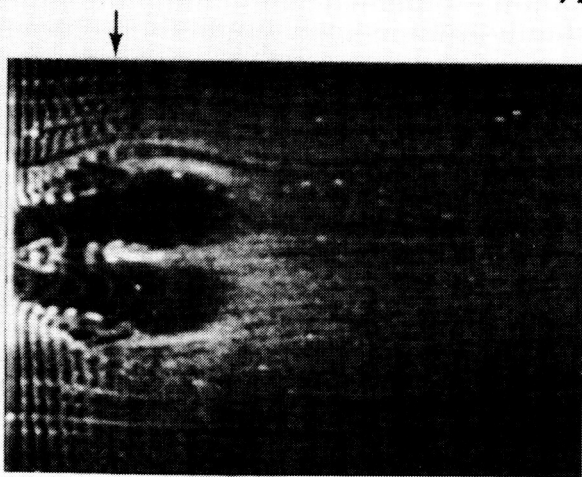
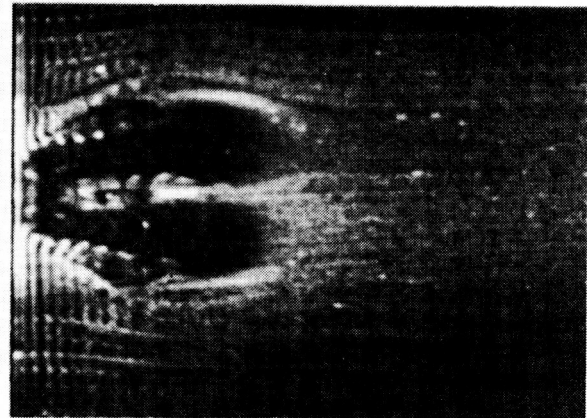


Figure 14. Withdrawing Fluid Through Four Suction Holes Results in the Generation of Five Low-Speed Streaks and Three Artificial Bursts

ORIGINAL PAGE IS
OF POOR QUALITY $t = 0.38 \text{ sec}$  $t = 0.55 \text{ sec}$

FLOW

 $t = 0.70 \text{ sec}$  $t = 0.78 \text{ sec}$

3 cm

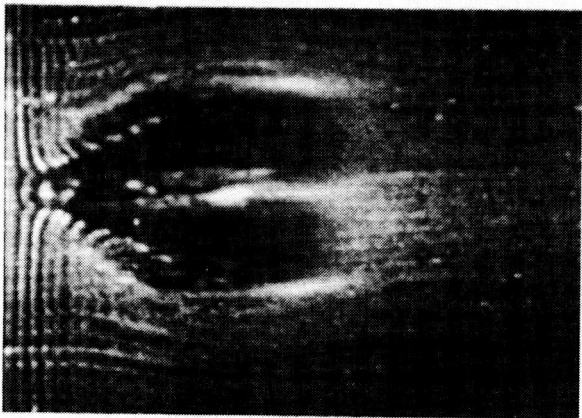
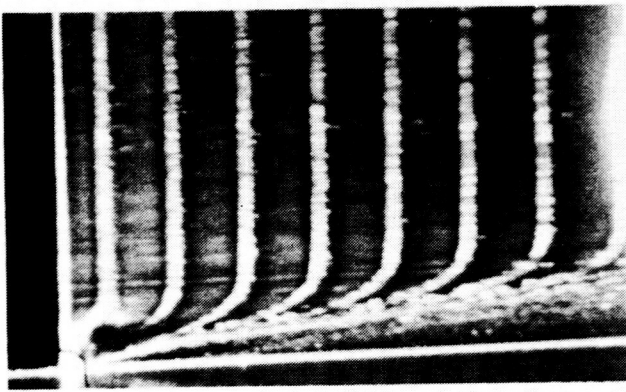
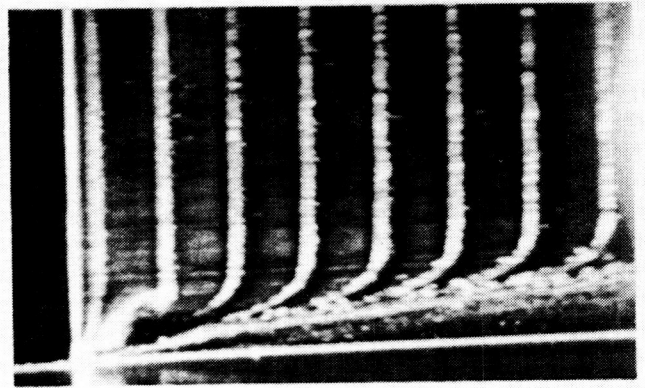
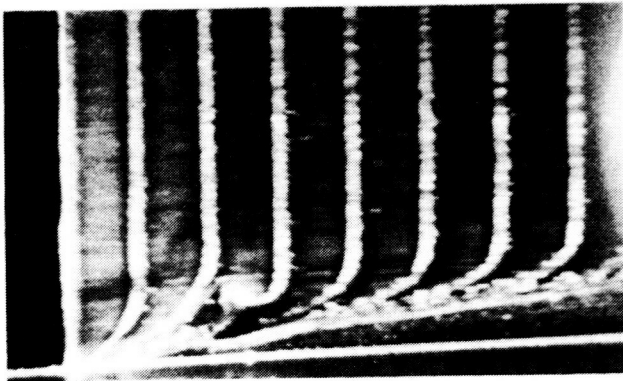
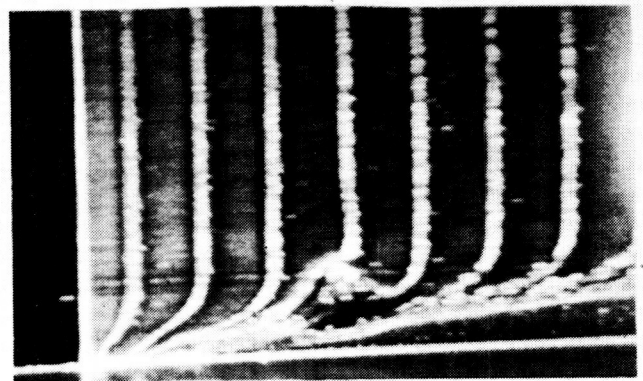
 $t = 0.94 \text{ sec}$  $t = 1.09 \text{ sec}$

Figure 15. Generation of an Artificial Event in a Laminar Boundary Layer Using Two Suction Holes. Top View is Visualized Using Hydrogen Bubbles and a Horizontal Sheet of Laser Light.

 $t = 0.63 \text{ sec}$  $t = 0.66 \text{ sec}$

FLOW →

 $t = 0.73 \text{ sec}$  $t = 0.81 \text{ sec}$

3 cm

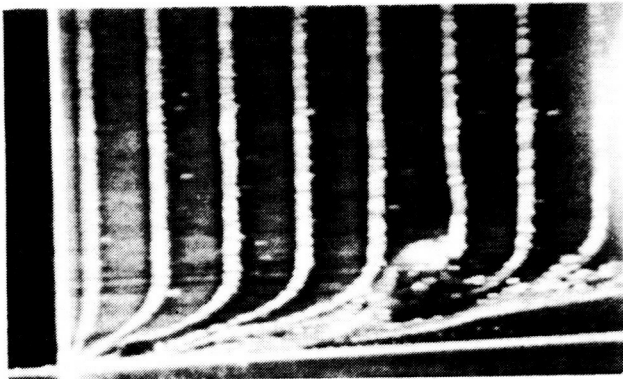
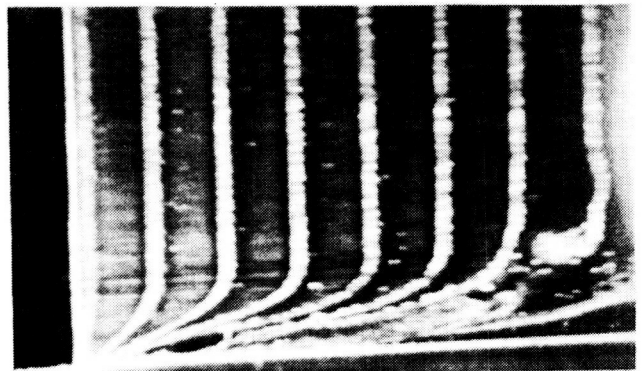
 $t = 0.89 \text{ sec}$  $t = 0.97 \text{ sec}$

Figure 16. Side View of the Artificial Burst in a Laminar Boundary Layer. Flow is Visualized Using Hydrogen Bubbles and a Vertical Sheet of Laser Light

Artificial bursts were also generated by pitching a flush-mounted delta wing as shown in the schematic in Figure 17. The negative angle of attack of 30° leads to the formation of two longitudinal vortices (Gad-el-Hak & Ho, 1985a; 1985b; 1986). An unstable low-speed region is formed between the two vortices. The low-speed streak lifts up away from the wall causing a strongly inflectional velocity profile and rapidly breaks down into a completely random pattern much the same as the streaks generated by suction from spanwise holes.

7.2 BURSTS IN A TURBULENT BOUNDARY LAYER

A bursting event is, of course, a characteristic structure of a turbulent boundary layer. The artificial burst generators were used to generate burst-like events in a laminar flow as described in the previous section to allow easy visualization free of the random background that characterizes a turbulent flow. In this section, we describe the visualization of natural and artificial bursts in a turbulent boundary layer. The photographs in Figure 18 show the sequence of events leading to the breakup of a natural low-speed streak in a turbulent boundary layer. The wall region of the boundary layer is visualized by injecting fluorescent dye from the spanwise slot located just upstream of the view shown in the photographs. A horizontal sheet of laser at the wall clearly shows the natural low-speed streaks, manifested as bright regions of dye, with the typical spanwise spacing. In particular, the low-speed streak whose tail is marked with the vertical and horizontal arrows on the first photograph undergoes a large-amplitude oscillation at $t = 0.28$ s (origin of time is arbitrary). At $t = 0.41$ s, the breakup process has started and it is completed at $t = 0.81$ s, as shown in the last photograph in Figure 18.

The breakup of a natural low-speed streak is compared to that of the artificially generated one in Figure 19. Here, the origin of time coincides with the onset of suction from two spanwise holes. In the first frame, the vertical and horizontal arrows indicate the position of the midpoint between the two suction holes. A low-speed streak is formed due to the pumping action of the longitudinal vortices that result from distorting the originally spanwise vortex lines. The artificially generated low-speed streak undergoes oscillation and breakup much the same as the natural one.

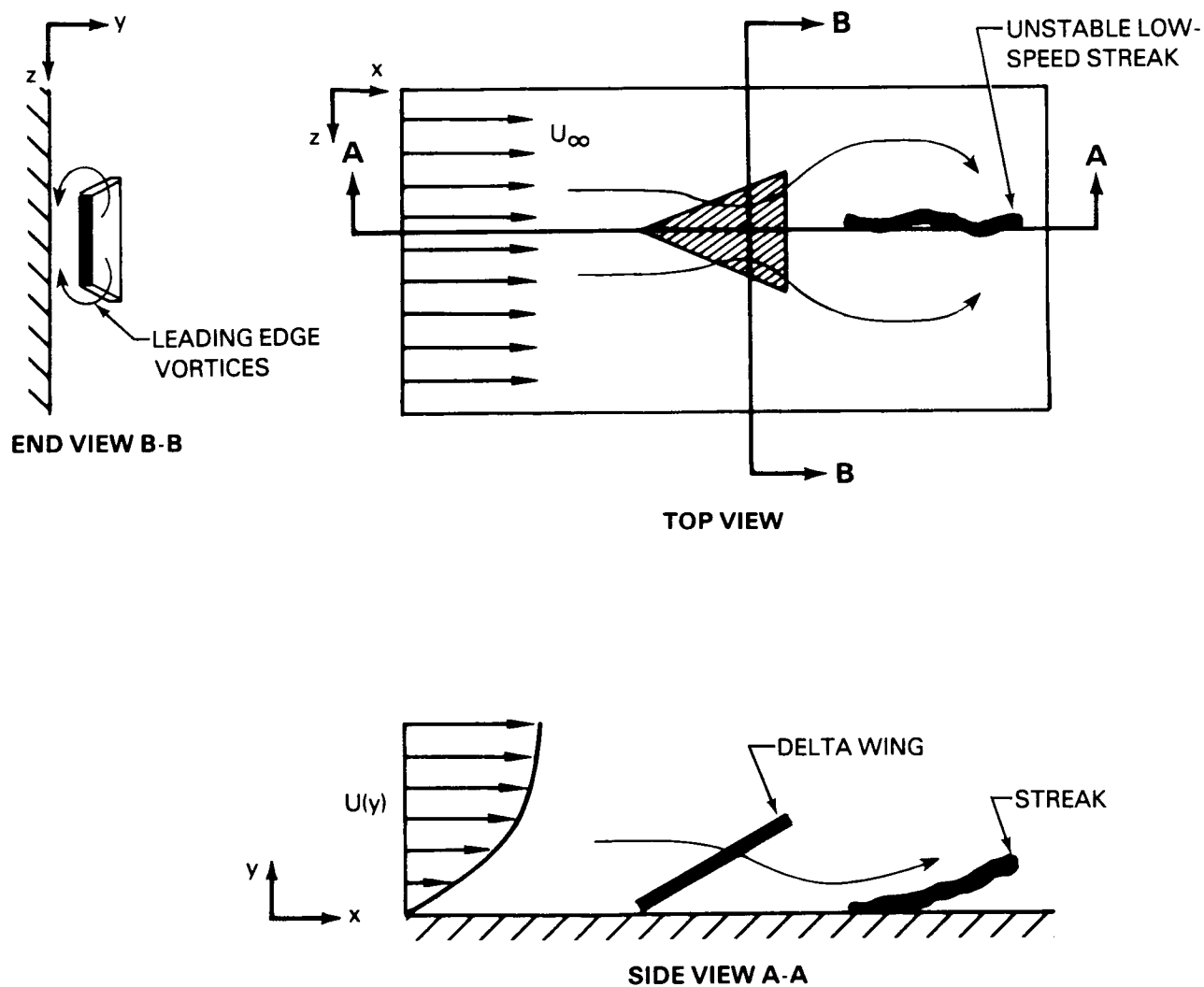


Figure 17. Resulting Streamlines When a Delta Wing, Originally Flush with the Surface, is Impulsively Pitched to Generate Negative Lift.

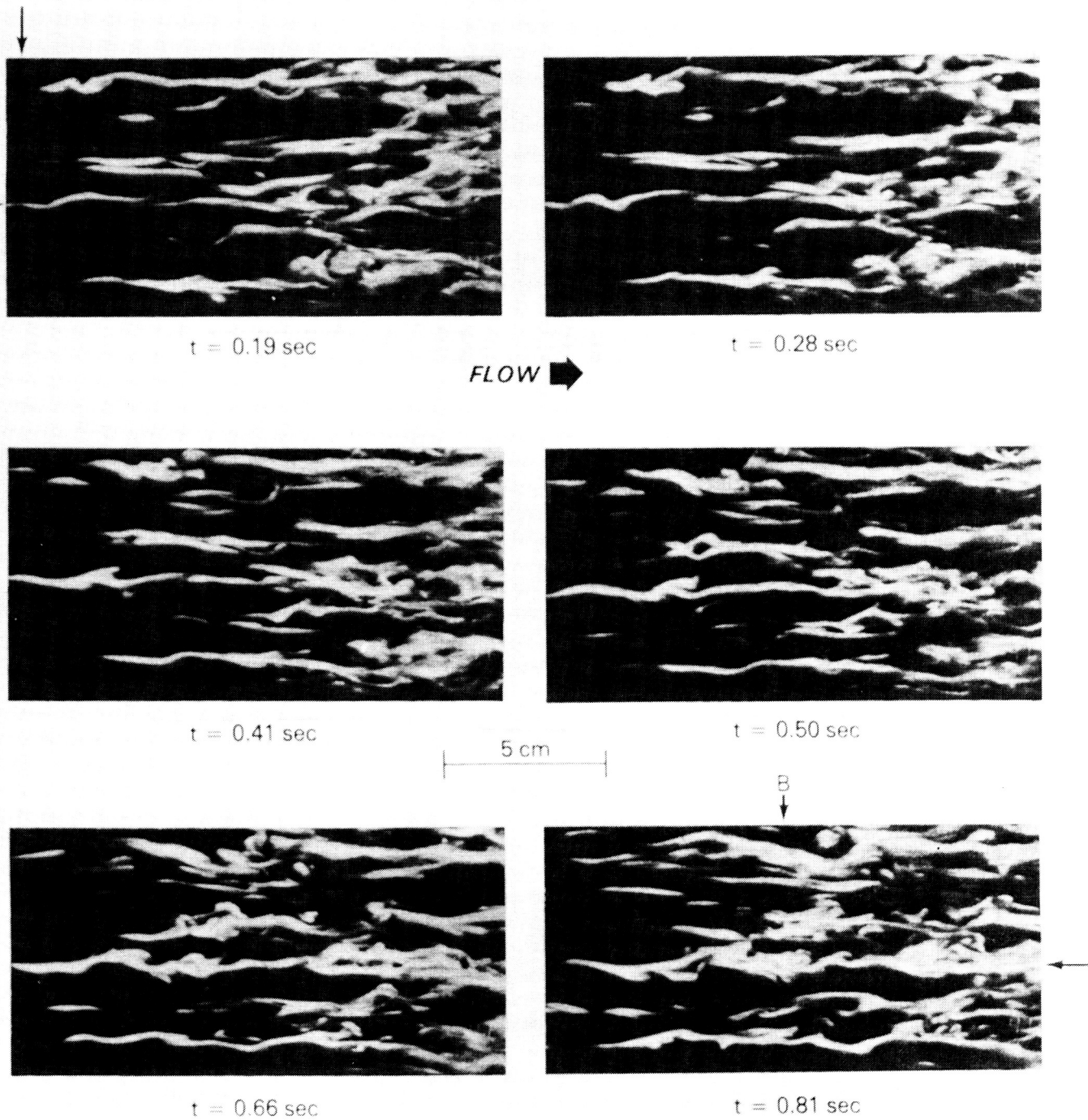


Figure 18. Top View of a Turbulent Boundary Layer Visualized Using Fluorescent Dye and a Horizontal Sheet of Laser Light. Sequence of Events Leading to the Break-Up of a Natural Low-Speed Streak

ORIGINAL PAGE IS
OF POOR QUALITY

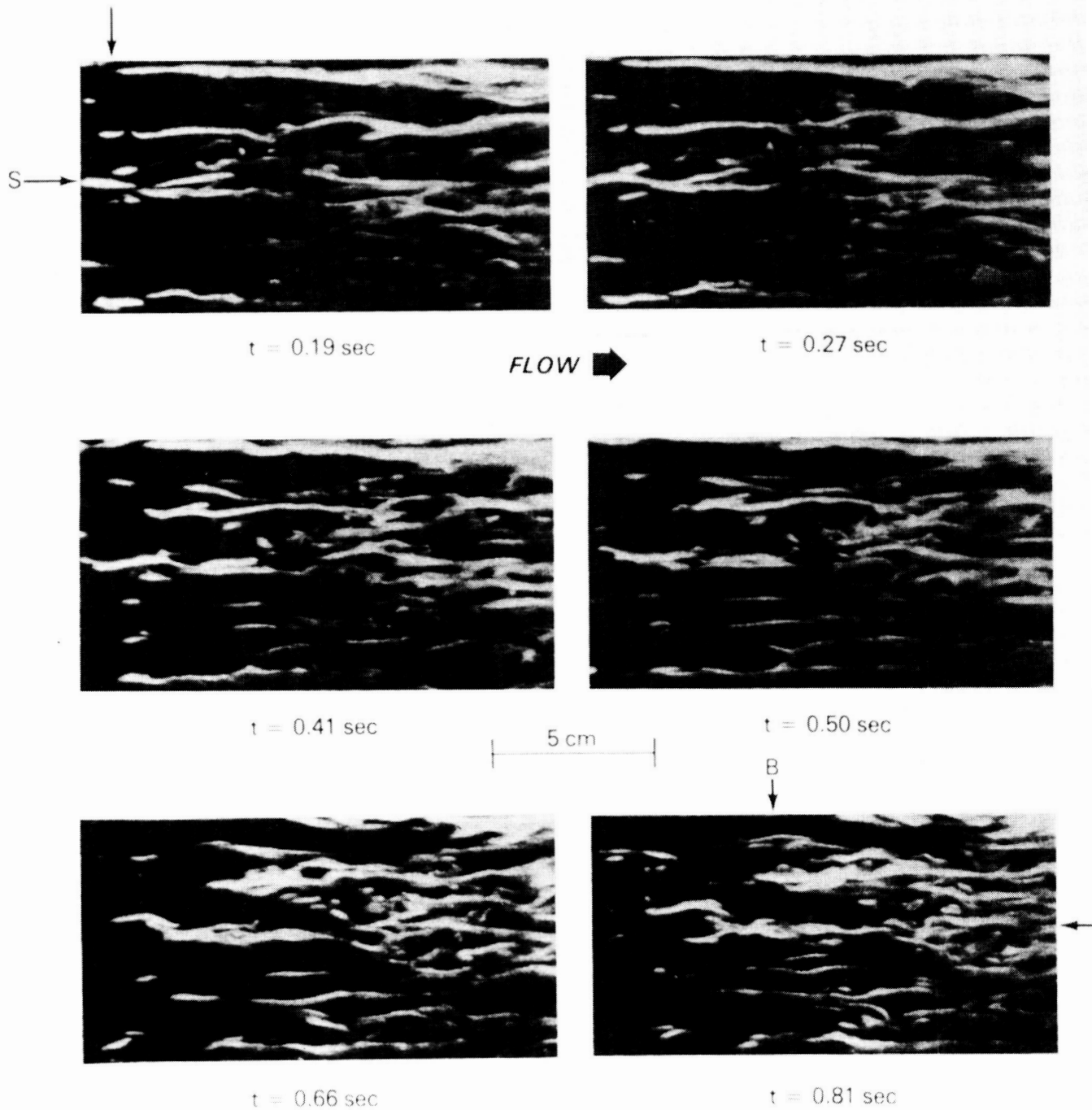


Figure 19. Sequence of Events Leading to the Break-Up of an Artificially-Generated Low-Speed Streak.

The similarity between the natural and artificial events is striking, considering the fact that the natural phenomenon under consideration is random in space and time.

A side view of the breakup of an artificially generated low-speed streak is shown in Figure 20. The turbulent boundary layer is visualized using fluorescent dye injected from the spanwise slot and a vertical sheet of laser light parallel to the flow. The dye accumulation near the wall indicates the formation of a low-speed region. In the first photograph in Figure 20, the streak lifts up as marked by the vertical arrow. The low-speed streak undergoes a large-amplitude oscillation and breaks up violently as shown in the sequence of movie frames.

A different perspective of the natural and artificial bursts is obtained from side views using a vertical hydrogen-bubble wire and a vertical sheet of laser light. Figures 21 and 22 show the sequence of events leading to natural and artificially generated bursts, respectively. The formation of inflectional velocity profiles is clearly indicated in both figures. These profiles are inviscidly unstable, and the flow rapidly breaks down into a completely random pattern. It is interesting to note the different time scales associated with the bursting event in laminar and turbulent boundary layers (e.g., Figures 16 and 22). This is due to the different friction velocities and thus different viscous scales in the two boundary layers.

7.3 PATTERN RECOGNITION OF BURSTS AND STREAKS

The visualization results presented in Sections 7.1 and 7.2 indicate the sequence of events associated with the generation of an artificial burst in laminar and turbulent boundary layers, respectively. The observed flow patterns agree qualitatively with observations of naturally occurring bursts and streaks in a turbulent boundary layer. The length and time scales of the artificial events also agree with those for natural structures. For quantitative comparison between natural and artificial bursts, hot-film probes were used together with pattern recognition algorithms aimed at detecting low-speed regions and bursting events.

The miniature hot-film probes were first used to obtain mean and rms streamwise velocity profiles. In the laminar case, the mean velocity profiles were found to agree with the Blasius

ORIGINAL PAGE IS
OF POOR QUALITY

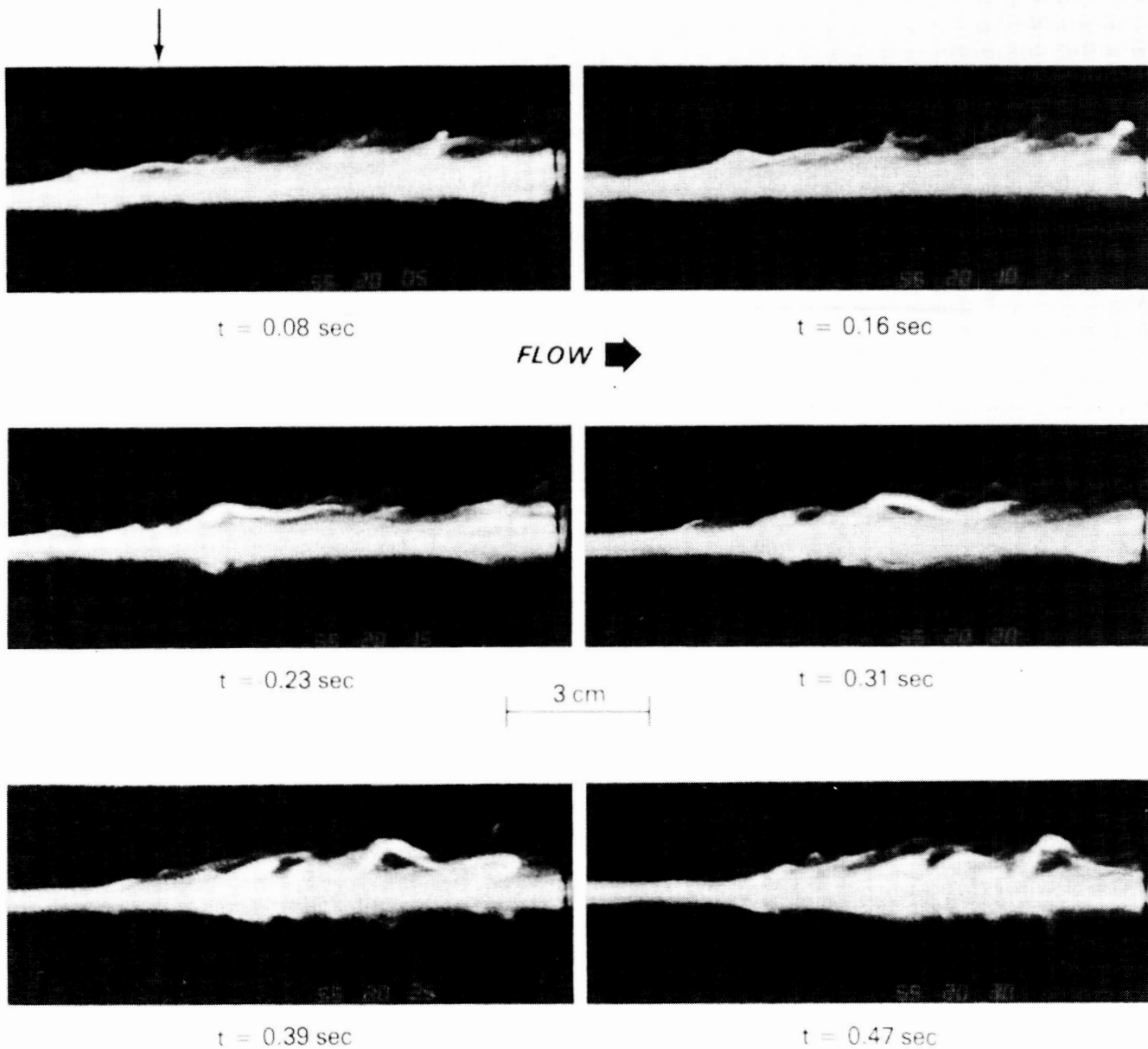


Figure 20. Side View of the Break-Up of an Artificially-Generated Low-Speed Streak. The Fluorescent Dye and the Vertical Sheet of Laser Light Show a Cut in the Hairpin Vortex Stretching and Lifting Away from the Surface

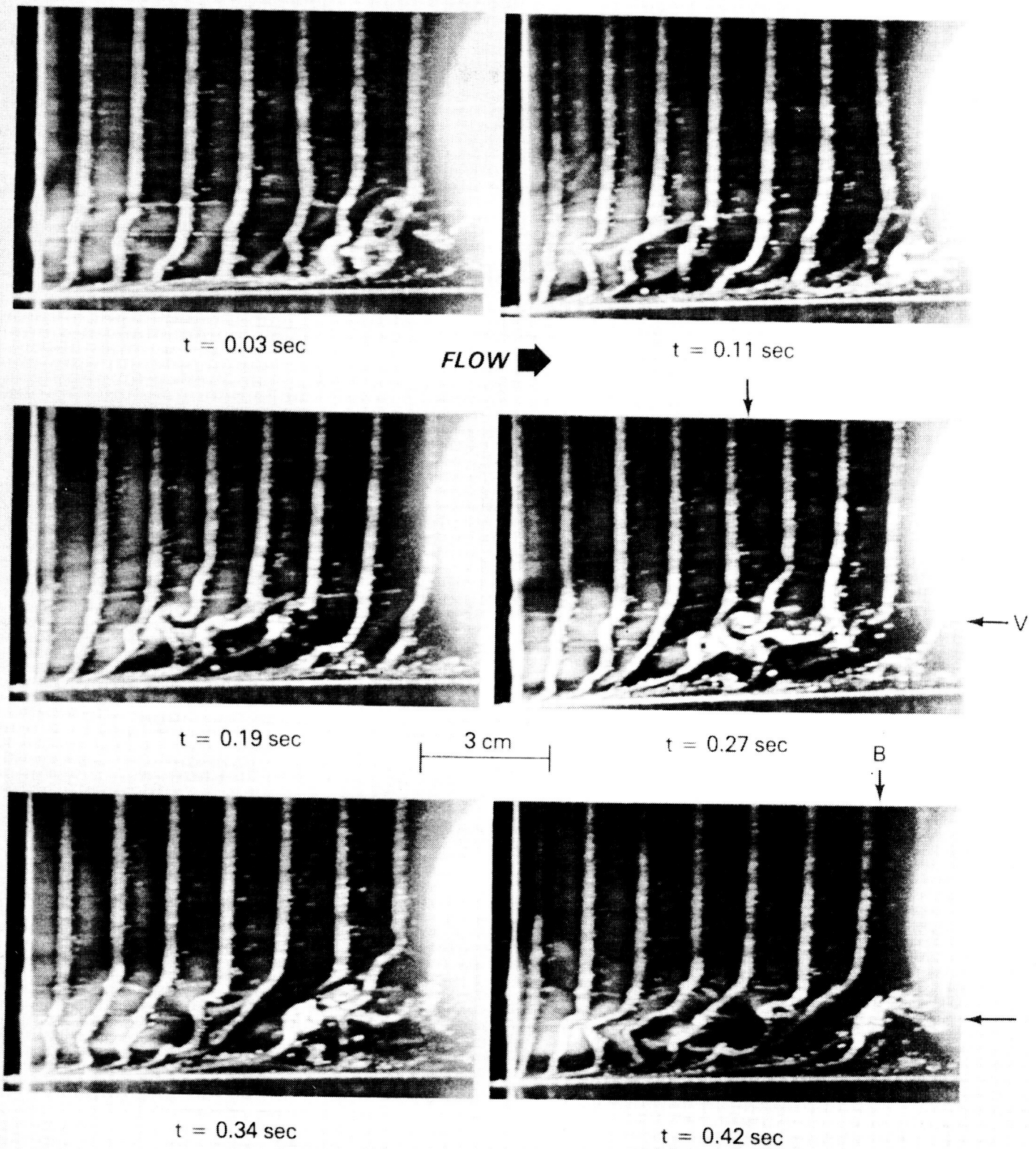


Figure 21. Side View of a Natural Burst in a Turbulent Boundary Layer Using Hydrogen Bubbles and a Vertical Sheet of Laser Light

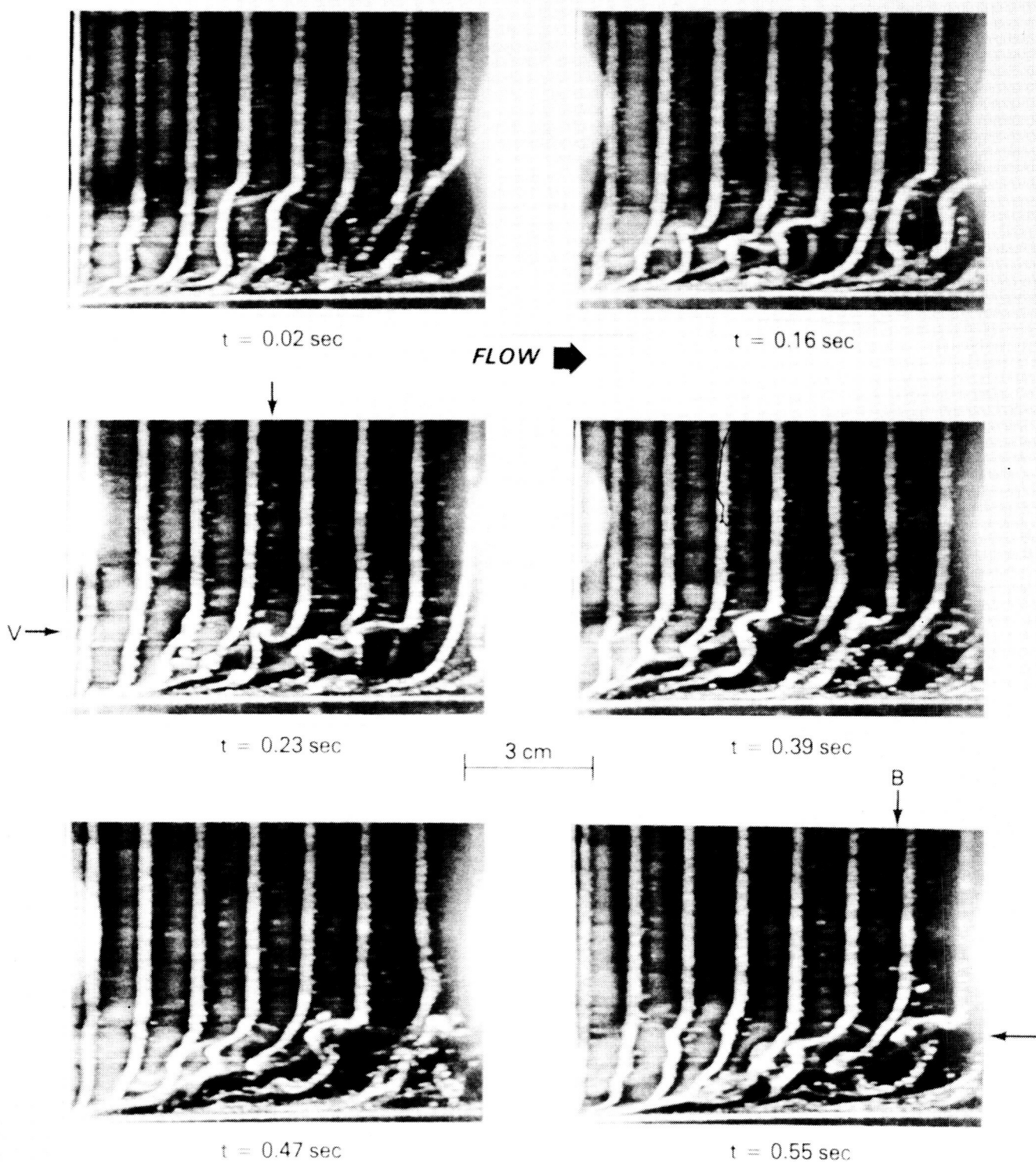


Figure 22. Side View of an Artificial Burst Generated by Withdrawing Fluid from the Turbulent Boundary Layer Using Two Suction Holes.

solution for a zero-pressure-gradient boundary layer. Similarly, the mean and rms velocity profiles in the turbulent case agreed well with those for a standard flat-plate boundary layer. The mean profiles always had well-defined linear, logarithmic and wake regions. Clauser's (1956) method was used to determine the friction velocity used for normalizing the data and in the pattern recognition algorithms described below.

The hot-film probes used to detect the bursts and streaks were placed 100 to 1000 wall units downstream of the artificial burst generator, and at a height above the wall in the range of 10 to 20 wall units (a wall unit was about 0.1 mm at a freestream speed of 20 cm/s and a streamwise distance from the leading edge of 80 cm). The instantaneous longitudinal velocity signal was mapped at these locations. In the laminar case, the initiation of an event using either the suction holes or the pitching delta wing was always associated with the passage of a velocity "spike" before the flow broke down into turbulence. These velocity spikes are consistent with the passage of the head of a hairpin vortex and are similar to the spikes observed by Klebanoff et al. (1962) in their classical vibrating ribbon experiment (see the discussion in Gad-el-Hak et al. , 1984b). In the case of a turbulent boundary layer, the artificial event caused a large streamwise velocity acceleration in the instantaneous velocity records similar to the accelerations observed by Blackwelder & Kaplan (1976) for natural bursts in a turbulent boundary layer. For a more objective assessment, the VITA technique was used to detect the passage of a burst, and the streak detection algorithm was used to recognize the formation and the evolution of a low-speed region.

The two pattern recognition algorithms, which have been described briefly in Section 6.8, search for recognizable patterns or structures. The burst detector searches for periods of high acceleration without necessarily larger fluctuations than the background turbulence. As shown by Blackwelder & Kaplan (1976), such periods are associated with events characterized by a high degree of coherence in time and in the direction normal to the wall and having a conditionally averaged Reynolds shear stress that is an order of magnitude greater than its conventionally averaged value. The detection scheme is then based on the dynamic properties of the organized

structure. Similarly, the streak detector searches for low-speed regions near the wall relative to the background mean velocity.

Whenever the artificial burst generator was triggered, a low-speed streak and a burst were detected, after an appropriate time delay, by the two pattern recognition algorithms. This confirms our hypothesis that the artificial event is dynamically similar to a natural burst.

8. SELECTIVE SUCTION IN LAMINAR BOUNDARY LAYER FLOWS

8.1 VISUALIZATION RESULTS

The sequence of events that result from withdrawing near-wall fluid from the two spanwise holes depends strongly on the rate of fluid withdrawn and whether the suction is continuous or impulsive. Weak impulsive suction results in the generation of one or more hairpin vortices. This vortex bursts when the rate of withdrawing the fluid is increased. Very strong impulsive suction yields to a turbulent spot. Injecting fluid from the spanwise holes, on the other hand, has a much more disturbing influence on the boundary layer compared to withdrawing the fluid, and even extremely small amounts of fluid injected impulsively into the flow results in the generation of a turbulent spot. Continuous suction from the two holes results in the generation of a periodic train of hairpin vortices that do not burst, as was first illustrated by Peter Bradshaw (see Van Dyke, 1982).

The above effects are illustrated in the photographs in Figures 23 through 27. Side views of the laminar boundary layer were visualized using a vertical hydrogen-bubbles wire located between the two spanwise holes. A vertical sheet of laser light parallel to the flow direction illuminated the hydrogen bubbles. The flow in all pictures is from left to right and the time in seconds, measured from the onset of suction, is indicated underneath each photograph. In Figure 23, the suction is applied for 0.5 s at a rate of $2.3 \text{ cm}^3/\text{s}$. A hairpin vortex is generated at the start of suction and a second one results when suction is terminated. Neither of these vortices bursts. When the suction rate is increased to $2.8 \text{ cm}^3/\text{s}$, only one hairpin vortex is generated and strong bursting occurs as evidenced in the photographs depicted in Figure 24.

A periodic train of hairpin vortices is generated when suction is applied continuously. At a freestream speed of 20 cm/s , the frequency of detachment of the vortices from the surface is about 4 Hz. Typical still pictures taken from the ciné film are shown in Figure 25. The suction rate in this case was about $2.35 \text{ cm}^3/\text{s}$. The vortex loops were seen to rise as they move downstream. Weaker vortices were generated at lower suction rates and stronger ones were produced at higher

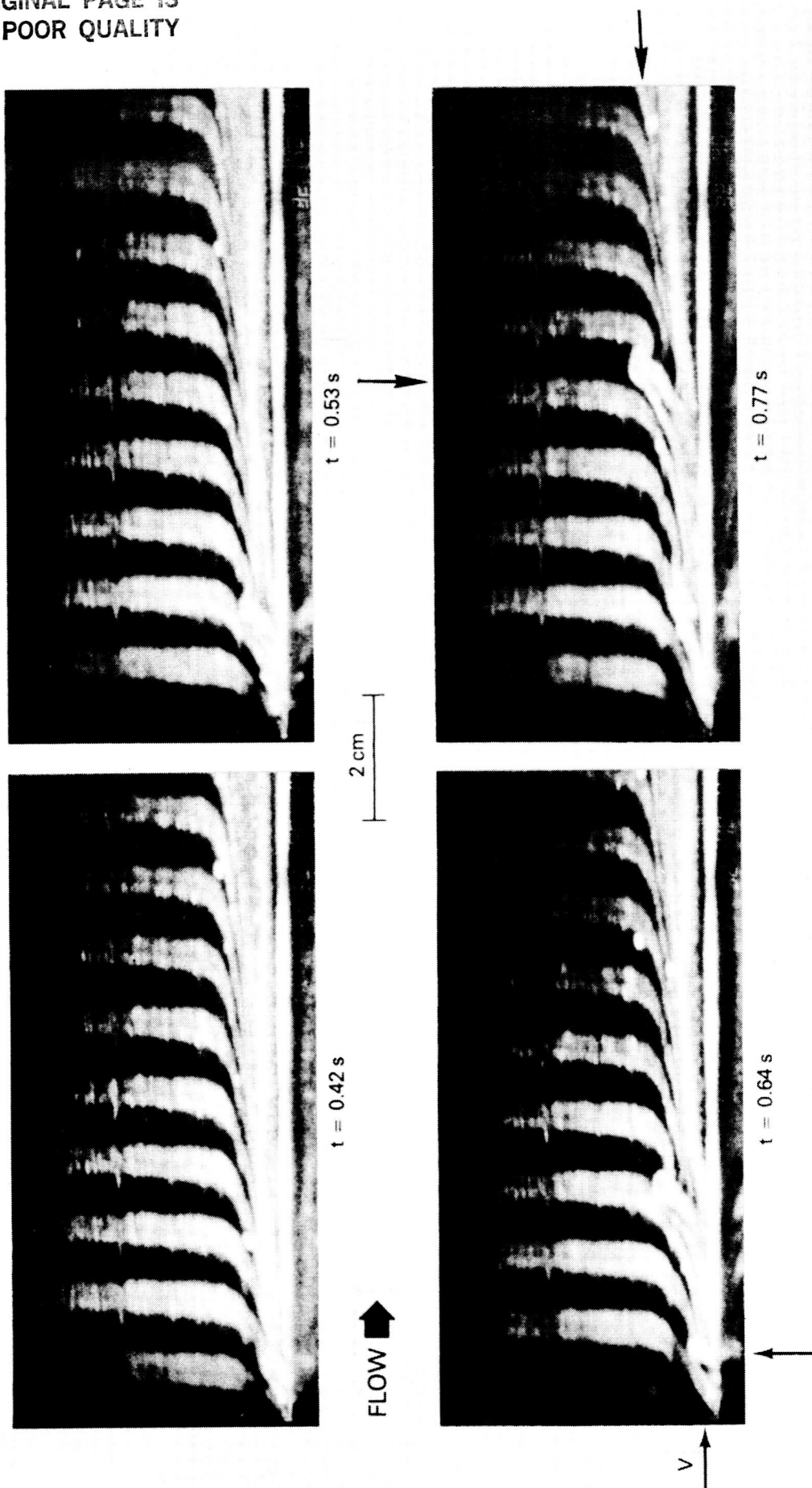


Figure 23. Side View of the Laminar Boundary Layer Visualized Using Hydrogen Bubbles from a Vertical Wire. Suction from the Two Spanwise Holes is Applied for 0.5 s at a Rate of $2.3 \text{ cm}^3/\text{s}$

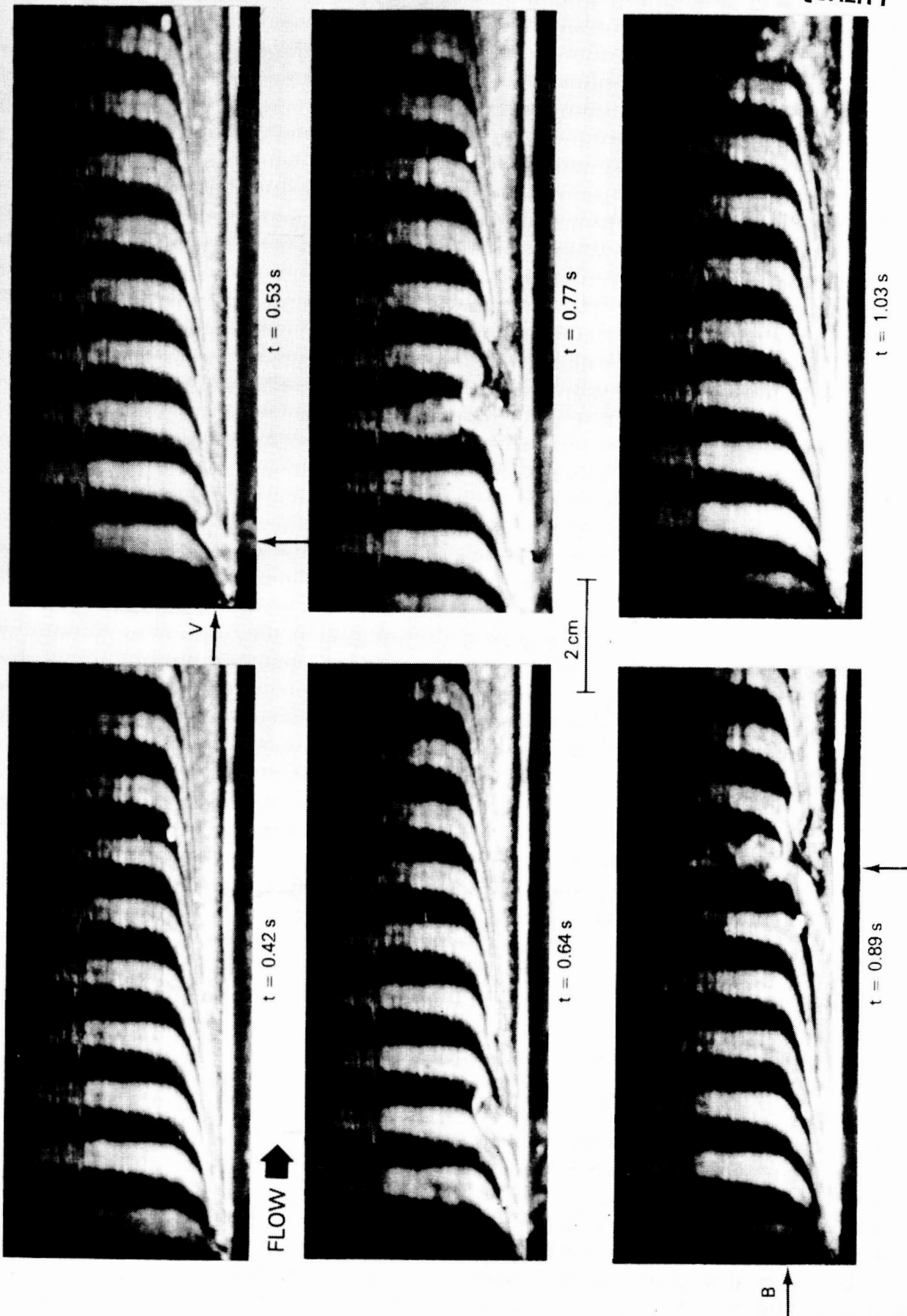


Figure 24. The Hairpin Vortex Undergoes Bursting when Suction Rate from the Two Spanwise Holes is Increased. Suction Lasts for 0.5 s at a Rate of $2.8 \text{ cm}^3/\text{s}$

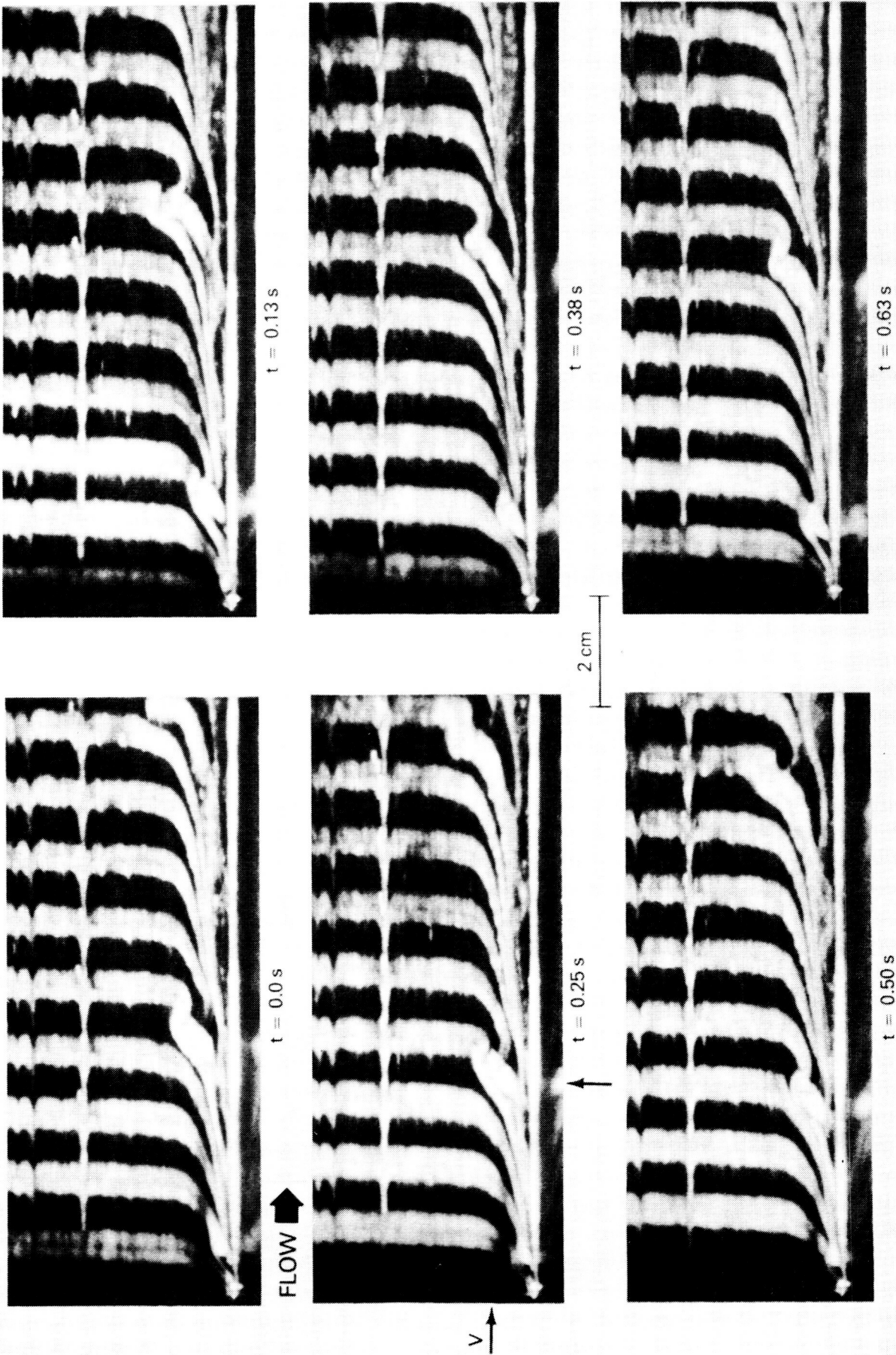


Figure 25. A Periodic Train of Hairpin Vortices is Generated in a Laminar Boundary Layer when Suction is Applied Continuously from Two spanwise Holes at a Rate of $2.35\text{ cm}^3/\text{s}$.

ORIGINAL PAGE IS
OF POOR QUALITY

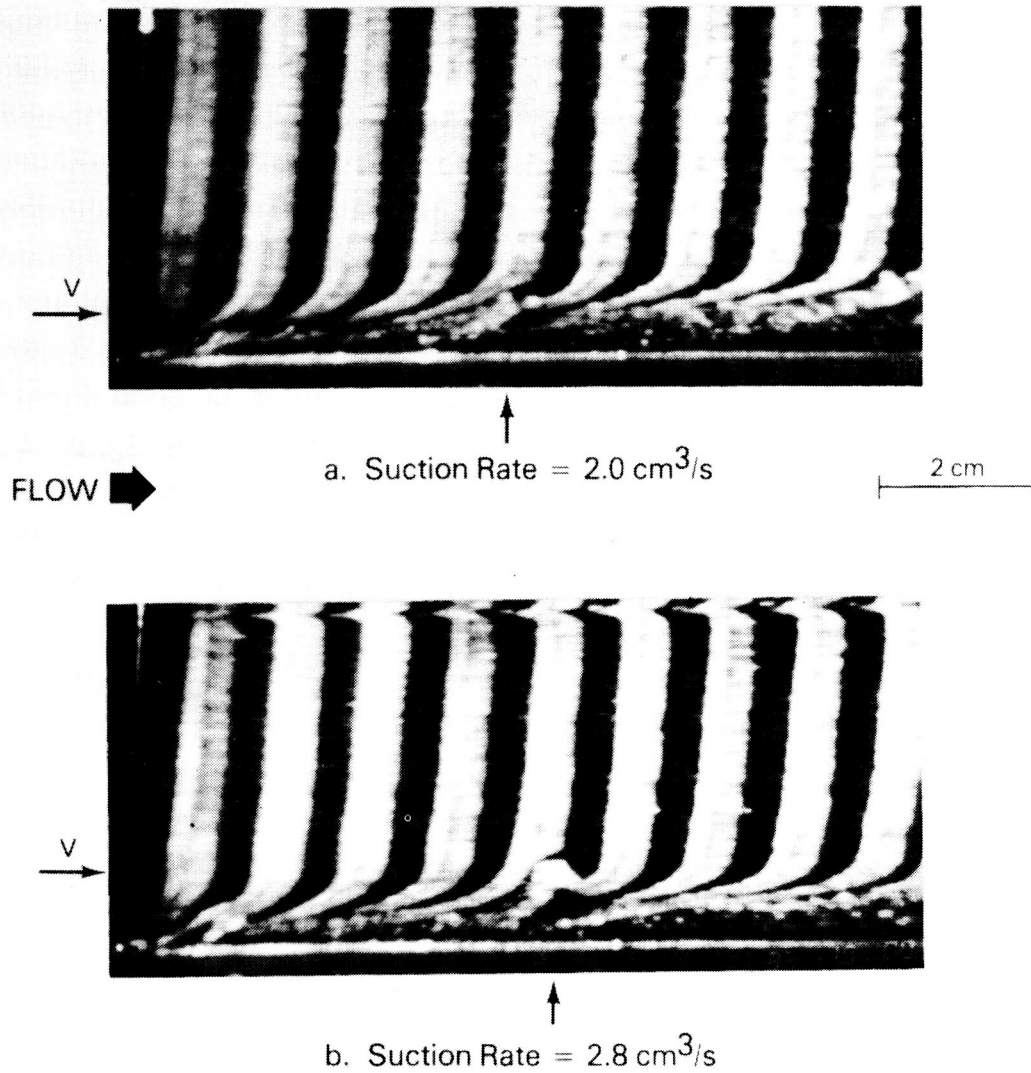


Figure 26. Effects of Rate of Continuous Suction from the Two Spanwise Holes on the Resulting Hairpin Vortex. $U_{\infty} = 20$ cm/s.

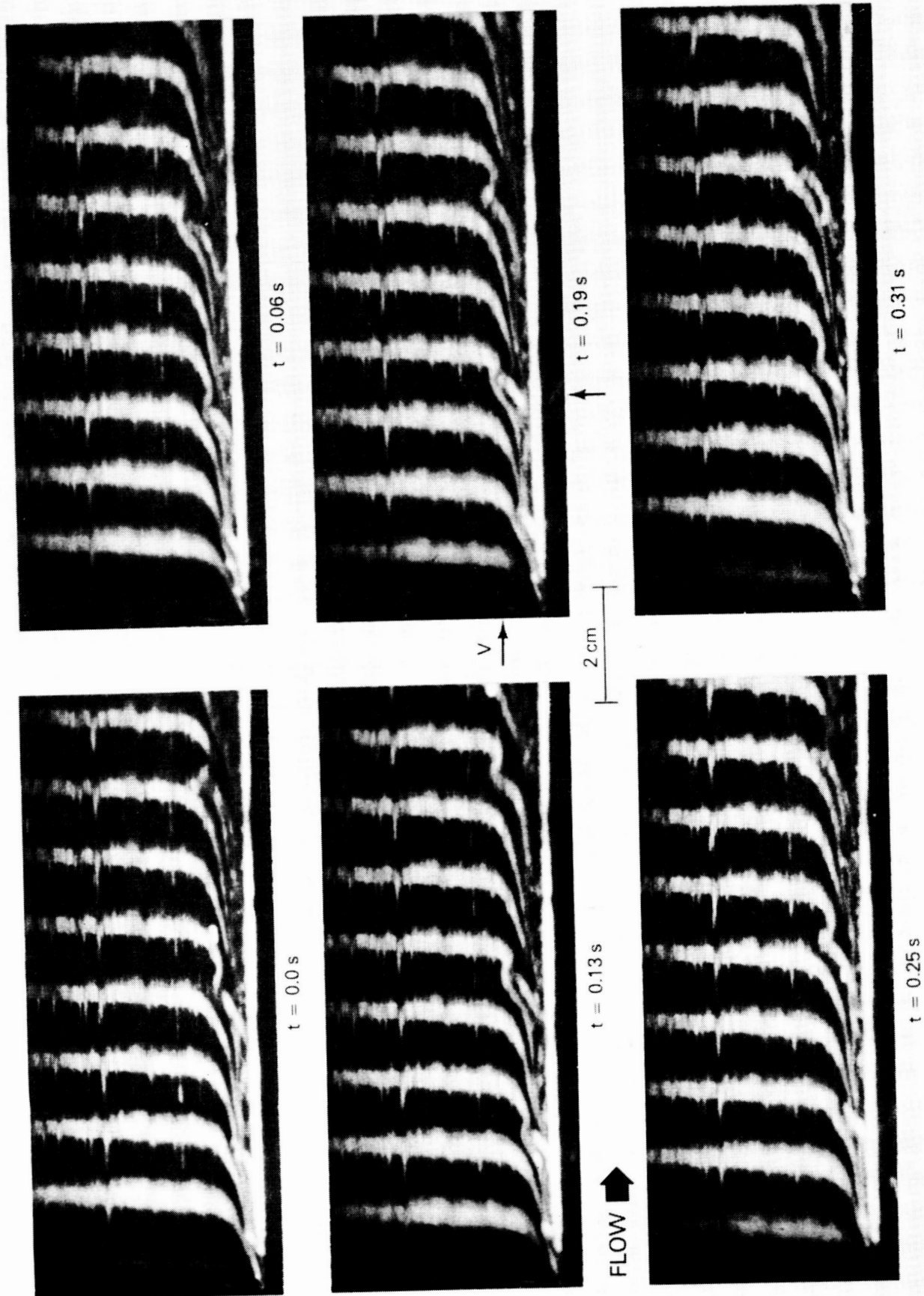


Figure 27. The Frequency of the Train of Periodic Burst-Like Events is Increased at Higher Flow Speeds. $U_{\infty} = 30$ cm/s; Suction from Two Spanwise Holes is Applied Continuously at a Rate of 2.35 cm³/s

rates, as shown in Figure 26 for the suction rates of $2 \text{ cm}^3/\text{s}$ and $2.8 \text{ cm}^3/\text{s}$, respectively. Note that the hairpin vortices generated as a result of continuous suction from the two spanwise holes did not burst even at the higher suction rate. In contrast, the hairpin vortex generated as a result of impulsive suction burst when the suction rate was the same as that depicted in Figure 26b (see Figure 24).

The frequency of detachment of the hairpin vortices from the surface of the plate appears to be a unique function of the flow speed. As shown in Figure 24 and 27, this frequency is increased from 4 Hz to 7 Hz when the flow speed is increased from 20 cm/s to 30 cm/s. It appears that the hairpin vortices result from a shear layer instability and that the frequency of the most unstable disturbance scales with the flow speed to the $3/2$ power as observed by Klebanoff et al. (1962) and Blackwelder (1979).

Suction from the streamwise slot can also be applied continuously or impulsively. Two low-speed streaks result from withdrawing the near-wall fluid using this slot. Similar to the suction from a single hole (see Figure 10), these two streaks are stable if the rate of suction is small. Stronger impulsive suction from the streamwise slot results in the development of a turbulent spot, but continuous suction appears to have no destabilizing effect on the laminar boundary layer.

The burst-like event generated from the two spanwise holes can be obliterated by withdrawing the fluid from the streamwise slot either impulsively or continuously. In Figure 28, the continuous suction from the slot was at a rate of $4 \text{ cm}^3/\text{s}$, and two hairpin vortices were generated by withdrawing the near-wall fluid from the two spanwise holes for 0.5 s at a rate of $2.3 \text{ cm}^3/\text{s}$.* As shown in the figure, both vortices were nearly obliterated. Higher suction rate from the streamwise slot was more effective in eliminating the artificial hairpin vortices as shown in Figure 29. In this case, the continuous suction from the slot was at a rate of $5.5 \text{ cm}^3/\text{s}$, and the two hairpin vortices generated from the holes have completely disappeared.

* As shown in Figure 23 at the same suction rate and duration from the two spanwise holes, one vortex is generated as a result of starting the suction and the second vortex is produced when suction from the holes is terminated.

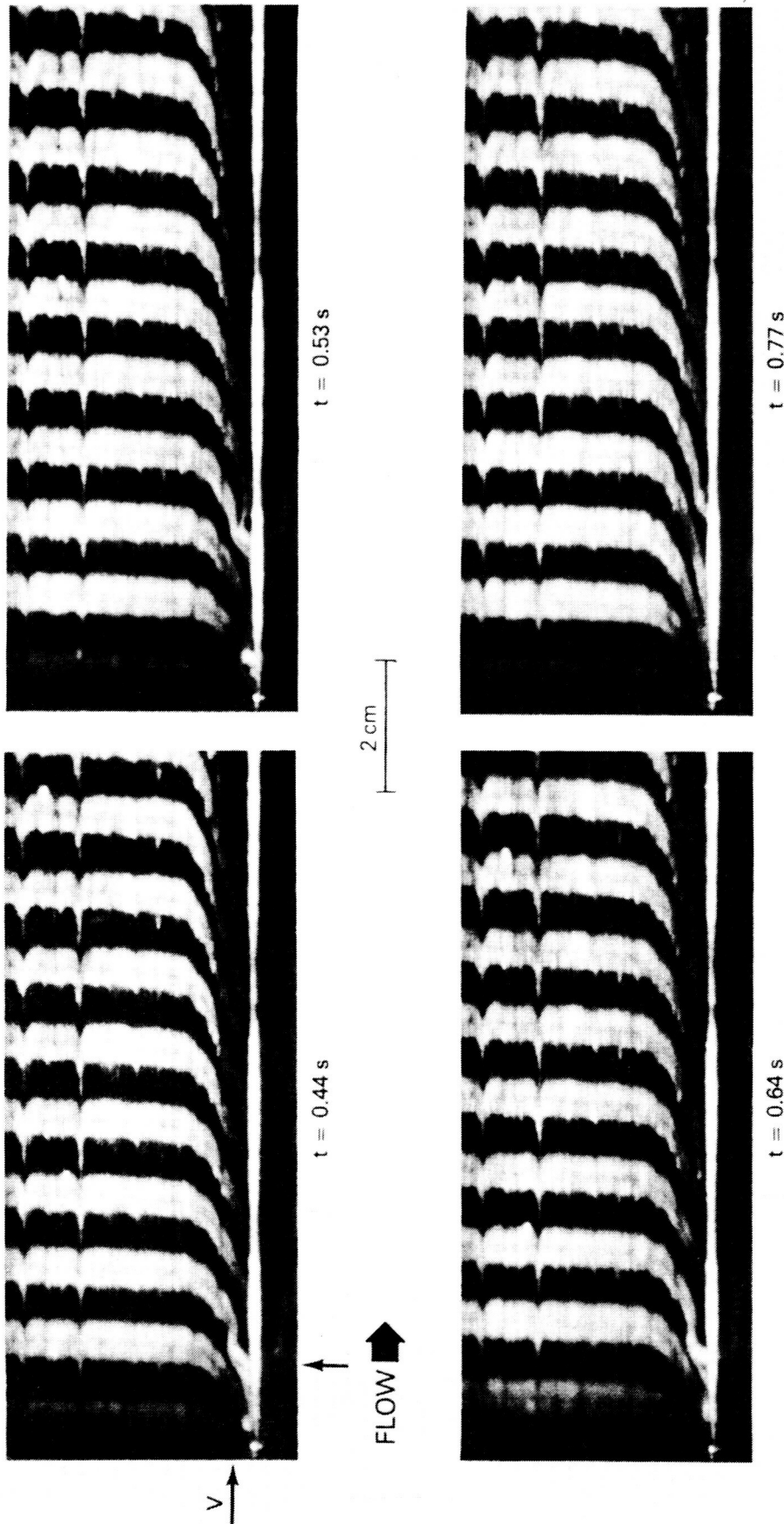


Figure 28. A Burst-Like Event is Generated in the Laminar Boundary Layer by Withdrawing Fluid from Two Spanwise Holes for 0.5 s at a Rate of $2.3 \text{ cm}^3/\text{s}$. The Streamwise Slot is Used to Obliterate the Resulting Hairpin Vortex. Suction from the Slot is Continuous at a Rate of $4 \text{ cm}^3/\text{s}$.

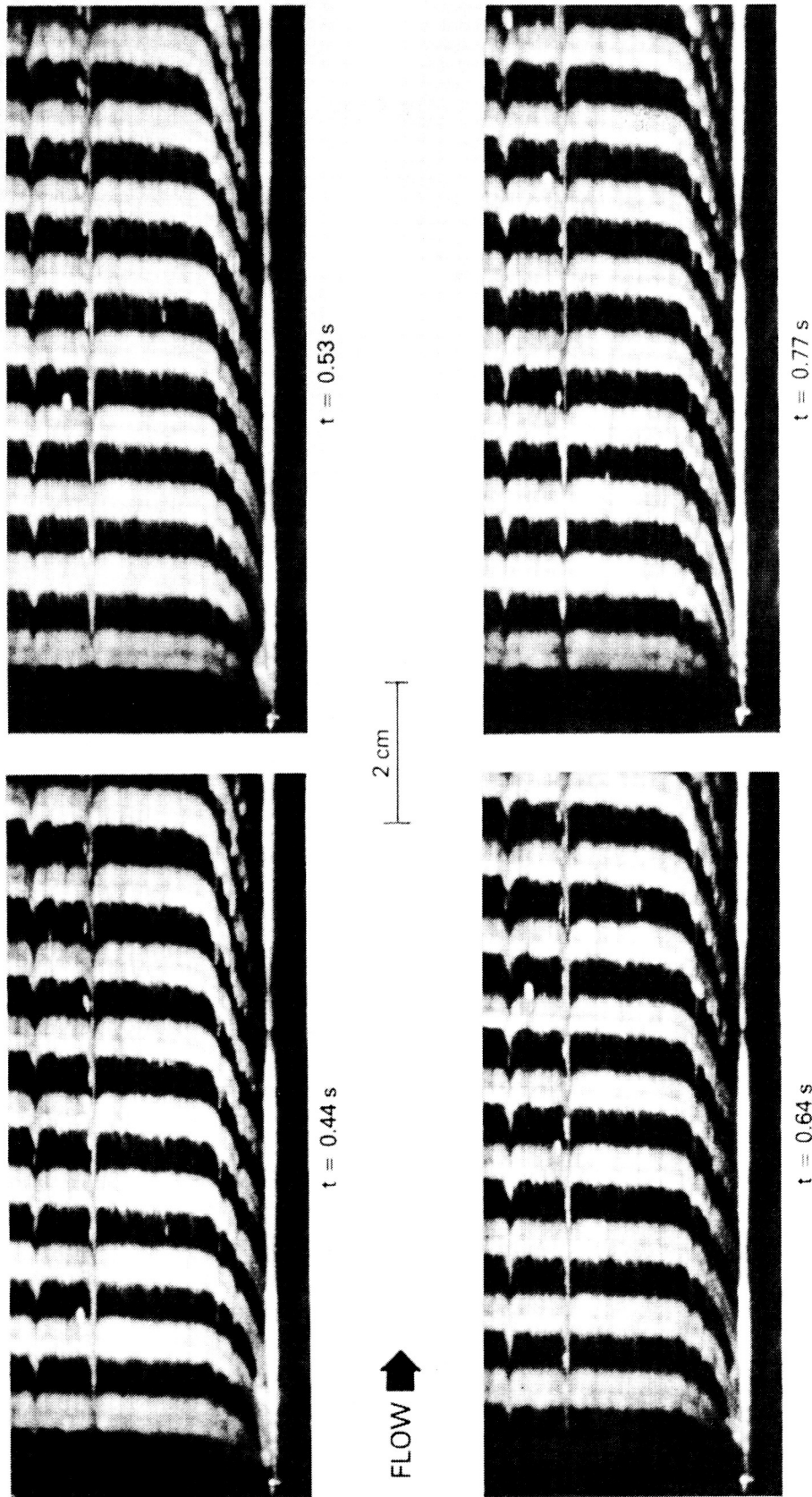


Figure 29. Higher Suction Rate from the Streamwise Slot is More Effective in Eliminating the Hairpin Vortex. The Continuous Suction from the Slot is at a Rate of $5.5 \text{ cm}^3/\text{s}$

The streamwise suction slot is also effective in eliminating the periodic train of hairpin vortices generated when the near-wall fluid is continuously withdrawn through the two spanwise holes. A comparison of four different runs is instructive and is depicted in the four photographs in Figure 30. In the first picture, a periodic train of hairpin vortices was generated by continuously withdrawing near-wall fluid through the two spanwise holes at a rate of $2.35 \text{ cm}^3/\text{s}$ (see Figure 25). In Figure 30b, continuous suction is applied only from the streamwise slot at a rate of $3 \text{ cm}^3/\text{s}$ and has no apparent effect on the laminar boundary layer. A downwardly displaced Blasius profile is evident from the time lines shown in the figure. When continuous suction is applied from both the two spanwise holes and the single streamwise slot, the periodic train of hairpin vortices seems to disappear as shown in Figures 30c and 30d. As expected, the larger suction rate from the slot shown in Figure 30d ($5.5 \text{ cm}^3/\text{s}$) is more effective in eliminating the artificial disturbances compared to the more moderate rate of $3 \text{ cm}^3/\text{s}$ shown in Figure 30c.

Top views of the flow field were also useful in showing the effects of the streamwise suction slot on the artificial events. Fluorescent dye was seeped from a spanwise slot located just upstream of the two spanwise holes. A horizontal sheet of laser light was projected very near the surface of the flat plate to excite the fluorescent dye. The sequence of events associated with the withdrawal of near-wall fluid from the two spanwise holes is shown in Figure 31. The flow is from left to right, and the ambient speed was 20 cm/s . The suction from the holes was applied for 0.5 s at a rate of $2.3 \text{ cm}^3/\text{s}$. Three low-speed streaks were generated and the middle one was unstable and broke down into a burst-like structure, as shown in the figure.

When suction from the streamwise slot was applied, the middle streak was obliterated and bursting was prevented, as shown in the sequence of photographs in Figure 32. In here, the suction from the holes lasted for 0.5 s and was at a rate of $2.3 \text{ cm}^3/\text{s}$, while the suction from the slot lasted for 0.5 s and was at a rate of $6.6 \text{ cm}^3/\text{s}$. Although this latter rate may seem excessive, the area of the slot, while much larger than the combined area of the two spanwise holes, is far smaller than the area over which a typical burst evolves.

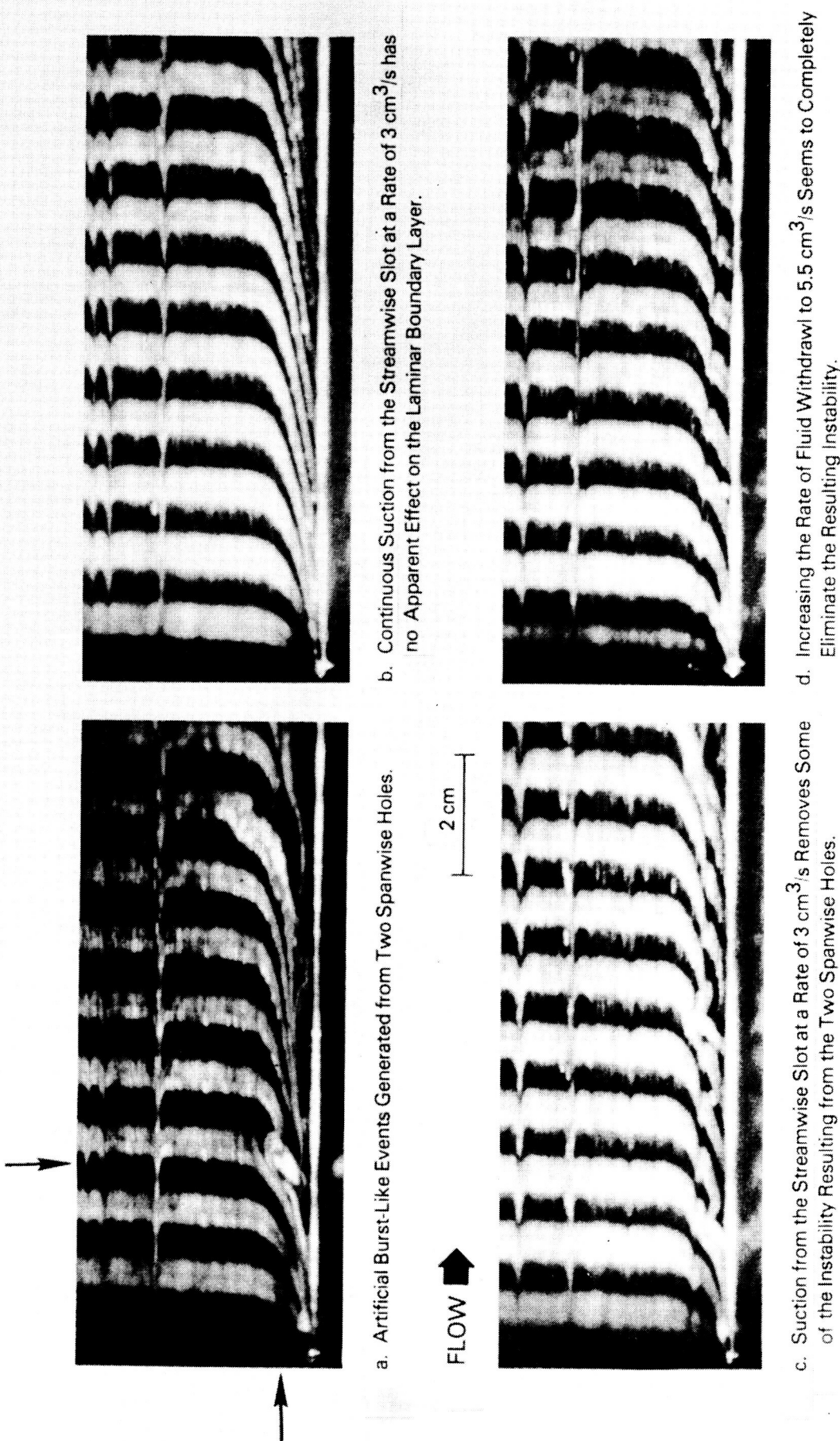


Figure 30. Effects of Suction from the Streamwise Slot on the Artificially Generated Bursts in a Laminar Boundary Layer.

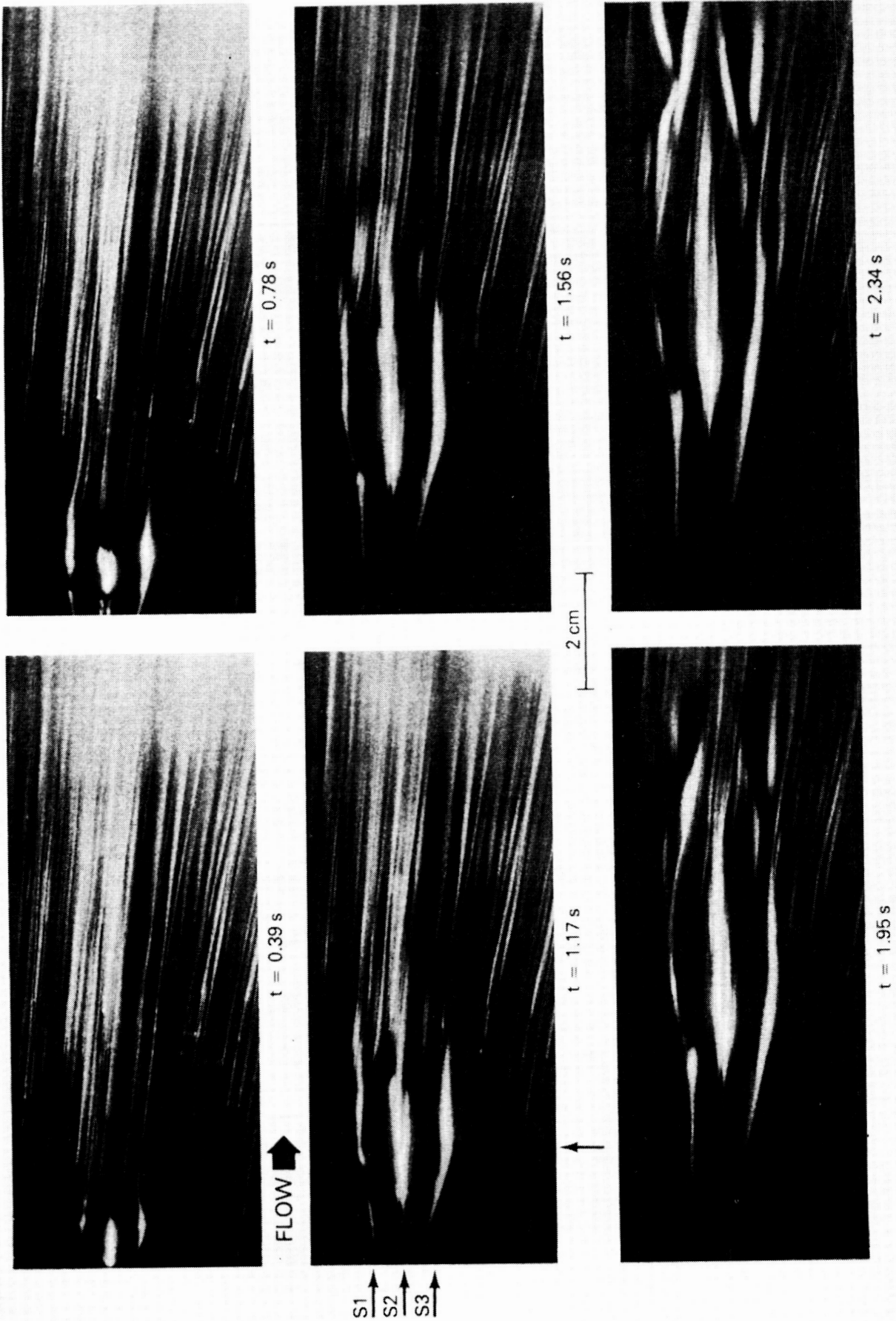
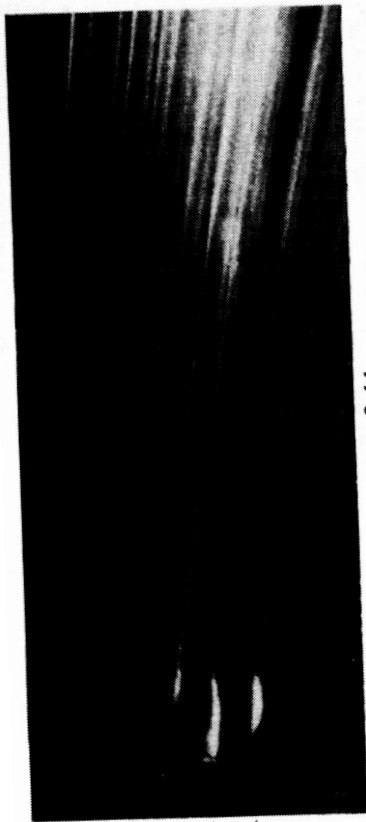
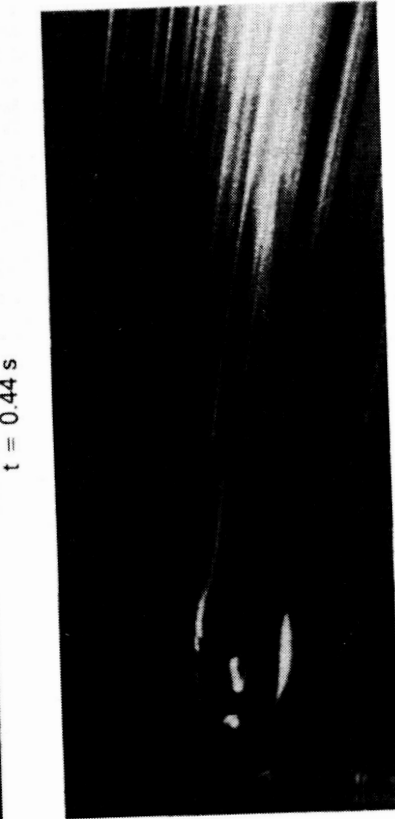


Figure 31. Top View Showing Sequence of Events Associated with the Withdrawal of Near-Wall Fluid from Two Spanwise Holes. $U_{\infty} = 20 \text{ cm/s}$; Suction is Applied for 0.5 s at a Rate of $2.3 \text{ cm}^3/\text{s}$.


S1
S2
S3



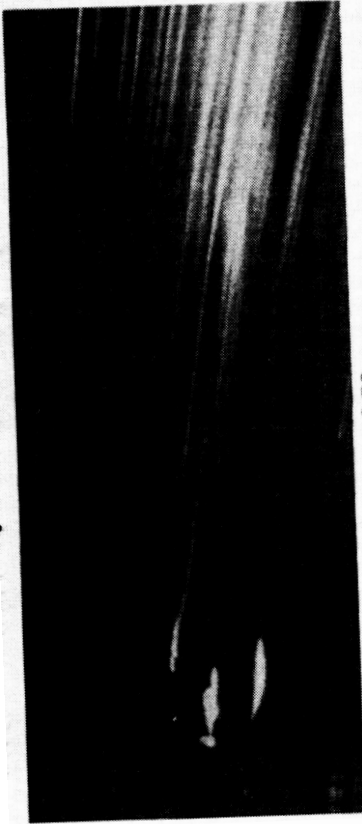
$t = 0.44 \text{ s}$



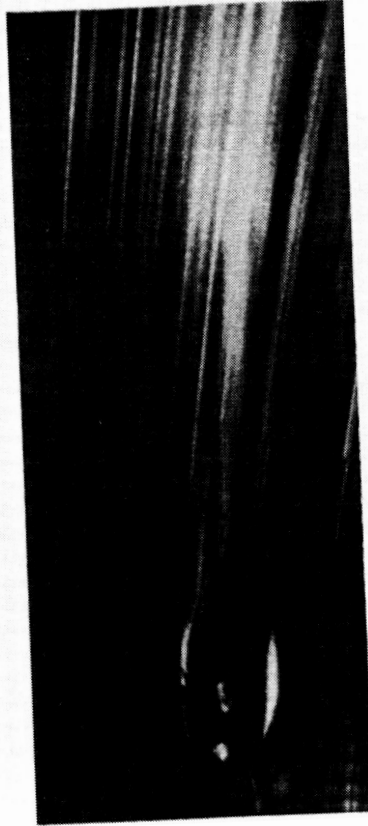
$t = 0.56 \text{ s}$

FLOW 

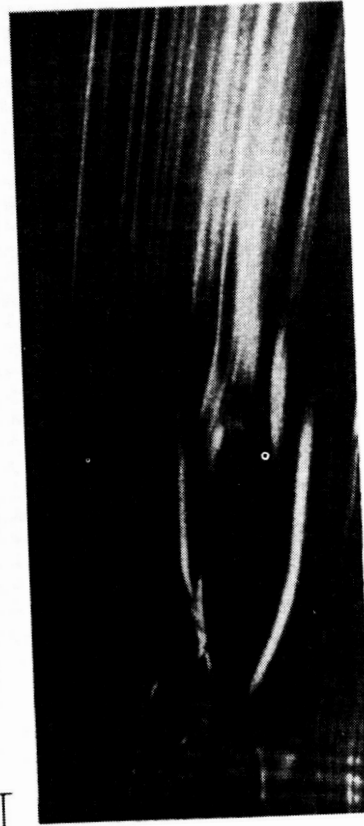
4 cm



$t = 0.53 \text{ s}$



$t = 0.59 \text{ s}$



$t = 1.17 \text{ s}$

$t = 0.67 \text{ s}$

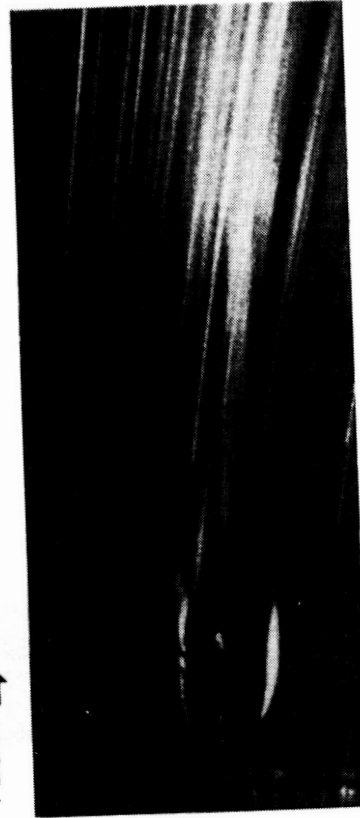


Figure 32. Three Streaks are Generated when Fluid is Withdrawn from the Two Spanwise Holes for 0.5 s at a Rate of $2.3 \text{ cm}^3/\text{s}$. The Middle Streak Disappears as a Result of Activating the Suction from the Streamwise Slot for 0.5 s at a Rate of $6.6 \text{ cm}^3/\text{s}$. Delay Time Between the Slot and the Holes is 0.5 s

As mentioned earlier, stronger impulsive suction from either the spanwise holes or the streamwise slot results in the generation of a turbulent spot. Continuous suction, on the other hand, does not have the same effect on the flow. Evidently, the unsteadiness plays a major role in the development of disturbances caused by the suction. The evolution of typical turbulent spots generated as a result of impulsive suction or the start of continuous suction from the streamwise slot is depicted in Figures 33 and 34, respectively. Top views of the left to right flow are visualized using fluorescent dye and a horizontal sheet of laser light. Note the initial convergence of the two low-speed streaks, their subsequent divergence, and the generation of two new streaks. The sequence of events leading to the generation of turbulent spots depicted in the present photographs is consistent with the vortex filaments model presented by Perry et al. (1981).

8.2 FAST RESPONSE PROBE RESULTS

To more quantitatively study the effects of the streamwise suction slot on the burst-like events generated in a laminar boundary layer, hot-film probes were used. A time record of 5 artificial events is shown in Figure 35a. The probe was located at $x = 84$ cm (5 cm downstream of the two spanwise holes) and $y = 0.5$ cm ($y/\delta = 0.49$). Suction was applied from the two spanwise holes for 0.5 s at a rate of $2.3 \text{ cm}^3/\text{s}$. A negative spike was observed in the velocity record whenever an artificial event was triggered. Note that the spike's strength and sign depend on both the probe location and the parameters of the impulsive suction. This is because the hairpin vortex that results from the artificial disturbance evolves differently for different suction rates and duration.

Attempts were made to eliminate these events using impulsive or continuous suction from the streamwise slot. This process has to be optimized, since too much suction from the slot would have a destabilizing effect on the boundary layer and weak suction would be insufficient to remove the artificial disturbance. Figure 35b indicates a successful attempt to remove the hairpin vortices shown in Figure 35a. In here, suction from the streamwise slot was applied 5 times, each for 0.1 s

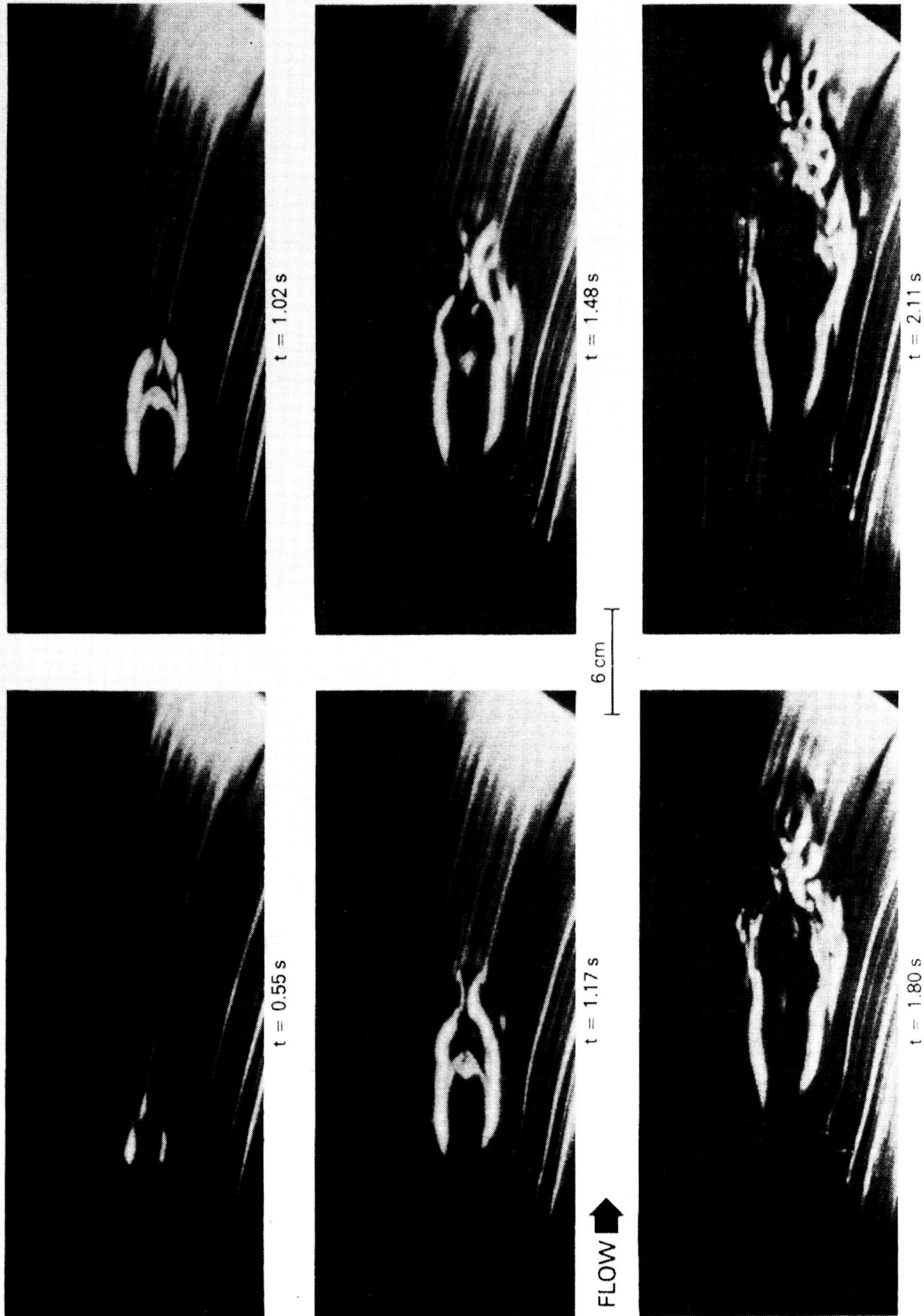


Figure 33. Evolution of a Turbulent Spot Initiated as a Result of Impulsive Suction from the Streamwise Slot. $U_{\infty} = 20 \text{ cm/s}$; Suction Lasts for 0.5 s at a Rate of $9.5 \text{ cm}^3/\text{s}$

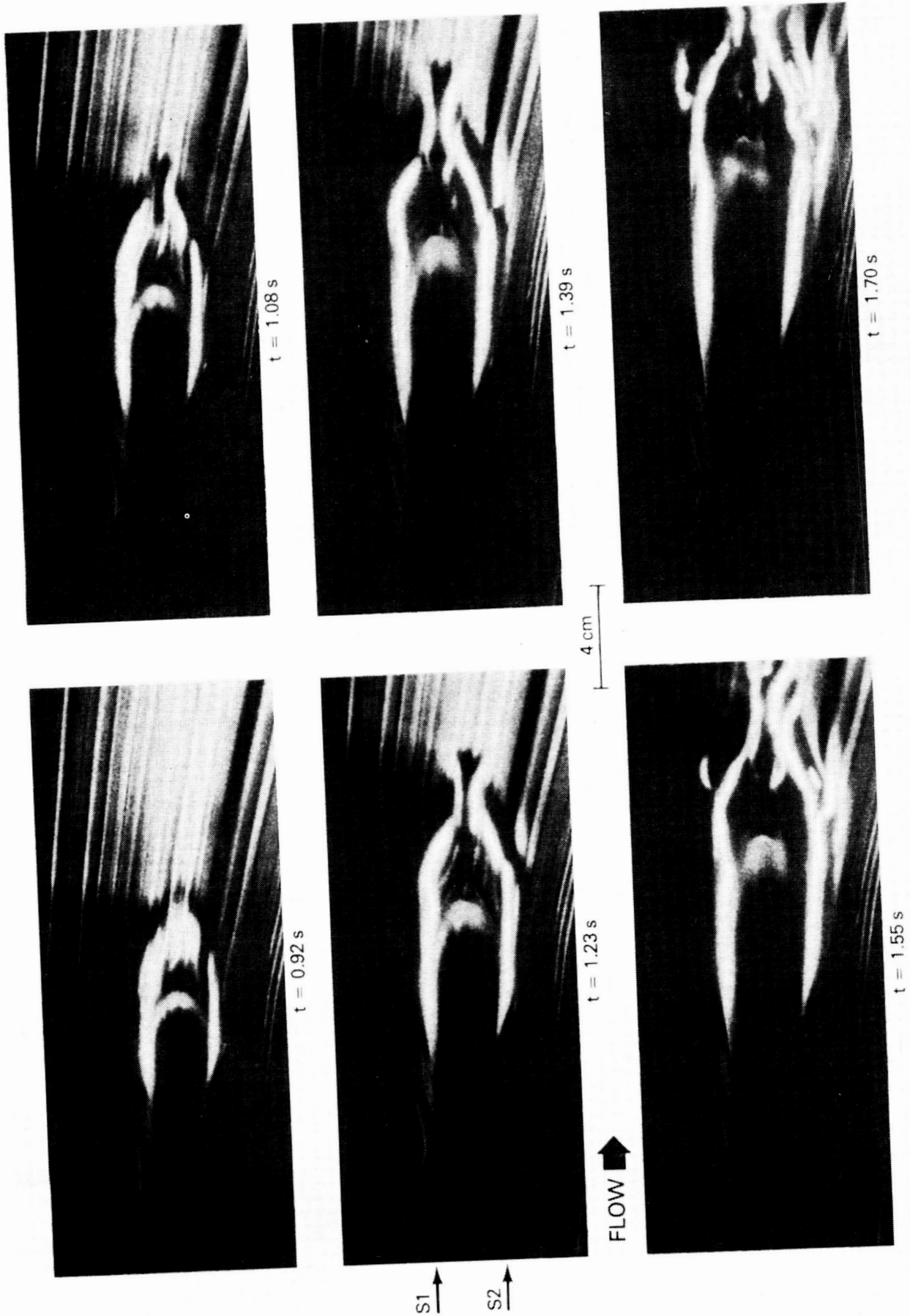
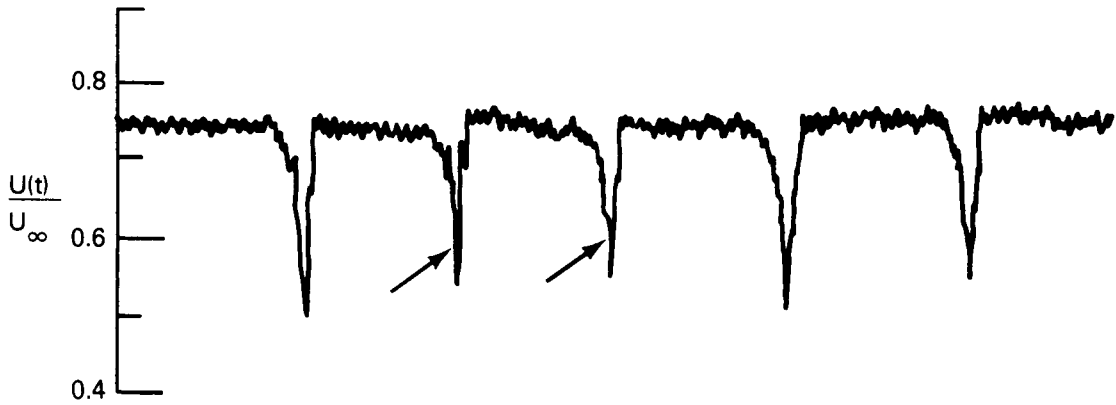
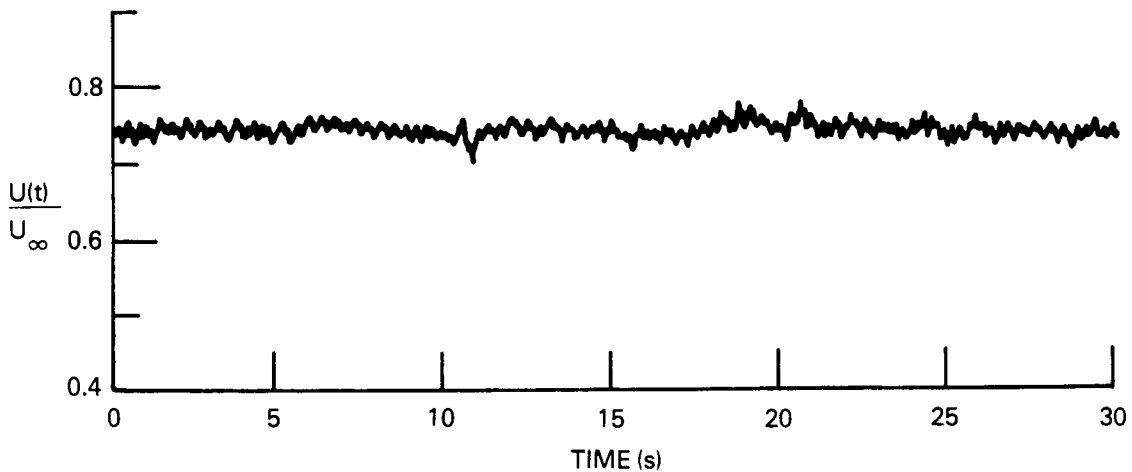


Figure 34. Evolution of a Turbulent Spot Initiated at the Start of Suction from the Streamwise Slot. $U_{\infty} = 20$ cm/s; Suction Rate from Slot = $9.4 \text{ cm}^3/\text{s}$



- a. Suction from Two Spanwise Holes Repeated 5 Times, Each Lasting 0.5 s at a Rate of $2.3 \text{ cm}^3/\text{s}$



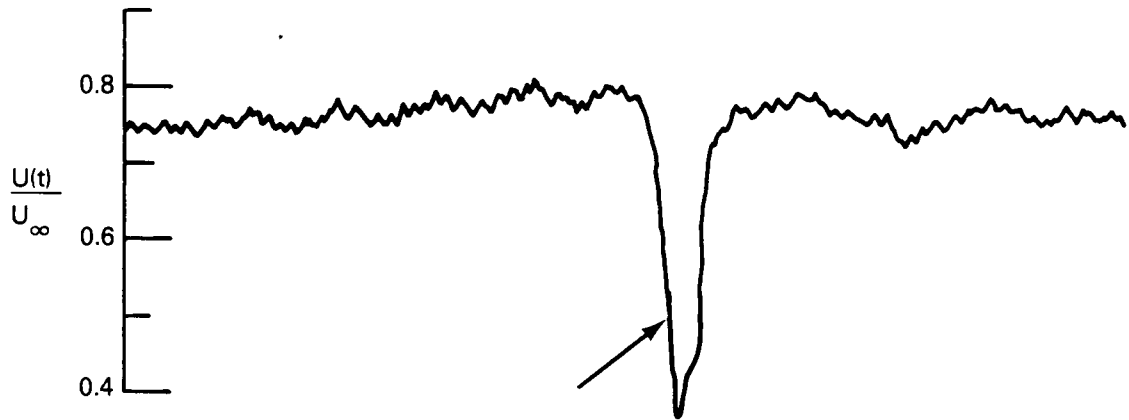
- b. In Addition to Suction from Two Holes, Fluid is Withdrawn from the Streamwise Slot for 0.1 s at a Rate of $1.5 \text{ cm}^3/\text{s}$. Suction from Slot Starts 0.25 s after Suction from Holes.

Figure 35. Effects of Suction from Streamwise Slot on Five Artificially Induced Burst-Like Events in a Laminar Boundary Layer. $U_\infty = 20 \text{ cm/s}$; $x = 84 \text{ cm}$; $y = 0.5 \text{ cm}$

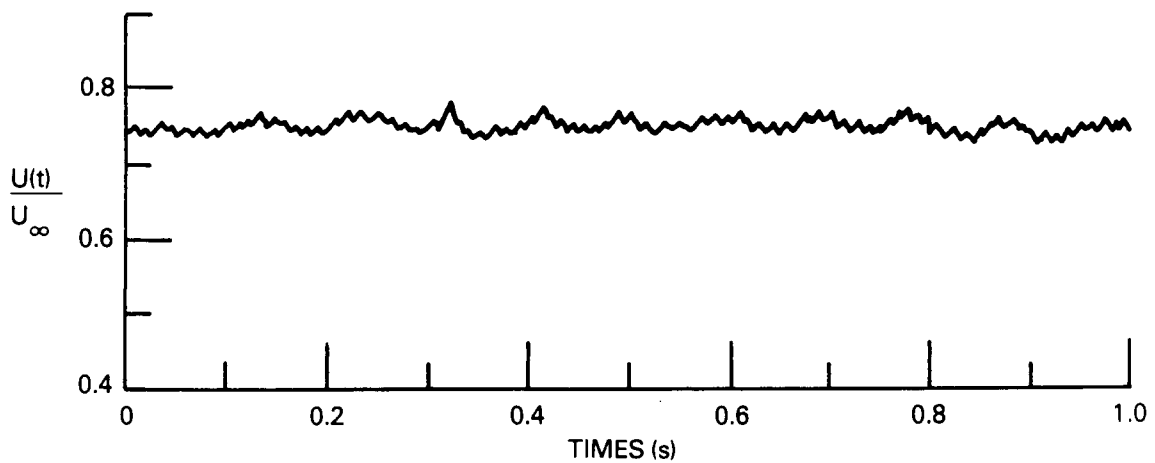
at a rate of $1.5 \text{ cm}^3/\text{s}$. The impulsive suction from the slot always started 0.25 s after the onset of suction from the two spanwise holes. The time record shown in Figure 35b shows no sign of the artificial events. A close-up of one of the artificial events and its obliteration is shown in Figure 36. All other run conditions are similar to those depicted in Figure 35.

The vertical velocity through the streamwise slot was 30 cm/s for the conditions in Figure 35b. Since the slot width was 1% of the average spanwise streak's spacing, the average continuous normal velocity would have been 0.3 cm/s. However, the suction was only applied for 0.1 s to remove each burst. In a corresponding turbulent boundary layer this duration would represent 4% of the total time. Thus, the equivalent suction coefficient is $C_q = 0.0006$. This equivalent rate is 5 times smaller than that reported by Rotta (1970) and Verollet et al. (1972) as the rate of uniform transpiration necessary to yield zero growth of the boundary layer's momentum thickness. Additionally, as mentioned in Section 6.5, further savings are possible by using finite-length slots and periodically repeating the pattern in the streamwise direction. For example, if the length of the streamwise slot is 1000 wall units and the pattern is repeated every 3000 wall units, C_q will be reduced by a factor of 3.

Strong impulsive suction from the two spanwise holes resulted in the generation of a hairpin vortex that burst (broke down into turbulence). This is shown in the time record in Figure 37a. The hot-film probe was centered behind the two spanwise holes and was located at $x = 820 \text{ mm}$ and $y = 2 \text{ mm}$ ($y/\delta = 0.2$). Suction was applied from the holes for 0.5 s at a rate of $2.8 \text{ cm}^3/\text{s}$. The resulting fluctuations are different from the single spike associated with a hairpin vortex in Figure 36a, because the generation suction was increased by 20% and the velocity signal was obtained at a lower position in the boundary layer. The burst-like event was partially obliterated using continuous suction from the streamwise slot at a rate of $9.4 \text{ cm}^3/\text{s}$ as shown in Figure 37b. Clearly, this suction rate ($C_q = 0.09$) is too high to be of practical value and the process must be further optimized by using intermittent suction, etc. Also, the suction rate is so large that distortion of the flow field may have been present, e.g. the oscillations seen in Figure

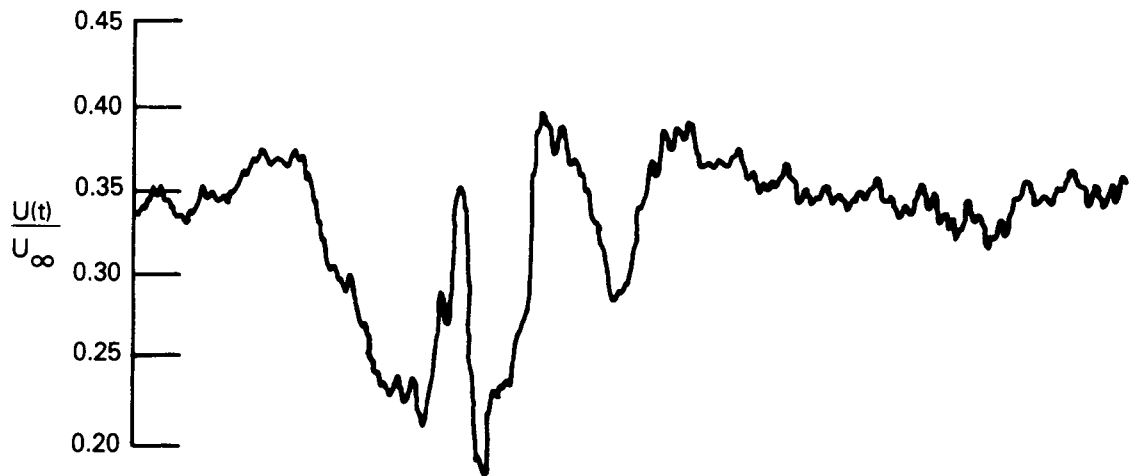


a. Single Burst-Like Event Generated in a Laminar Boundary Layer. Suction from Two Spanwise Holes Lasting for 0.5 s at a Rate of $2.3 \text{ cm}^3/\text{s}$

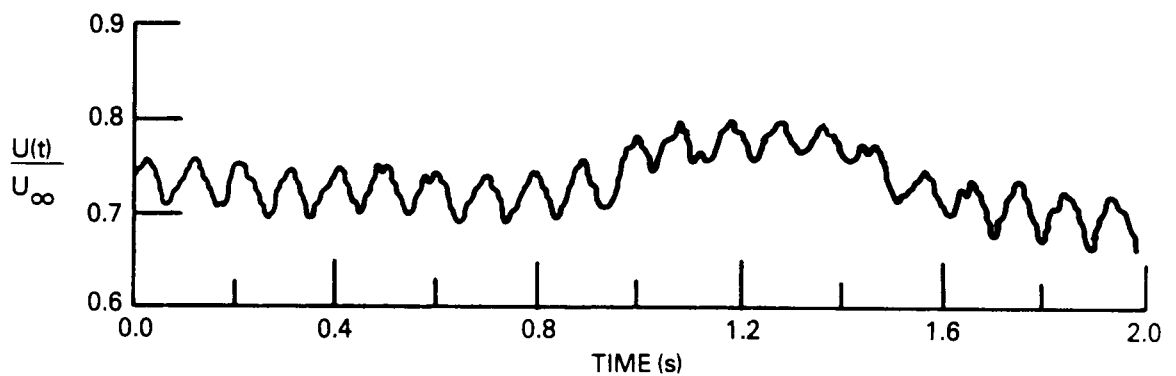


b. Suction from the Streamwise Slot Obliterate the Burst-Like Event

Figure 36. Effects of Suction from Streamwise Slot on a Single Burst-Like Event in a Laminar Boundary Layer.



a. Burst-Like Event is Generated when Suction is Applied from Two Spanwise Holes for 0.5 s at a Rate of $2.8 \text{ cm}^3/\text{s}$



b. Continuous Suction from Streamwise Slot at a Rate of $9.4 \text{ cm}^3/\text{s}$ Partially Obliterate the Burst

Figure 37. Effect of Slot Suction on a Single Artificial Burst in a Laminar Flow.
 $U_\infty = 20 \text{ cm/s}$; Probe at $x = 82 \text{ cm}$ and $y = 0.2 \text{ cm}$

37b. It is clear that a mature burst is more difficult to eliminate than a newly-developed hairpin vortex.

Continuous suction from either the two holes or the streamwise slot results in a downward shift of the Blasius profile and a corresponding increase of the streamwise velocity at a given height above the plate. For example at $y = 0.2 \text{ cm}$ ($y/\delta = 0.2$), continuous suction from the two spanwise holes at a rate of $2.35 \text{ cm}^3/\text{s}$ results in an increase of the streamwise velocity of about 20 percent. In this case, a periodic train of hairpin vortices was generated. Continuous suction from the streamwise slot at a rate of $5.5 \text{ cm}^3/\text{s}$ was sufficient to obliterate the artificially generated vortices.

9. SELECTIVE SUCTION IN TURBULENT FLOW

The ultimate application of the selective suction technique will be to reduce the skin friction drag in a turbulent boundary layer. The previous section of this report illustrated the feasibility of the concept in a laminar flow where flow visualization and probe measurements are relatively easy to conduct and interpret. The problem in a turbulent flow is much more complex. The background turbulence fluctuations make it hard to see or to measure the organized structures that we are attempting to control. Nevertheless, some limited measurements were conducted in a turbulent boundary layer during the present investigation. This section summarizes the results of this task.

Figure 38 is a sequence of photographs depicting a natural bursting event in a turbulent boundary layer. The flow is from left to right and the side view was visualized using a vertical hydrogen-bubbles wire and a vertical sheet of laser light parallel to the flow direction. The towing speed was $U_{\infty} = 20$ cm/s, and the field of view in each photograph was from $x \approx 79$ to 90 cm. The typical sequence of events associated with a burst is depicted in the figure and is very similar to the results of Kline et al. (1967).

Continuous suction from the streamwise slot was applied to attempt to reduce the frequency or the strength of bursting events at a given location. This task was not easy and required very careful optimization. A successful attempt is shown in Figure 39. In Figure 39a, a typical photograph in a natural boundary layer during bursting is depicted. Continuous suction from the slot is applied at a rate of 4 cm³/s and the effect on natural bursts is shown in Figures 39b and 39c. The flow seems to be much more quite in this case, although a shear layer appears to develop intermittently (Figure 39c).

More quantitative information were obtained using hot film probes and the two pattern recognition algorithms described in Section 6.8. Artificial bursting events were generated in the turbulent boundary layer by withdrawing fluid impulsively from the two spanwise holes, and attempts were made to prevent these bursting from developing using either continuous or impulsive suction from the streamwise slot. About 80 percent of these bursts were eliminated when suction from the slot was applied for 0.1 s at a rate of 4 cm³/s.

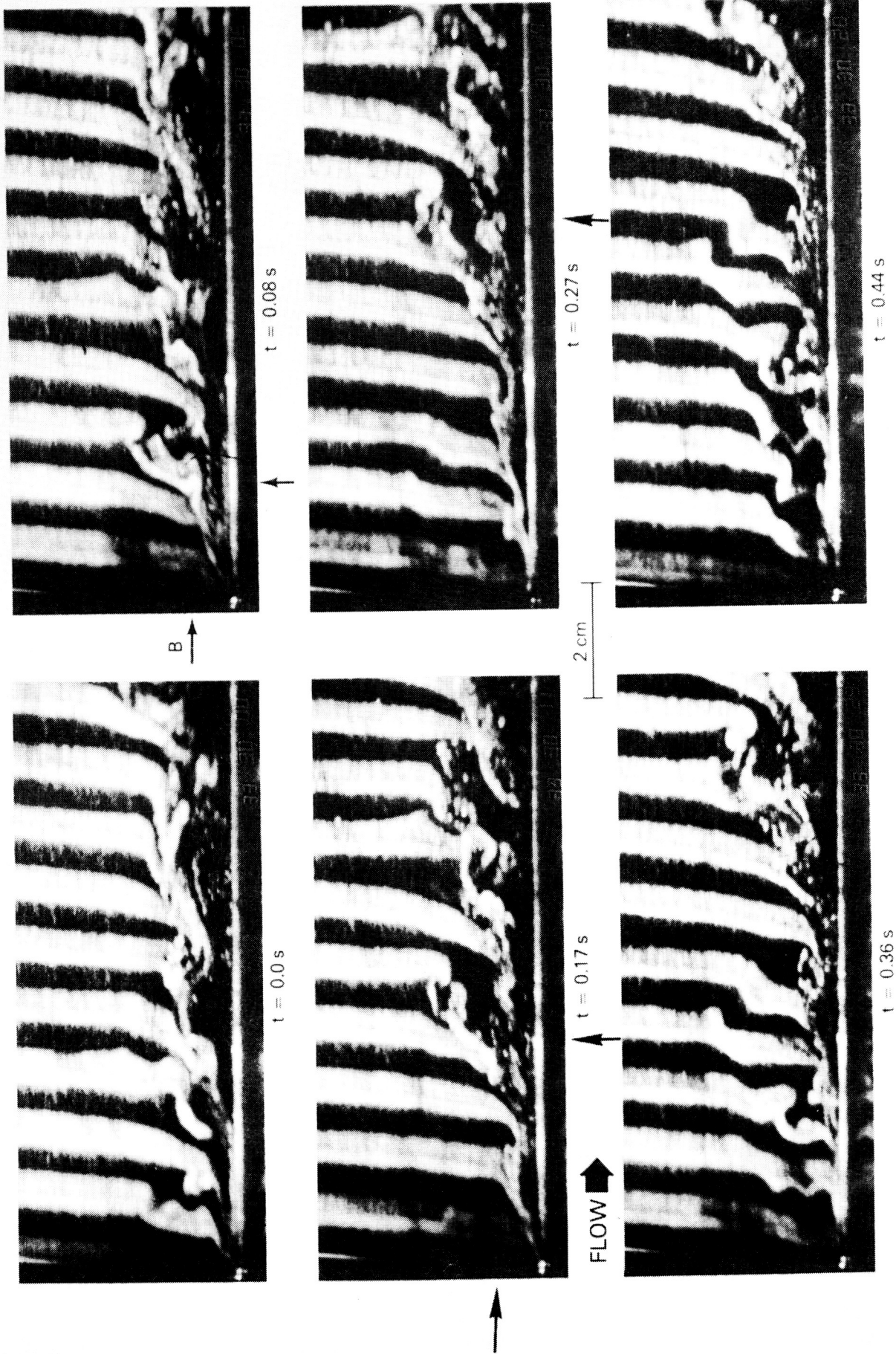


Figure 38. A Bursting Event in a Turbulent Boundary Layer. Flow is Visualized Using Hydrogen Bubbles Illuminated with a Vertical Sheet of Laser Light. $U_{\infty} = 20$ cm/s

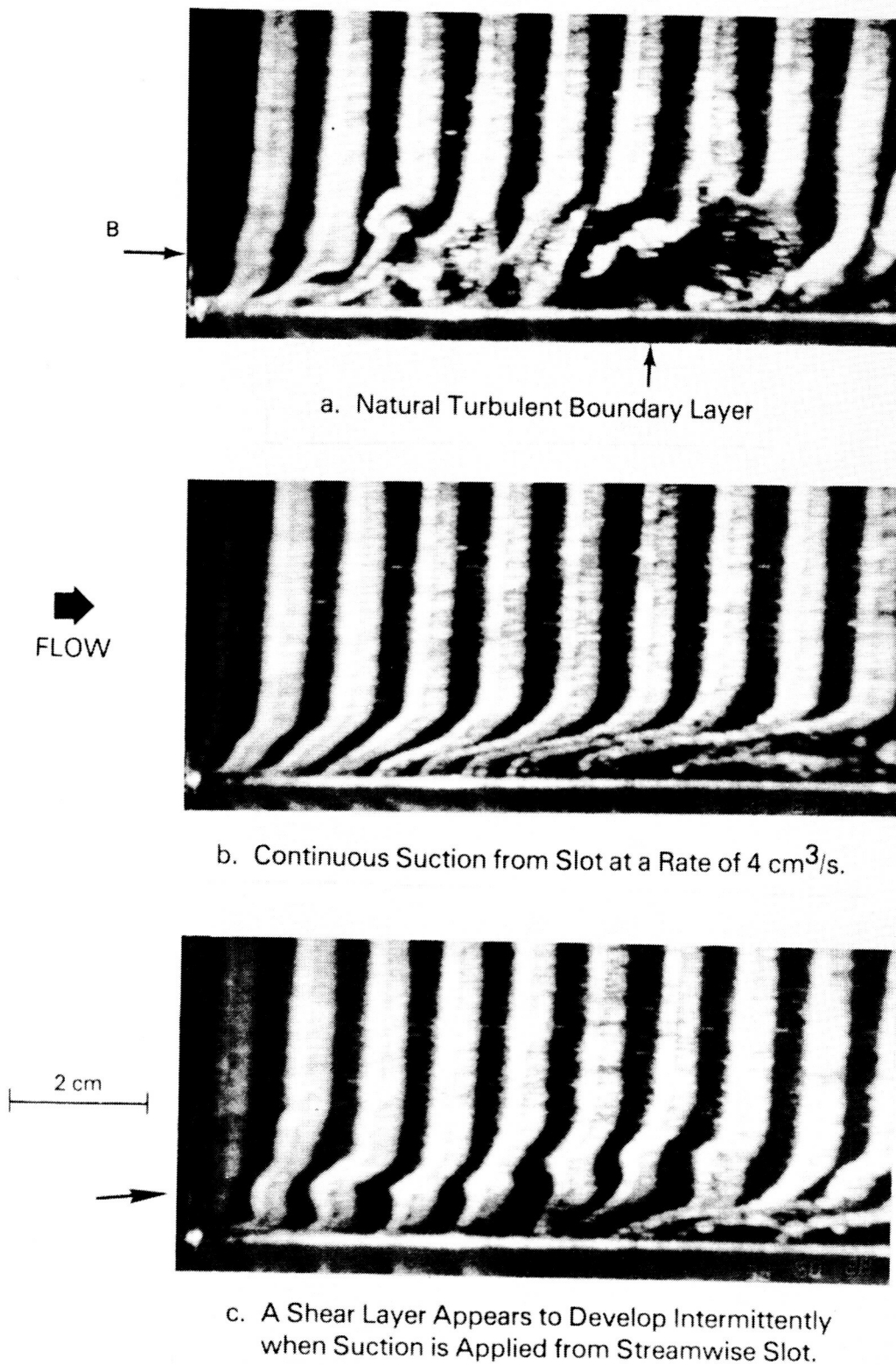


Figure 39. Effects of Suction from Streamwise Slot on Bursting Events in a Turbulent Boundary Layer. $U_{\infty} = 20$ cm/s

For natural bursts, continuous suction is obviously needed due to their random occurrence. When continuous suction was applied optimally from the streamwise slot, the natural bursting frequency as computed from the VITA algorithm was reduced by as much as 50 percent.

10. WIND-TUNNEL RESULTS

10.1 LONGITUDINAL ROUGHNESS ELEMENTS

Velocity profiles and bursting statistics were measured in the presence of the cylindrical longitudinal roughness elements (LREs) described in Section 6.3. A difficult question arose concerning which values to use for the reference mean and rms velocities. Both the VITA scheme for measuring bursting statistics and the low-speed streaks (LSS) algorithm presented here hinge upon the values used. As shown in Figure 40, a hot-wire over a string sees a lower mean and rms velocity due to the elevated no-slip condition imposed by the LRE. Two philosophies were developed to look at the data. The first was to assume that the presence of the LREs was unknown, and use the normal flat plate values as a reference. Since the velocity over the flat plate is larger than that over a string at the same height (relative to the plate), the LSS algorithm is triggered a greater portion of the time. The second idea was to use the local mean and rms velocities seen by each sensor, thus the various algorithms would be triggered at a lesser rate. All of the following data is presented and discussed under both viewpoints. The term "flat plate reference" refers to using the flat plate mean and rms velocities in the algorithms, and the term "local reference" refers to using the mean and rms velocities seen locally in those algorithms.

Velocity profiles directly over an LRE and between two LREs are shown in Figures 41a and 41b, respectively. The friction velocity was obtained with a Coles (1968) fit of the logarithmic region. The friction velocities obtained in this manner were the same for all of the profiles, indicating an insensitivity of the logarithmic region to the presence of the LREs. All of the profiles are identical for $y^+ > 15$, thus the LREs only effect the streamwise velocity in the sublayer and the buffer layer. Below $y^+ = 15$, there is a velocity deficit over a string, and an excess between them, as would be expected. It should be noted, however, that if the data over an LRE is shifted by the diameter of that LRE ($H^+ = 5$), the defect disappears and a normal boundary layer profile is obtained. Hence velocity profiles over an LRE appear to be simply elevated by the height of that LRE.

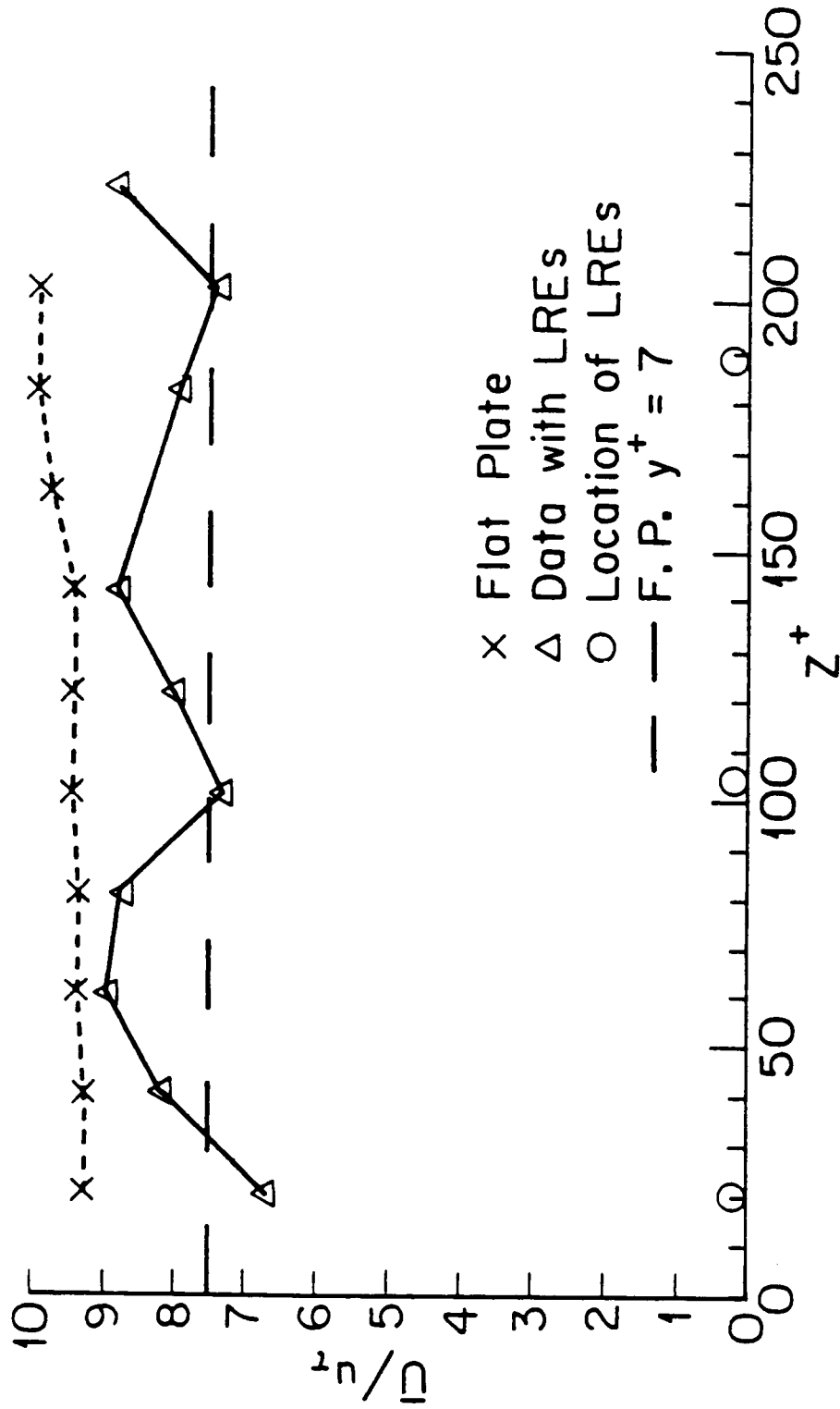


Figure 40 a. Average Velocity Across the Span with LRE's ($y^+ = 12$).

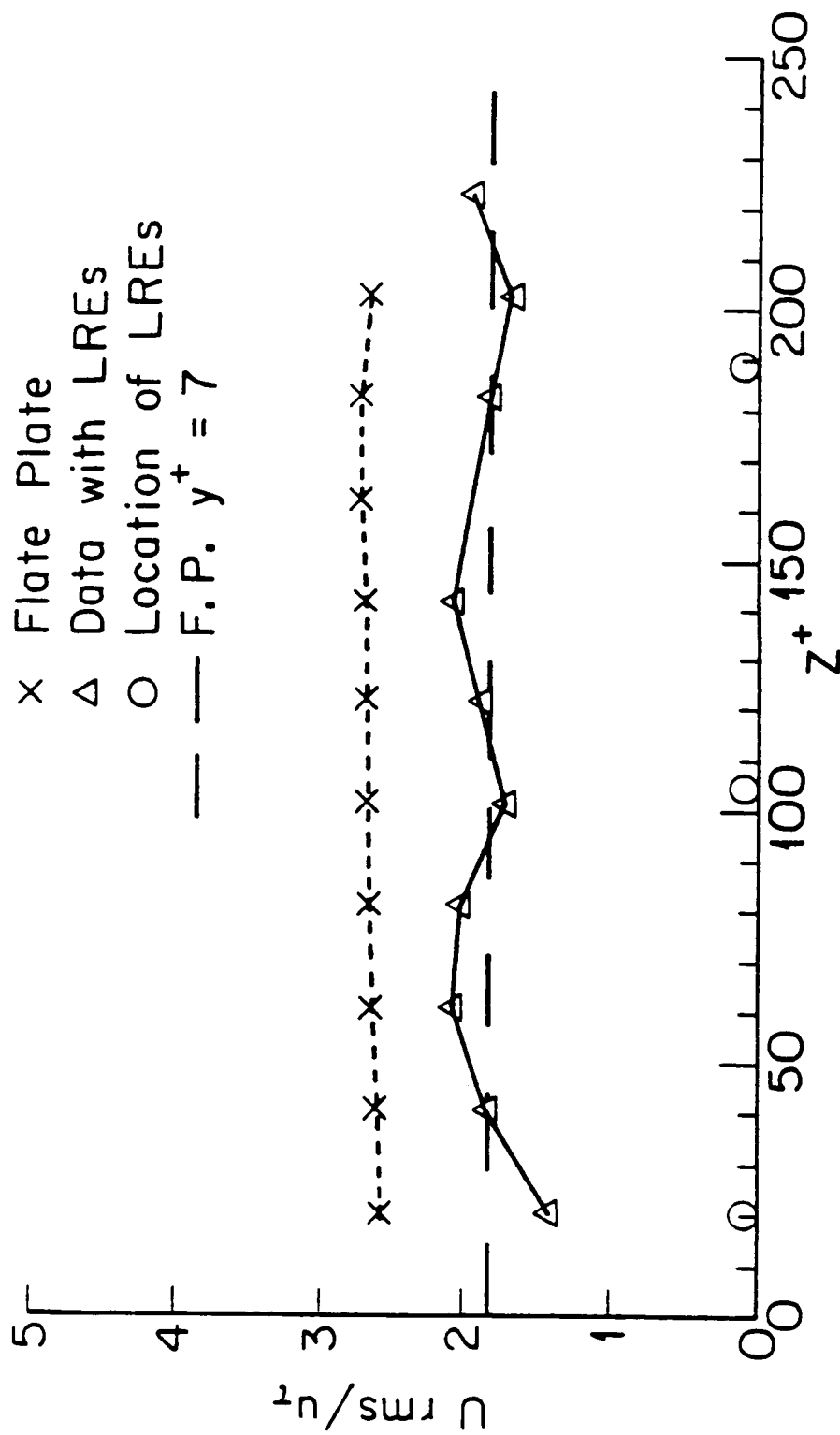


Figure 40 b. RMS Velocity Across the Span with LRE's ($y^+ = 12$).

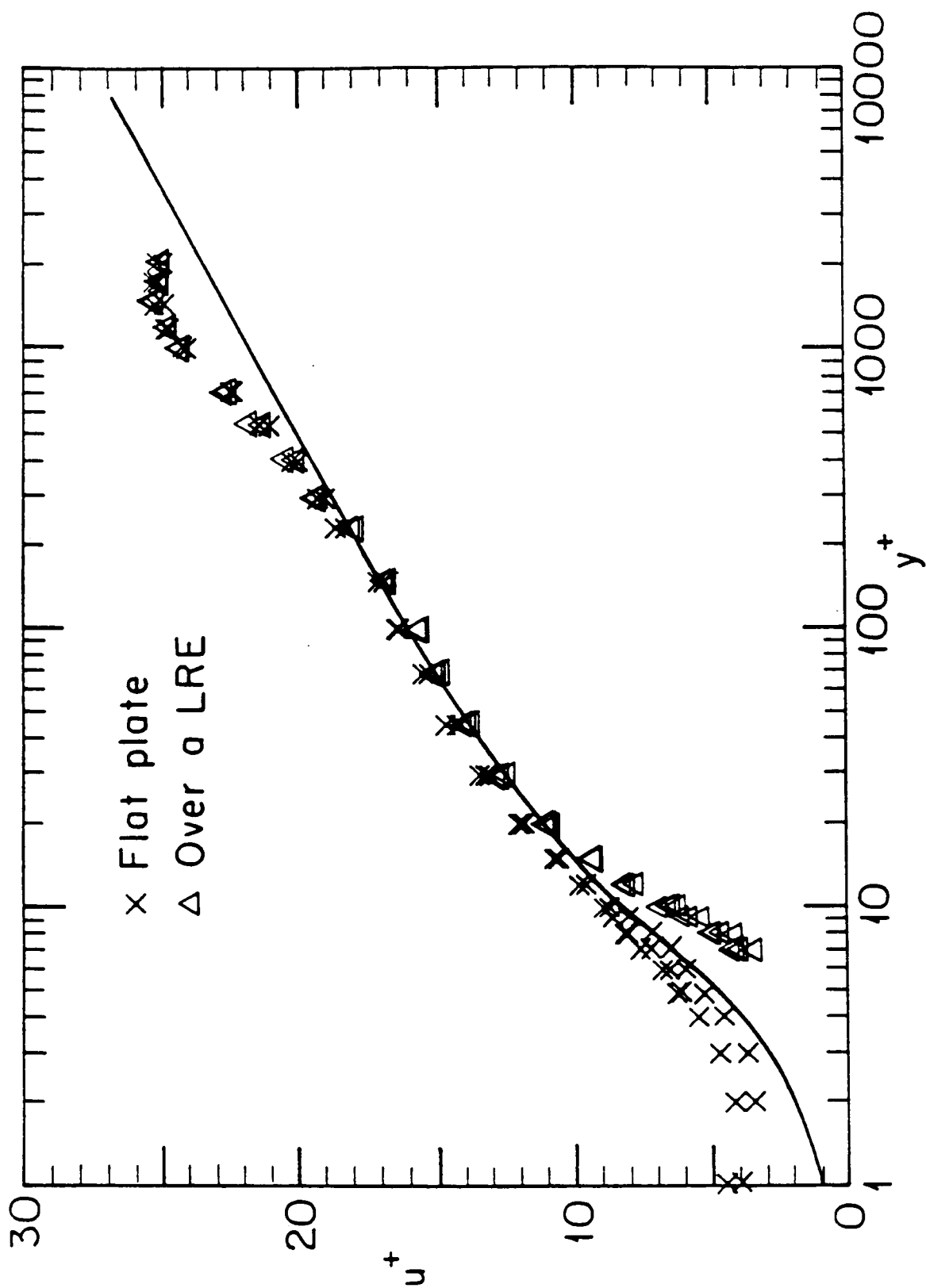


Figure 41 a. Velocity Profiles over an LRE. The Multiple Data Points are for Different Runs and Indicate the Repeatability of the Data.

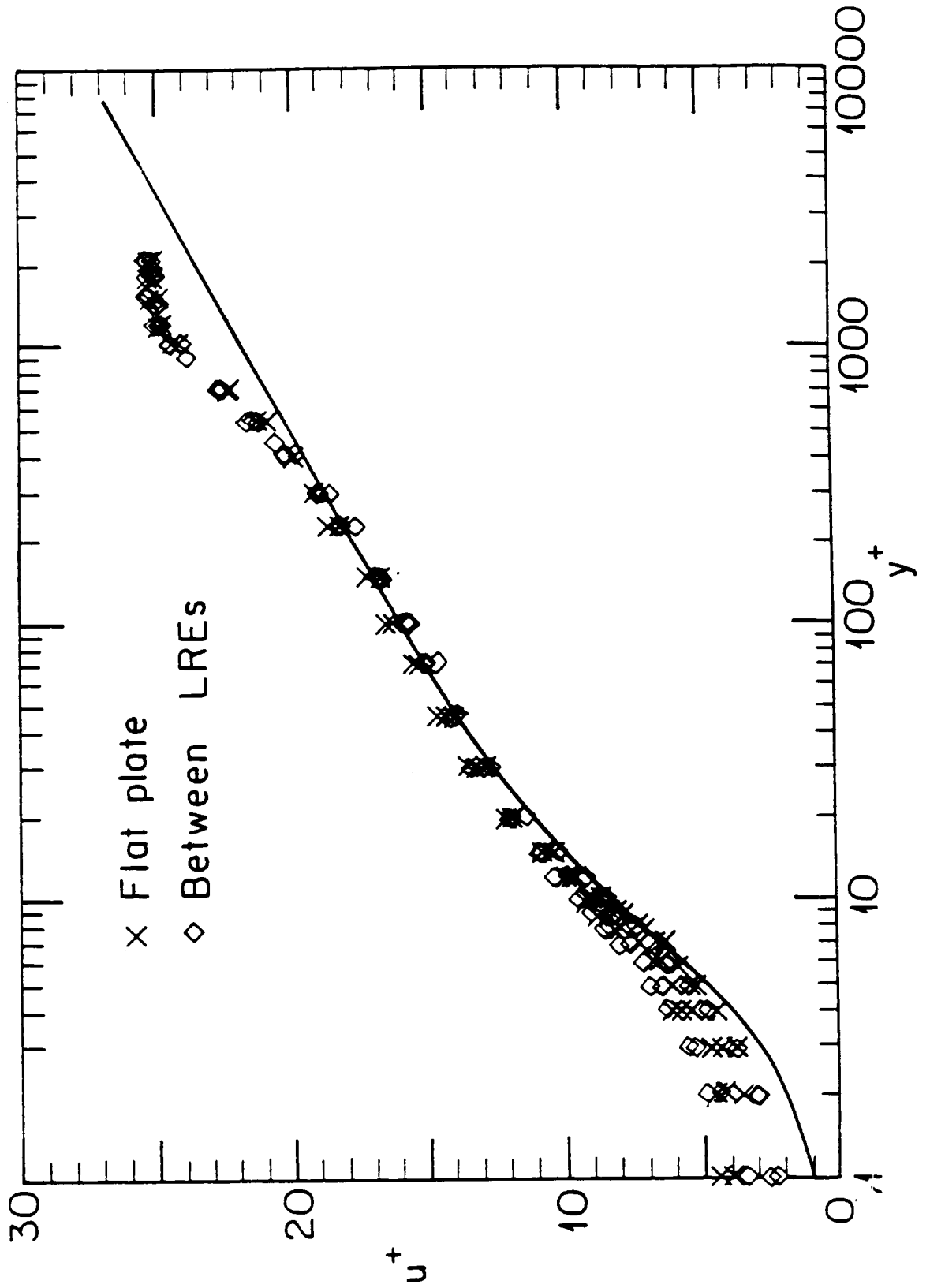


Figure 41 b. Velocity Profiles between LRE's.

For qualitative information, flow visualization experiments were conducted in a water channel using a single hydrogen-bubbles wire. Similar LRE modifications were used in the water and the air boundary layers. The horizontal wire was placed perpendicular to the freestream at various heights above the wall. At a height of $y^+ = 6$, the pictures indicated LSS over all but one of the streamwise strings. However, few streaks were also discernable between the roughness elements. First appearances would suggest that the LSS have a great affinity for the LREs. At a height of $y^+ = 12$, the actual location of the LSS was quite random with respect to the LREs, although the average spacing of the LSS was comparable to the spacing of the LREs by design. It was possible, however, to associate most of the streaks as "belonging" to one or more of the strings.

A sketch of iso-velocity contours over the LREs is depicted in Figure 42 and reveals that the no-slip condition imposed by an LRE requires that relatively low-speed fluid will surround the LRE. The right side of the sketch demonstrates that if the LSS were formed over corresponding LREs, the spanwise velocity fluctuations would move the streaks randomly perpendicular to the LREs. This dislocation would increase with elevation, and hence the LSS would appear randomly with respect to the LRE. Thus, above a certain height, it would be impossible to determine which streak originated at which LRE. The data presented here would place that height at $y^+ = 10$ to 15.

The question of what constitutes a low-speed streak in the hydrogen-bubbles visualizations is perhaps academic. On the one hand we have the "naturally" occurring streaks whose nature and origin are far from being understood. On the other hand, a retarded spanwise profile of U velocity is inevitably generated as a result of the no-slip condition at the strings and will manifest itself as low-speed regions at the peaks of these surface modifications. Whether or not these low-speed regions are "natural" streaks, they constitute the only discernable structures at this height above the wall. Therefore, boundary layer control should be achievable most effectively by interfering with these eddies, regardless of their exact nature.

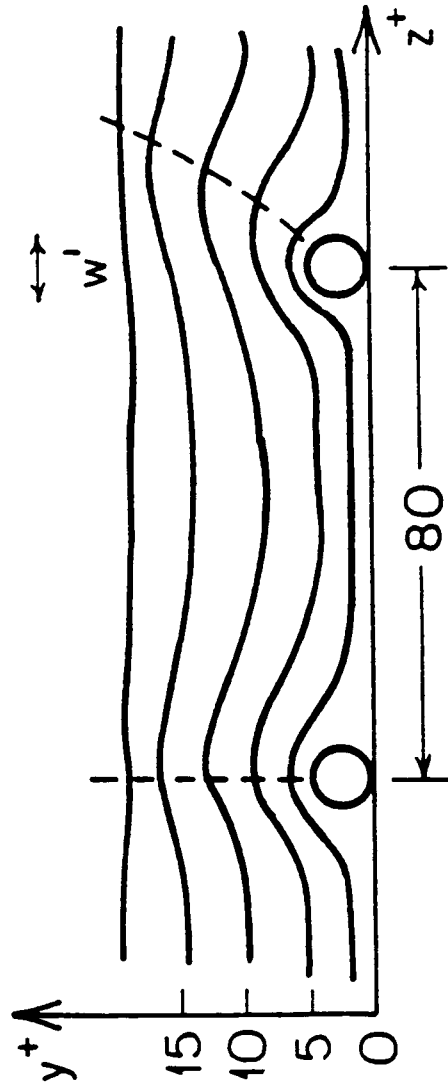


Figure 42. Sketch of Instantaneous Iso-Velocity Contours Over the LREs.

All of the hot-wire data plotted in Figures 43, 44, 45 and 46 were taken in the wind tunnel at a height of $y^+ = 12$ relative to the plate with the LREs. The data from a normal boundary layer on a clean plate at the same height are also plotted. The rake could not be operated below this height because heat conduction directly to the strings biased the results. If the only effect of the LREs was to elevate a normal boundary layer by their diameter, then the statistics over an LRE (when referenced locally) should compare to the flat plate values at a height of $y^+ = 7$. The extra dashed lines in Figures 43b, 44b, 45b, and 46b represent such flat plate information obtained with a single hot-wire.

In Figure 43a, the bursting frequency for the LREs and a clean plate are shown. These data were calculated with the flat plate reference velocity values. The bursting frequency decreases considerably over a string, while the values between the strings are comparable to the flat plate values. In Figure 43b, the local reference values were used in the VITA algorithm, and peaks in the bursting frequency are seen above the strings. This is expected since the VITA algorithm calculates its own mean value based upon a short temporal average, consequently it is independent of the mean velocity value. Thus the number of bursts detected is inversely proportional to the applied rms threshold. Since the LREs reduce the rms values, one expects a larger number of bursts detected. This is seen in Figure 43b as compared to 43a. An important indication that the LREs do not fully eliminate the randomness of the LSS is shown by the bursting frequency between the LREs which has the same magnitude as the flat plate value. The graphs show that while the streaks may "prefer" bursting over an LRE, there is no reduction of bursting between the LREs. Thus the spatial randomness of the entire bursting process is only effected near the LREs.

The number of LSS seen per second, based on the flat plate reference, are plotted in Figure 44a. The frequency of the detected LSS appears to have doubled over the LREs, but is not significantly reduced between them. At first glance, it would seem that the LREs are generating their own LSS in addition to those already existing in a normal boundary layer. But as discussed earlier (Figure 42c), the elevated no-slip condition creates lower velocities over the strings. Thus when referenced to the flat plate, the LSS algorithm is triggered more often. Using the local

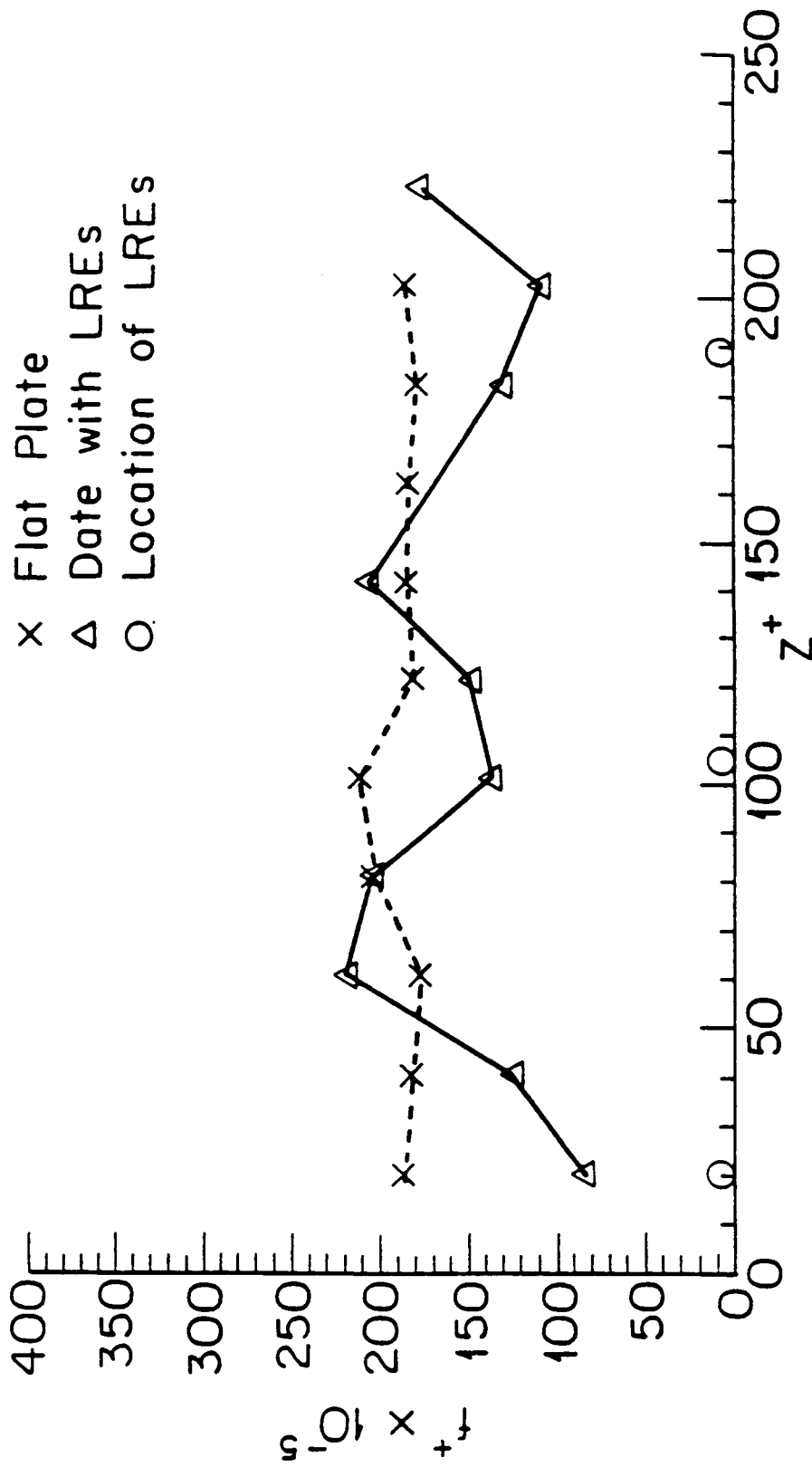


Figure 43 a. Bursting Frequency Across the Span (Flat Plate Reference;
 $y^+ = 12$).

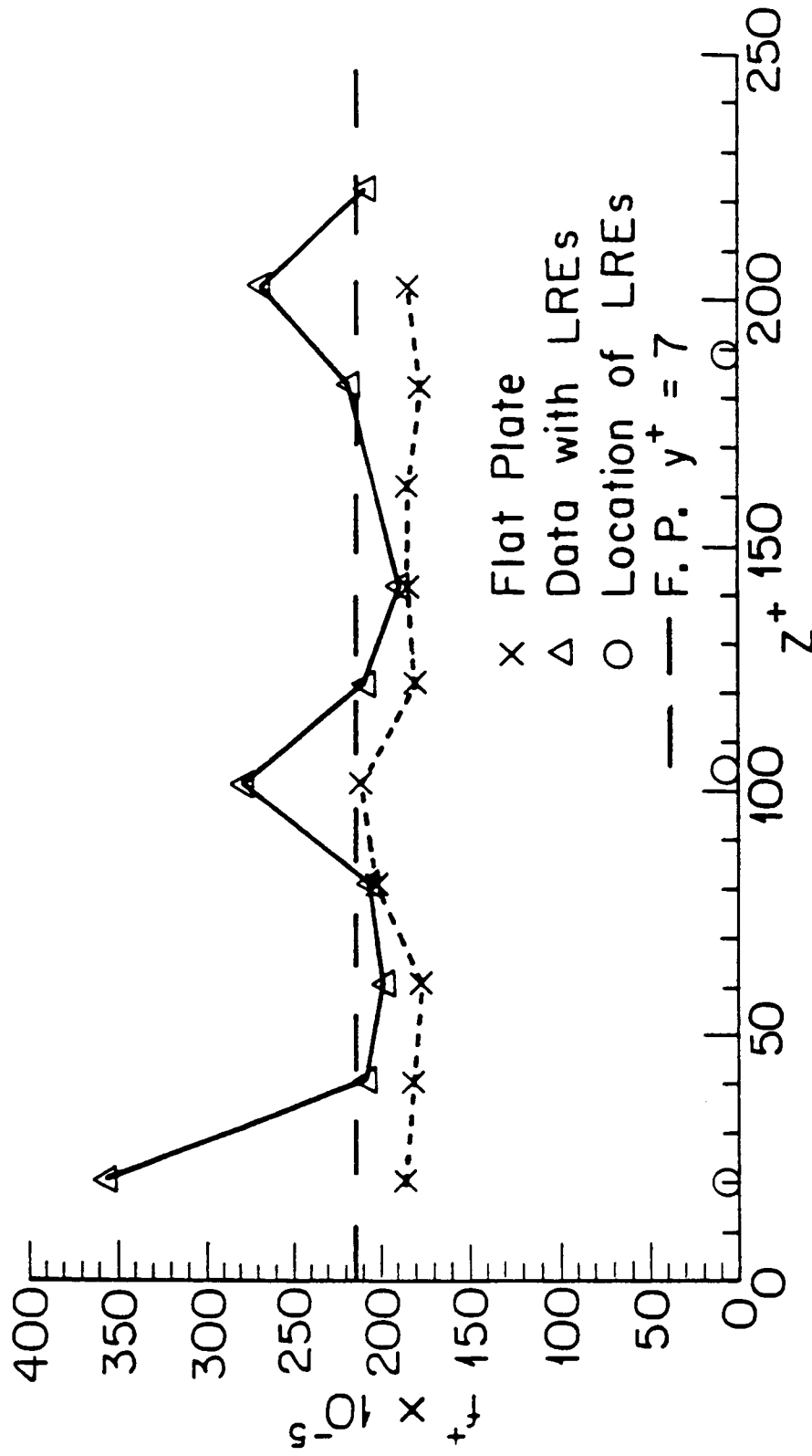


Figure 43 b. Bursting Frequency Across the Span (Local Reference;
 $y^+ = 12$).

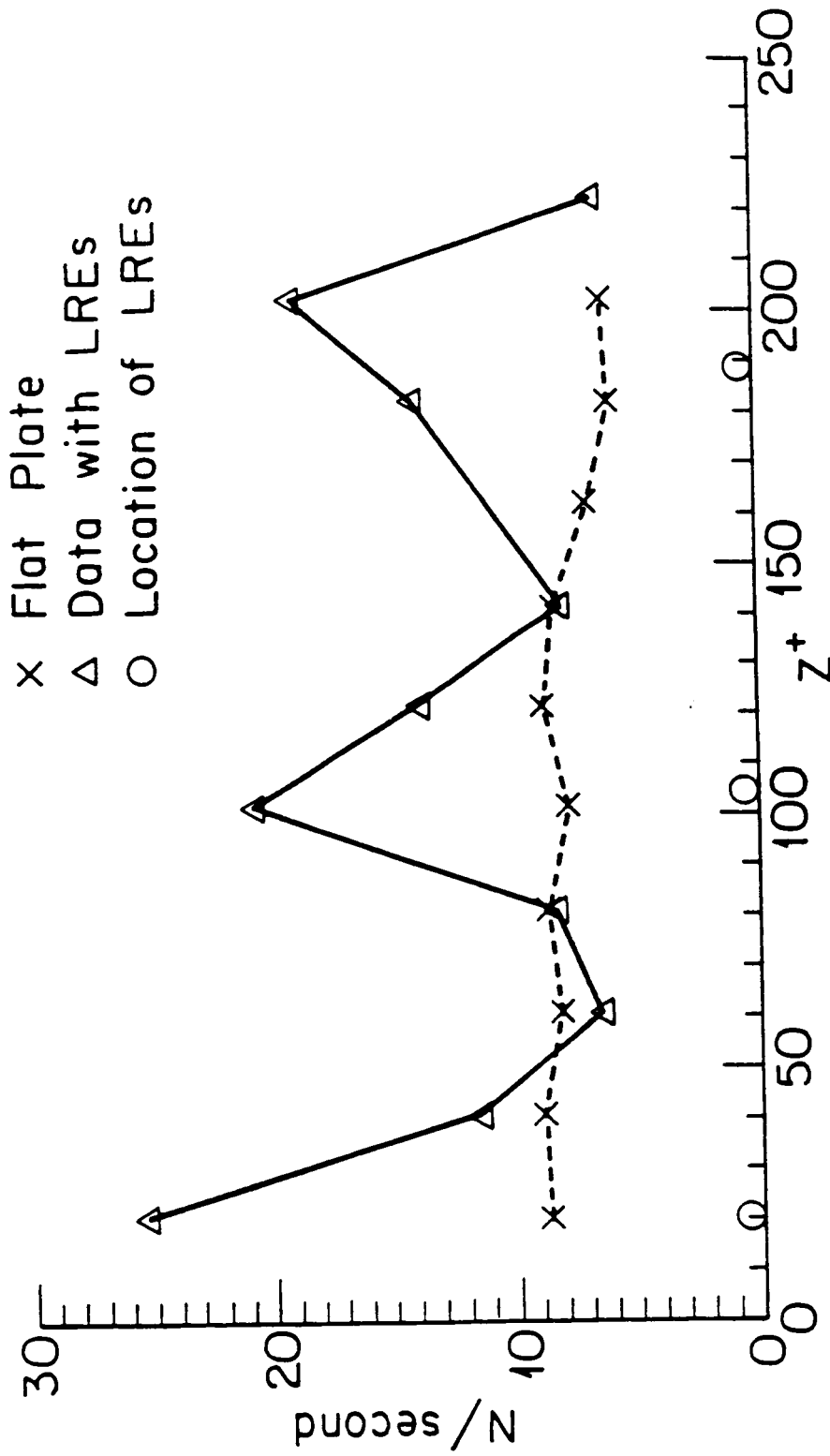


Figure 44 a. Number of LSS Seen per Second Across the Span (Flat Plate Reference; $y^+ = 12$).

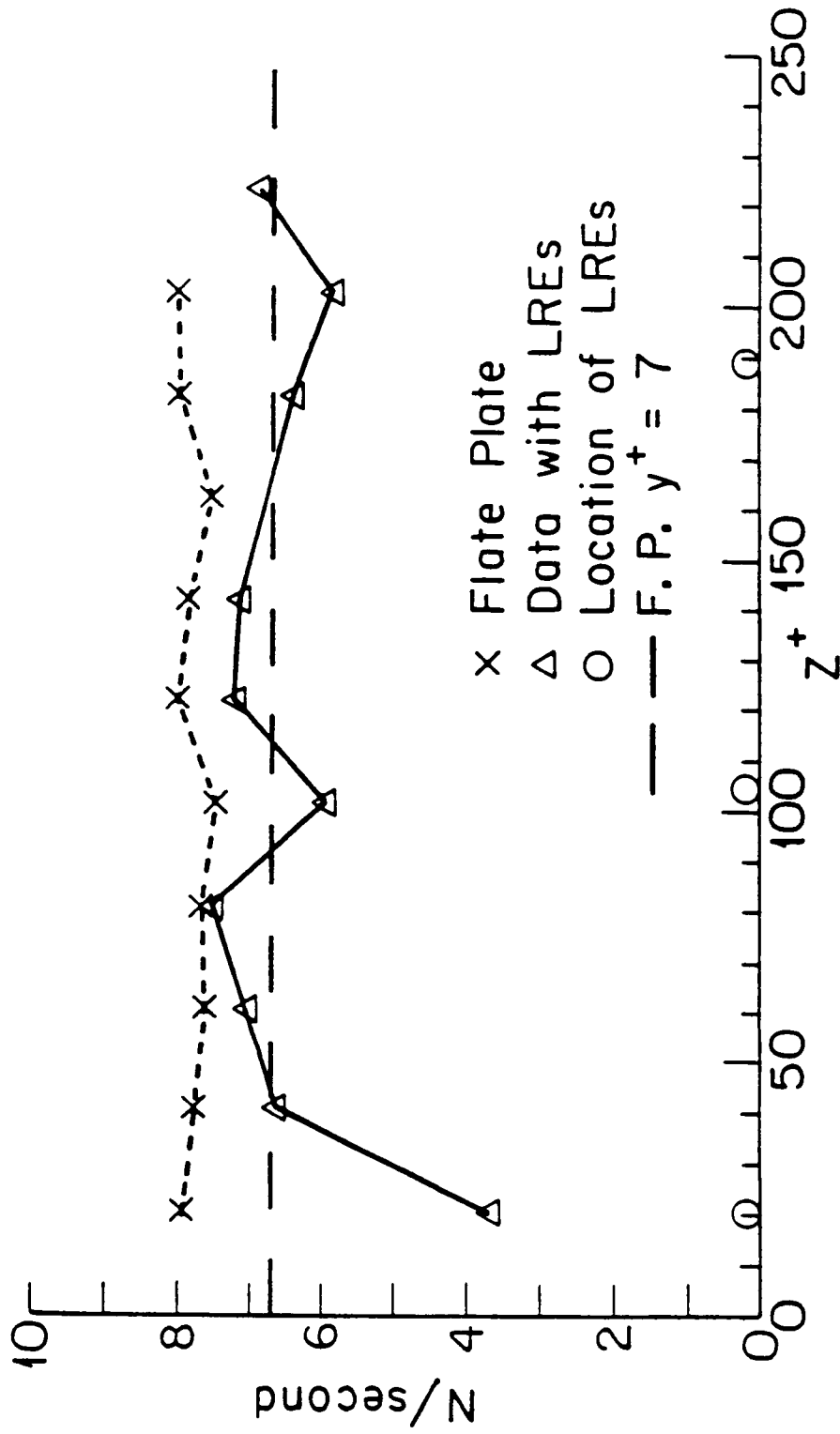


Figure 44 b. Number of LSS Seen per Second Across the Span (Local Reference; $y^+ = 12$).

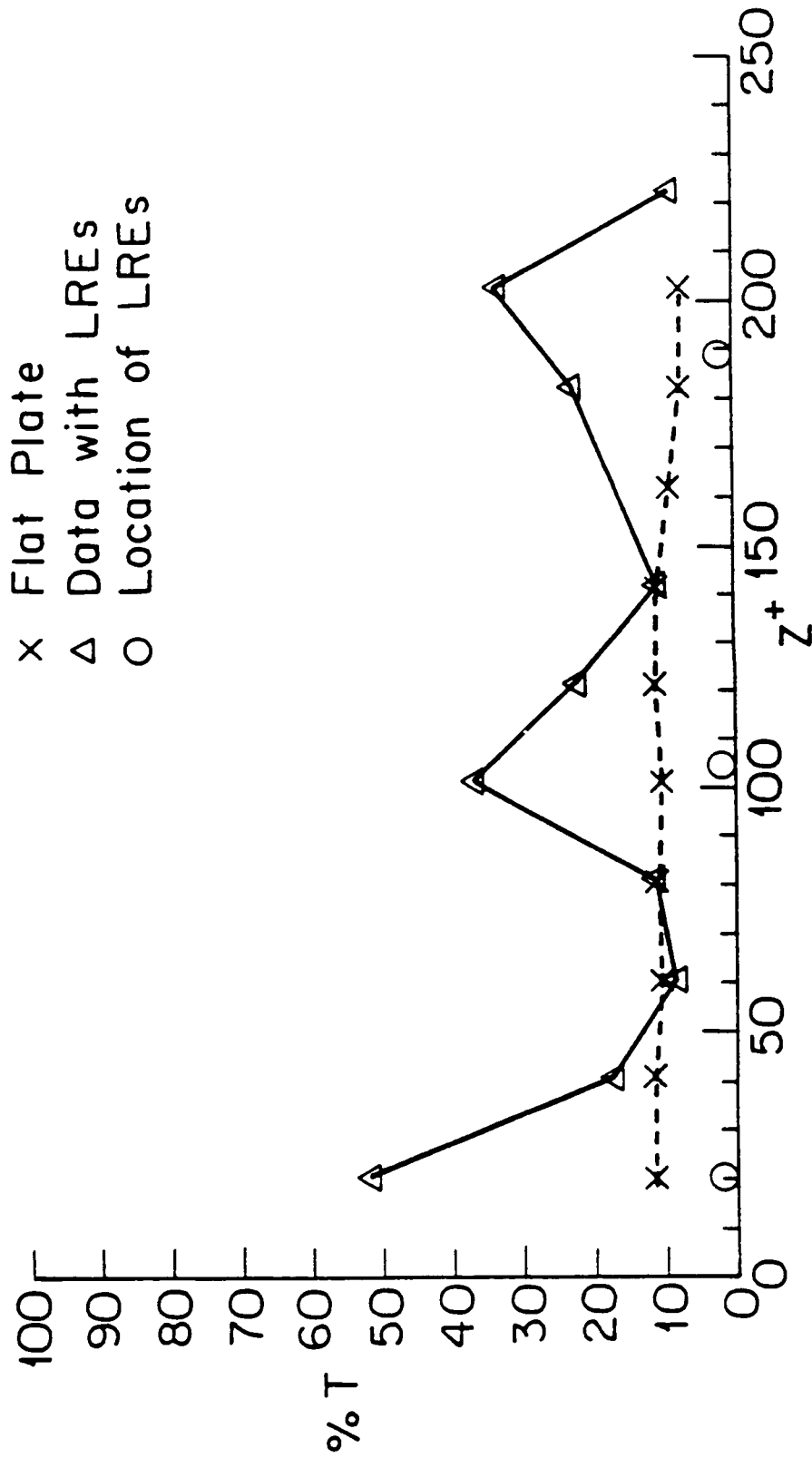


Figure 45 a. Percent of Time in an LSS Across the Span (Flat Plate Reference;
 $y^+ = 12$).

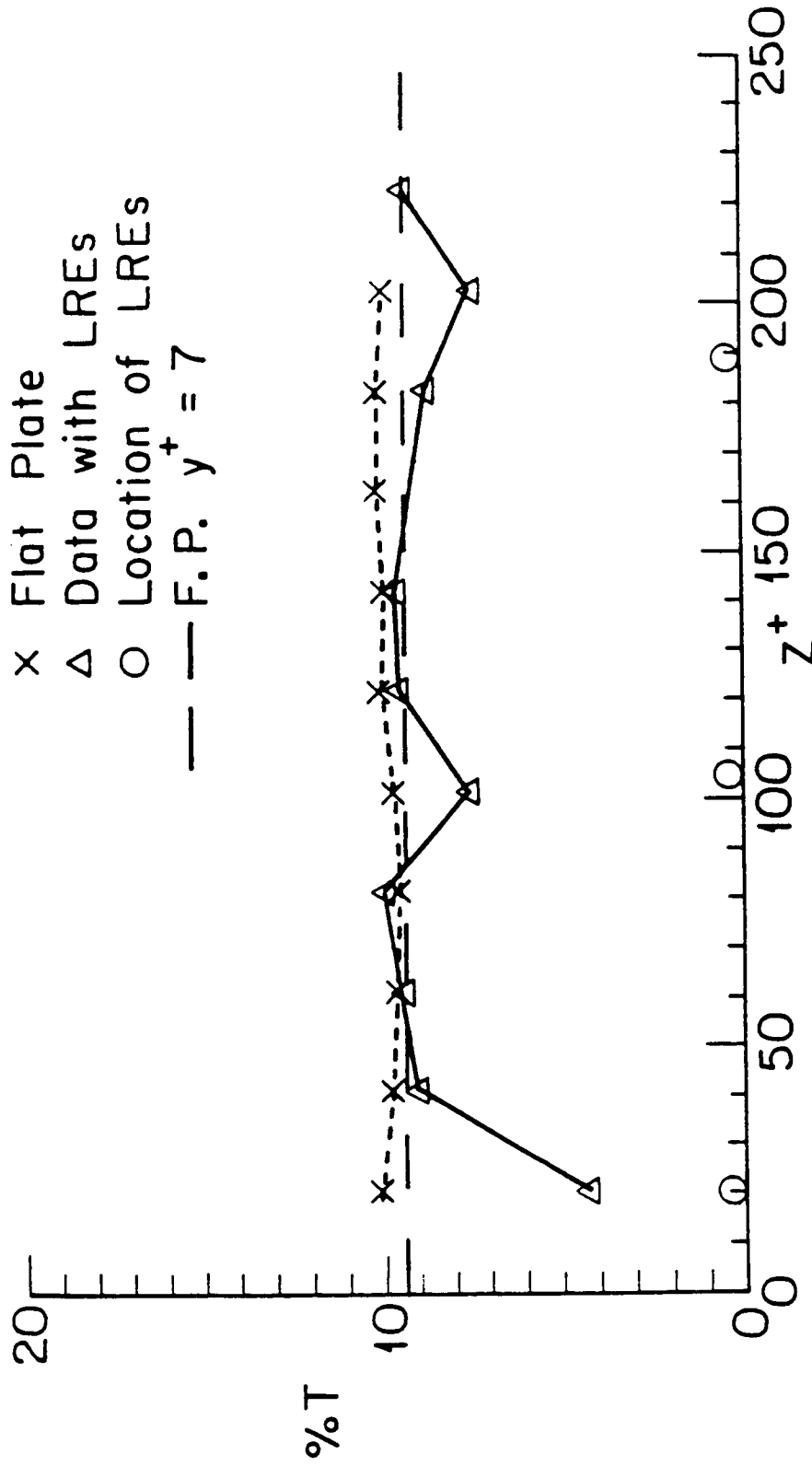


Figure 45 b. Percent of Time in an LSS Across the Span (Local Reference;
 $y^+ = 12$).

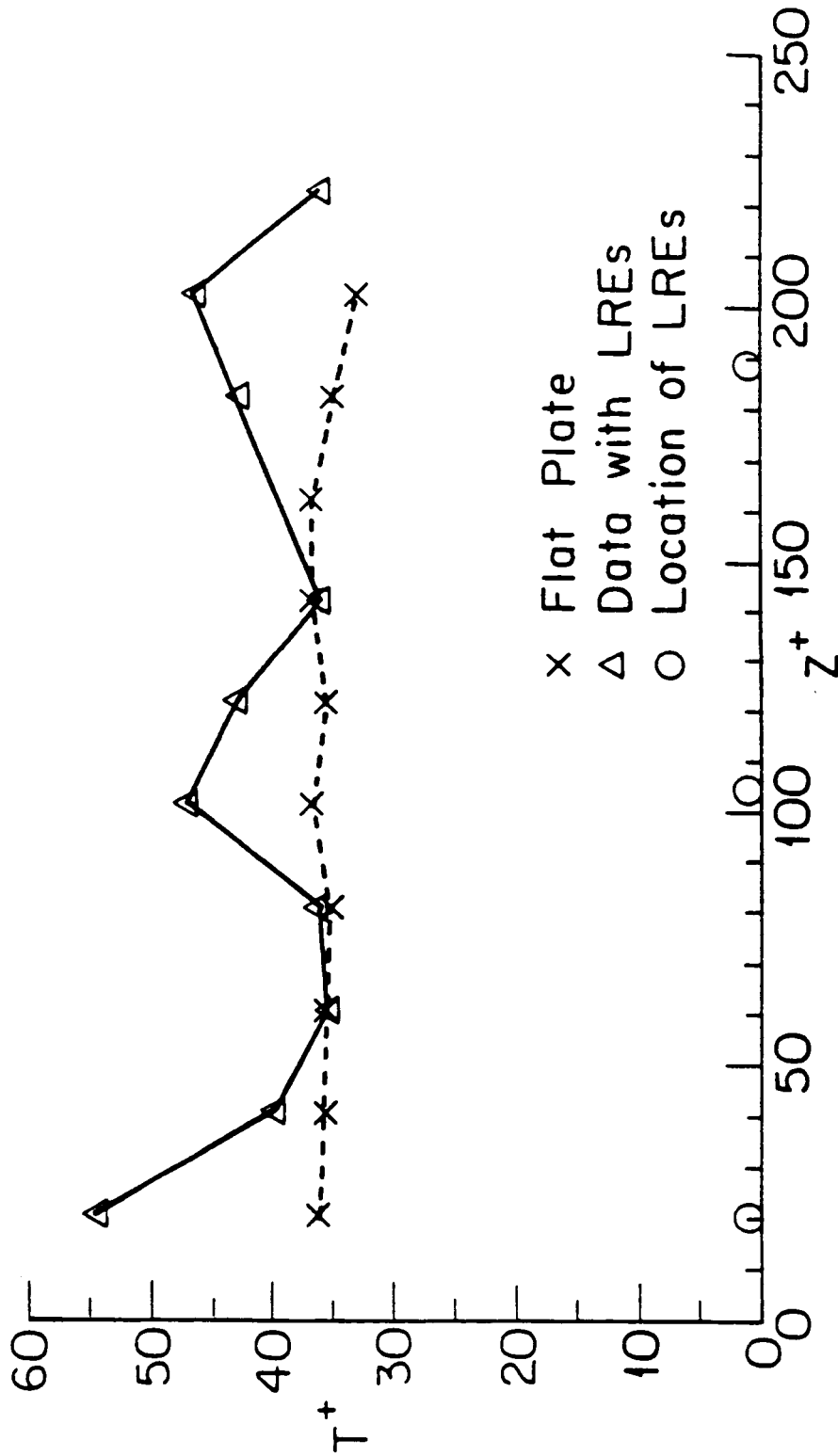


Figure 46 a. Average Time of Passage of an LSS Across the Span (Flat Plate Reference; $y^+ = 12$).

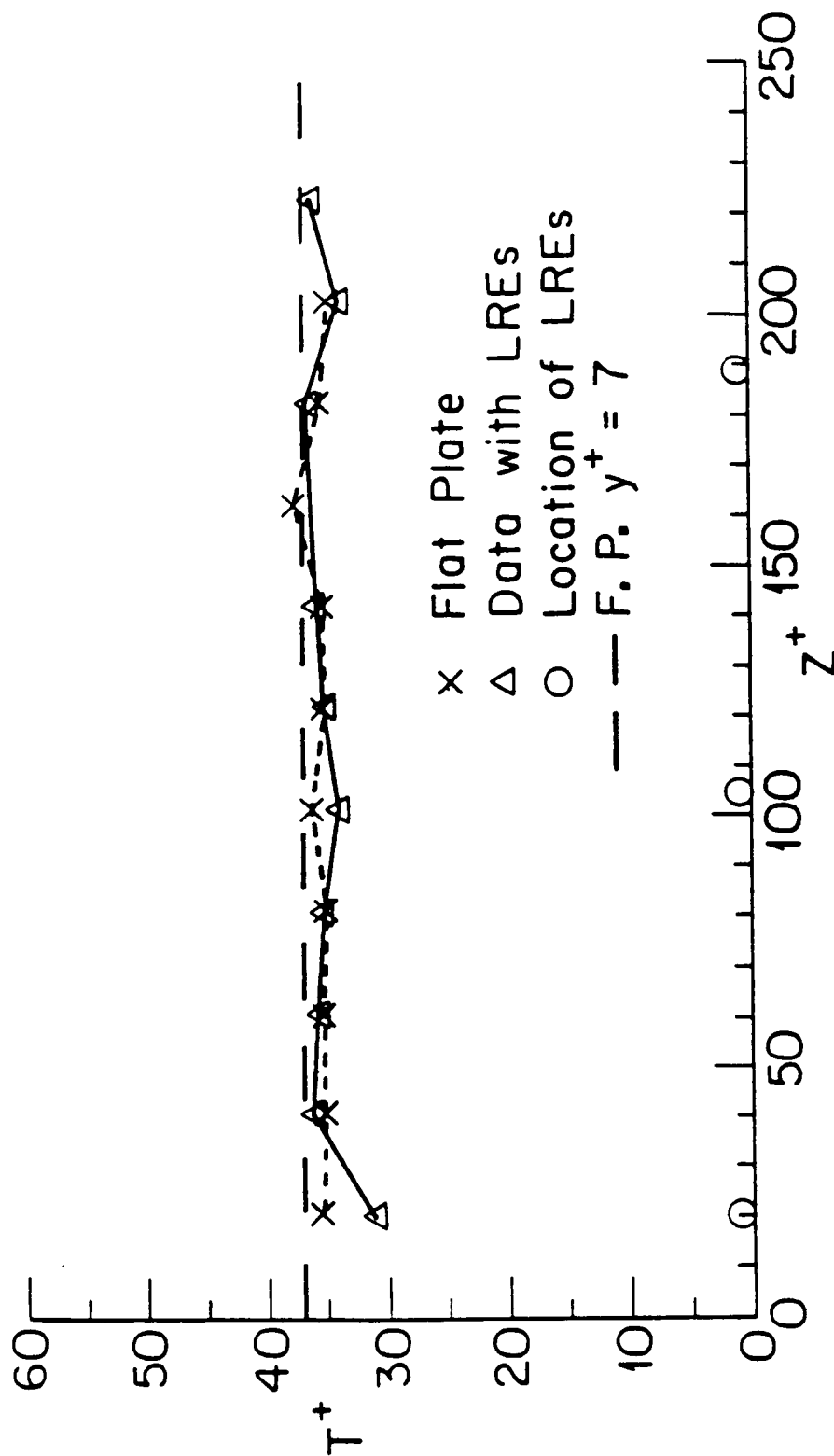


Figure 46 b. Average Time of Passage of an LSS Across the Span (Local Reference; $y^+ = 12$).

reference, Figure 44b shows a lower number of streaks seen per second over the LREs. Again, the values between the LREs are comparable to the flat plate data.

Figure 45a (flat plate reference) and Figure 45b (local reference) represent the percentage of time a hot-wire is inside of an LSS during the data run. The LREs impose a lower mean velocity, hence generate the appearance of additional low-speed streaks when referenced to the flat plate. Between the strings, a sensor spends the same percentage of time in an LSS as a sensor over a clean plate. For the local reference conditions, the velocity fluctuations over an LRE exceed the threshold less frequently. Correspondingly, Figure 45b shows a smaller percentage of time spent inside an LSS for the sensors directly over LREs.

Figures 46a and 46b show the average time of passage of an LSS over the sensors. This information could be converted into the average lengths of the LSS using Taylor's hypothesis, but the appropriate value of the convection velocity is unclear. The same trends due to the elevated no-slip condition are seen over the LREs. And again the values between the LREs are comparable with the clean flat plate values. A low-speed streak is in general oriented at some small angle in the x - z plane with respect to the freestream direction. If the LSS was actually locked onto the LREs, then this angle should decrease, and the streaks seen by the hot wires would appear "longer". In Figure 46b, all of the data lie within the scatter and no lengthening trend is apparent.

The dashed line in Figures 43b, 44b, 45b, and 46b that represents flat plate data for $y^+ = 7$ usually appears closer to the values over the LREs than any of the other data points. The exception is Figure 46b where the scatter prohibits any conclusions. Thus a crude first approximation would be to say that the LREs simply elevate the no-slip condition locally, and could be modeled by the normal flat plate statistics being raised by the diameter of the LREs.

Data were also obtained at other values of y^+ , but are not shown. At $y^+ = 18$ the data show a complete relaxation back to a clean flat plate, i.e. the sensors do not detect any change in the statistics due to the LREs. Any tendency for an LSS to be aligned with a particular LRE is apparently destroyed by the spanwise velocity fluctuations by the time the LSS extends out to this altitude.

10.2 SUCTION IN A TURBULENT BOUNDARY LAYER

Experiments were conducted using the LREs together with suction/injection through discrete holes located just downstream of the longitudinal roughness elements. The holes were 1.6 mm in diameter ($22\nu/u_\tau$). A single hole was located 6 mm ($87\nu/u_\tau$) behind each of the fish lines (diameter = $5\nu/u_\tau$, length = $17,000\nu/u_\tau$, and spanwise wavelength = $80\nu/u_\tau$). The freestream velocity in the tunnel was 500 cm/s and, at the measurement station, a fully-developed turbulent boundary layer existed with a nominal friction speed of 20.6 cm/s.

In order to test the effects of selective transpiration on the turbulent quantities, suction from the holes was applied in the present and in the absence of the fish lines. Additional reference runs were obtained with and without the longitudinal roughness elements. In addition, blowing through the holes was also tried. The continuous suction/blowing speed through each hole was 75 cm/s ($0.15U_\infty$), which is rather low considering the small area of each hole.

A single hot-wire probe was used to measure the instantaneous streamwise velocity component. The probe was located at $10\nu/u_\tau$ above the wall. The streamwise distance between the hot-wire probe and the transpiration hole was either $140\nu/u_\tau$ or $350\nu/u_\tau$. The raw signal was used to compute the local mean speed, the local rms velocity, and the nondimensional bursting frequency $f^+ = f\nu/u_\tau^2$. The bursting events were detected using the VITA technique and the reference plate's u_τ was used for threshold as well as for normalizing the bursting frequency. The results are summarized in Table 1. From this data we note the following:

1. Run #1-3 are repeat runs, and the repeatability of measuring mean velocity, turbulence level and bursting frequency is within 2%, 1% and 2.4%, respectively.
2. Comparison between Run #4 and the average of Run #1-3 reveals that, with no strings on the plate, suction increases the mean velocity by 40%, decreases the turbulence level by 30%, and increases the non-dimensional bursting frequency by 15%.

Table 1: Data Summary

Run #	Suction/Blowing	LRE's Yes/NO	Probe Location		\bar{U} (cm/s)	u_{rms} (cm/s)	$\frac{u_{rms}}{\bar{U}}$ %	f^+
			Δx^+	y^+				
1	None	No	140	10	168.36	51.52	30.6	0.00170
2	None	No	140	10	168.21	51.29	30.5	0.00171
3	None	No	140	10	171.85	52.13	30.3	0.00167
Average of Run Number 1-3	None	No	140	10	169.47	51.65	30.5	0.00169
4	Suction	No	140	10	235.26	49.74	21.1	0.00195
5	Blowing	No	140	10	162.45	48.88	30.1	0.00409
6	None	Yes	140	10	163.52	51.58	31.5	0.00149
7	Suction	Yes	140	10	226.71	48.63	21.5	0.00195
8	None	No	350	10	161.01	51.93	32.3	0.00139
9	Suction	No	350	10	195.56	50.81	26.0	0.00162

3. Comparison between Run #5 and the average of Run #1-3 reveals that, with no strings on the plate, blowing decreases the mean velocity by 4%, decreases the turbulence level by 1% (not significant), and increases the bursting frequency by 142%.
4. Comparison between Run #6 and the average of Run #1-3 reveals that the placement of the fish lines decreases the mean velocity by 4%, increases the turbulence level by 3%, and decreases the bursting frequency by 12%.
5. Comparison between Run #7 and Run #6 reveals that, with the strings in place, suction increases the mean velocity by 39%, decreases the turbulence level by 32%, and increases the bursting frequency by 31%.

Suction was also applied through a perforated stainless steel specimen instead of the (larger) discrete holes that we used above. The porous surface insert is a square piece 75 x 75 mm in size, and is kept in place with flush-mounted screws. The width and length of the active suction strips are controlled by blocking the undesired portions. After realigning the flat plate at a slight angle to allow for the displacement effects, the streamwise and spanwise pressure gradients were rechecked and were found to have the satisfactory values:

$$\frac{\partial C_p}{\partial x} \cong -6.9 \times 10^{-4} \quad \text{cm}^{-1} ,$$

$$\frac{\partial C_p}{\partial z} \cong -2.0 \times 10^{-4} \quad \text{cm}^{-1} .$$

A comparison of three cases is instructive and is reported in here. First, a 25 x 25 mm square area of the porous surface is exposed but the suction pump is not activated. Secondly, the porous surface is completely blocked with masking tape. Thirdly, the same 25 x 25 mm exposed

area and a peristaltic pump is used to achieve a suction coefficient of $C_q = 0.0018$. Hot-wire probes were used to measure the streamwise velocity component. Figures 47-49 depict the mean velocity profiles when the probe is centered over the porous surface, 1 cm downstream of the end of the screen, and 5 cm downstream, respectively. The three cases mentioned above are denoted by the circles (the stars in Figure 48 are for a repeat run), the pluses, and the triangles, respectively. None of the boundary layer parameters, such as momentum thickness, displacement thickness, or friction velocity (as determined from a Coles' fit of the log-region), changed significantly for any of the cases.

The profiles for the root-mean-square velocity do, however, have significant differences especially below $y^+ = 20$. This is shown in Figures 50-52, for the same runs in the earlier figures. Again, the circles are for an exposed porous surface but an idle pump (the stars in Figure 51 are for a repeat run), the pluses are for a blocked screen, and the triangles are for a 25 x 25 mm exposed area of the porous surface and an activated peristaltic pump to achieve a suction coefficient of $C_q = 0.0018$. In Figure 50, the probe is centered over the suction screen. In Figure 51, the hot-wire is 1 cm downstream of the porous strip, and in Figure 52 the profiles are taken 5 cm downstream.

A spanwise rake of 12 hot-wires at $y^+ = 7$ centered over the porous surface was used to obtain the spanwise profiles of mean velocity, rms velocity, and bursting frequency. This is shown in Figures 53-55 respectively, for the case of $C_q = 0.0018$ (triangles). No surprises from the mean or rms plots, just that the suction seems uniform. The bursting frequency tends to be lower with suction.

Centered over suction screen

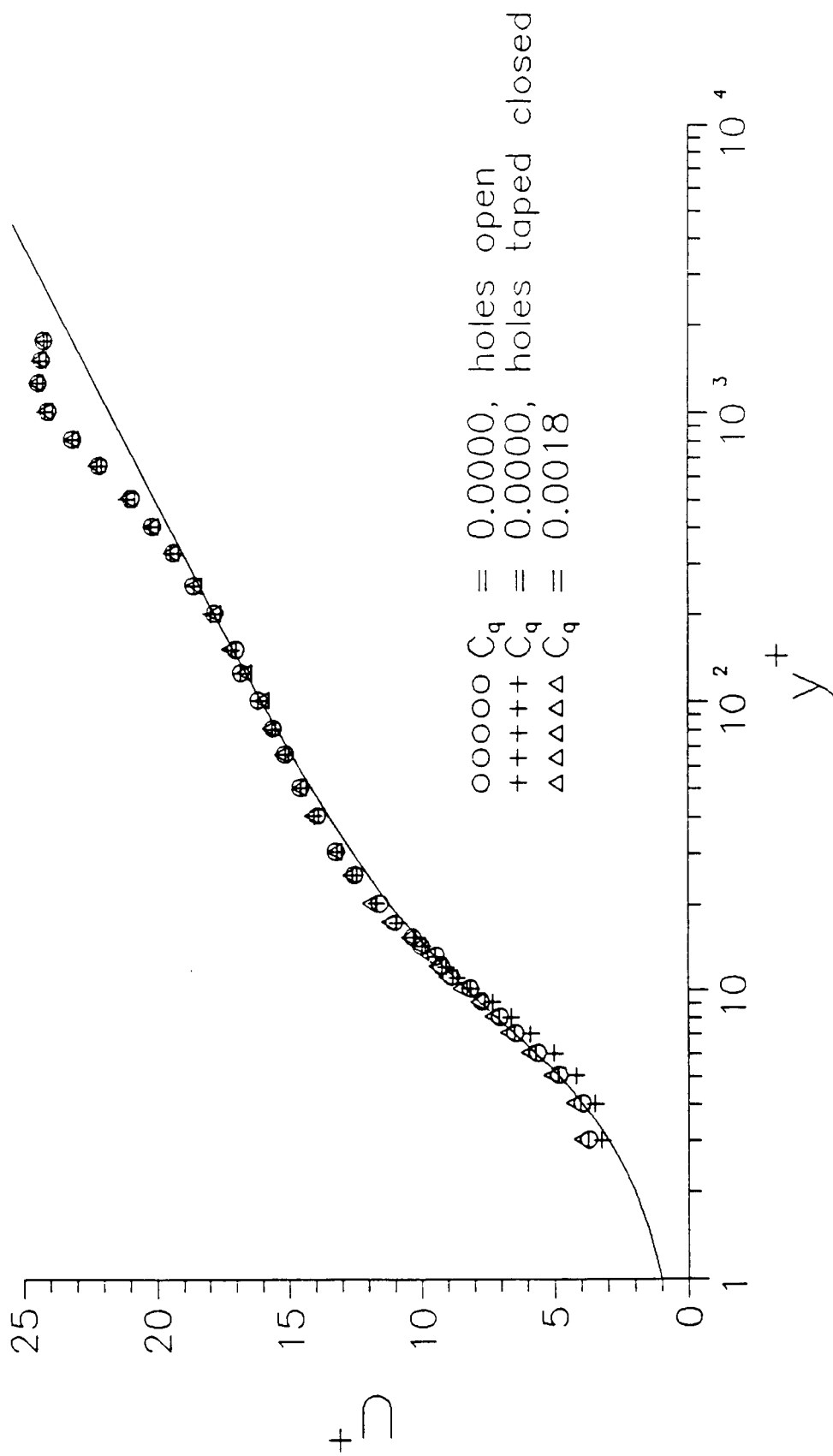


Figure 47. Normal Profiles of Mean Velocity.

1 cm downstream of suction screen

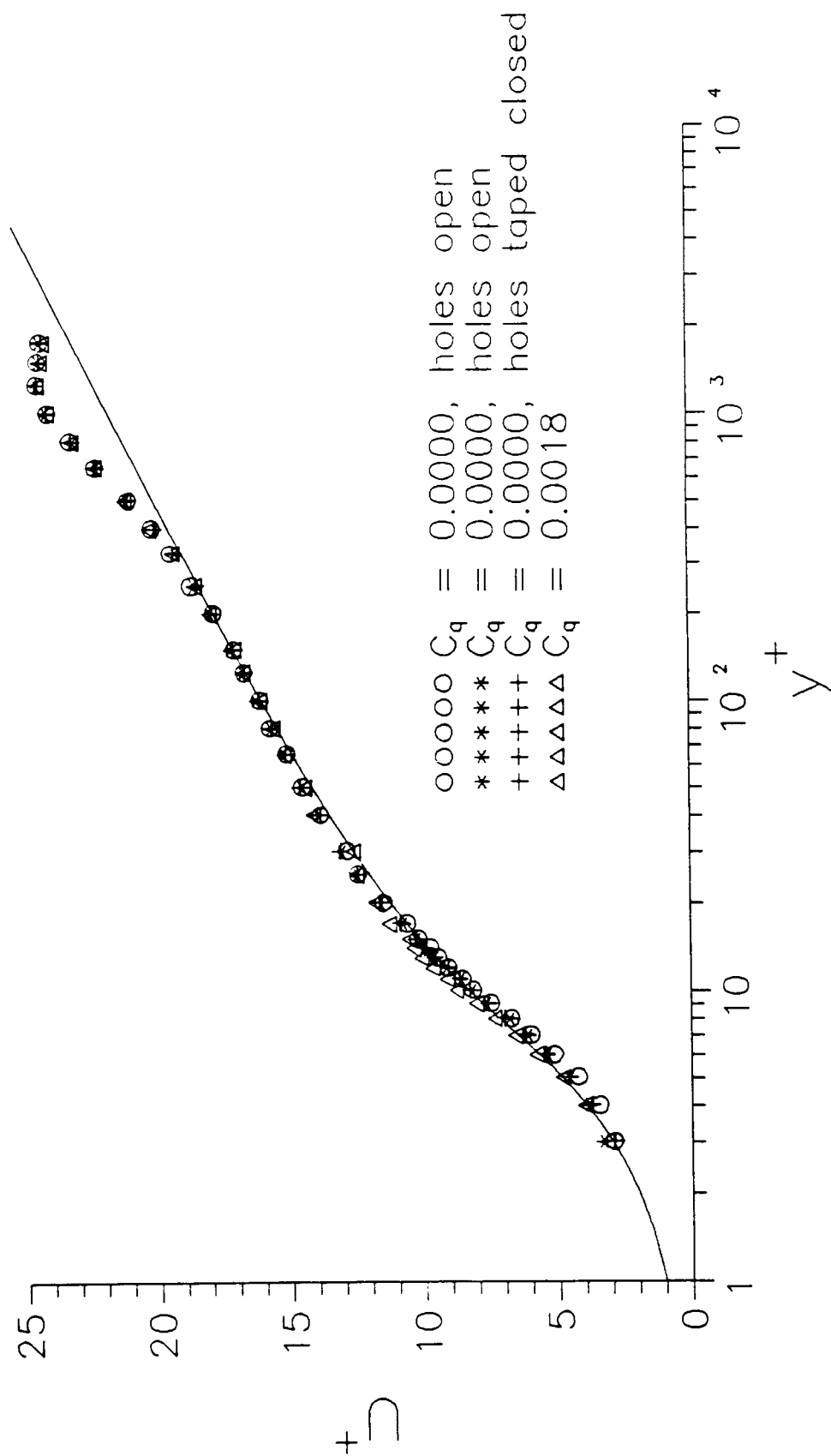


Figure 48. Normal Profiles of Mean Velocity.

5 cm downstream of suction screen

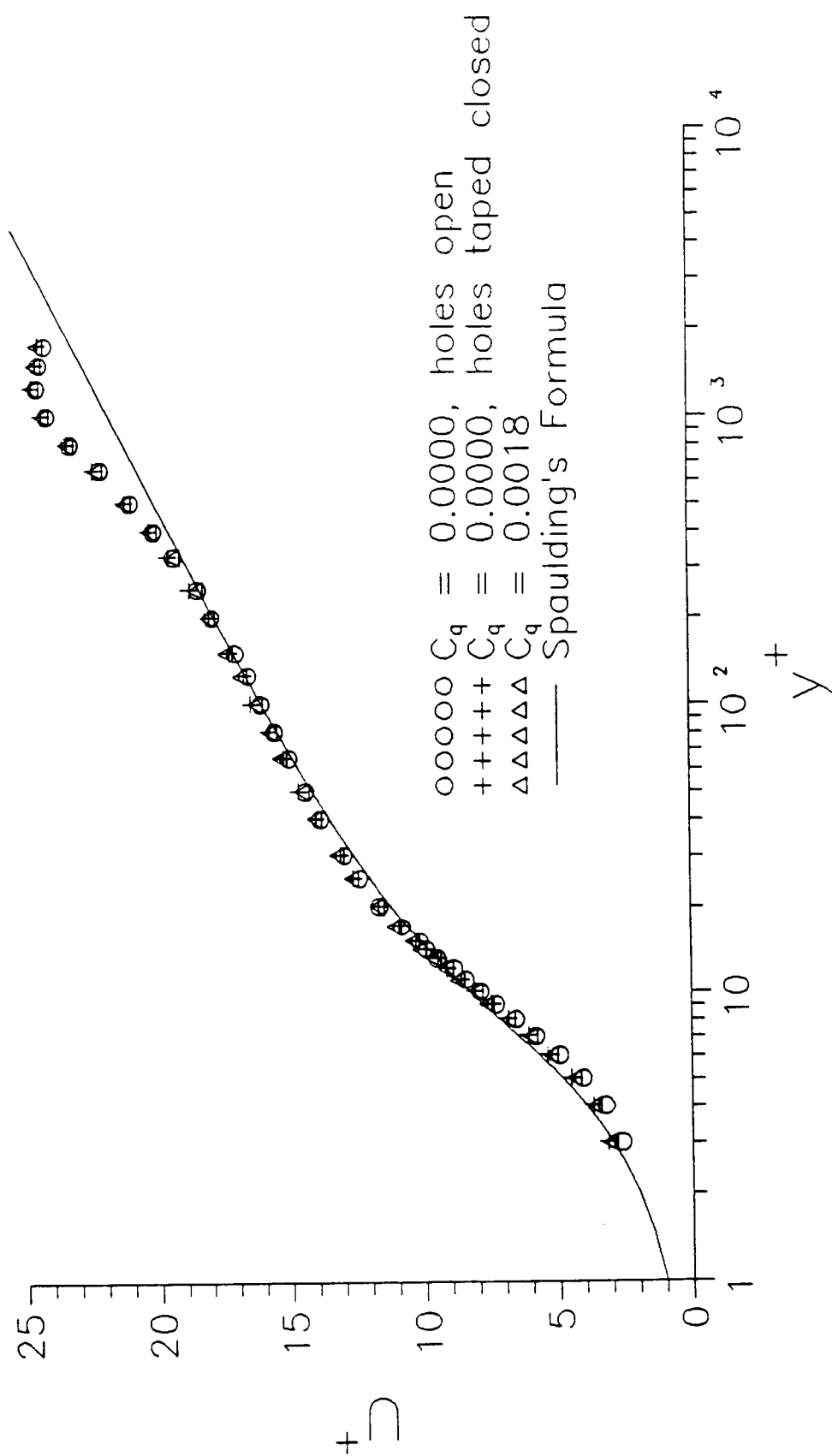


Figure 49. Normal Profiles of Mean Velocity.

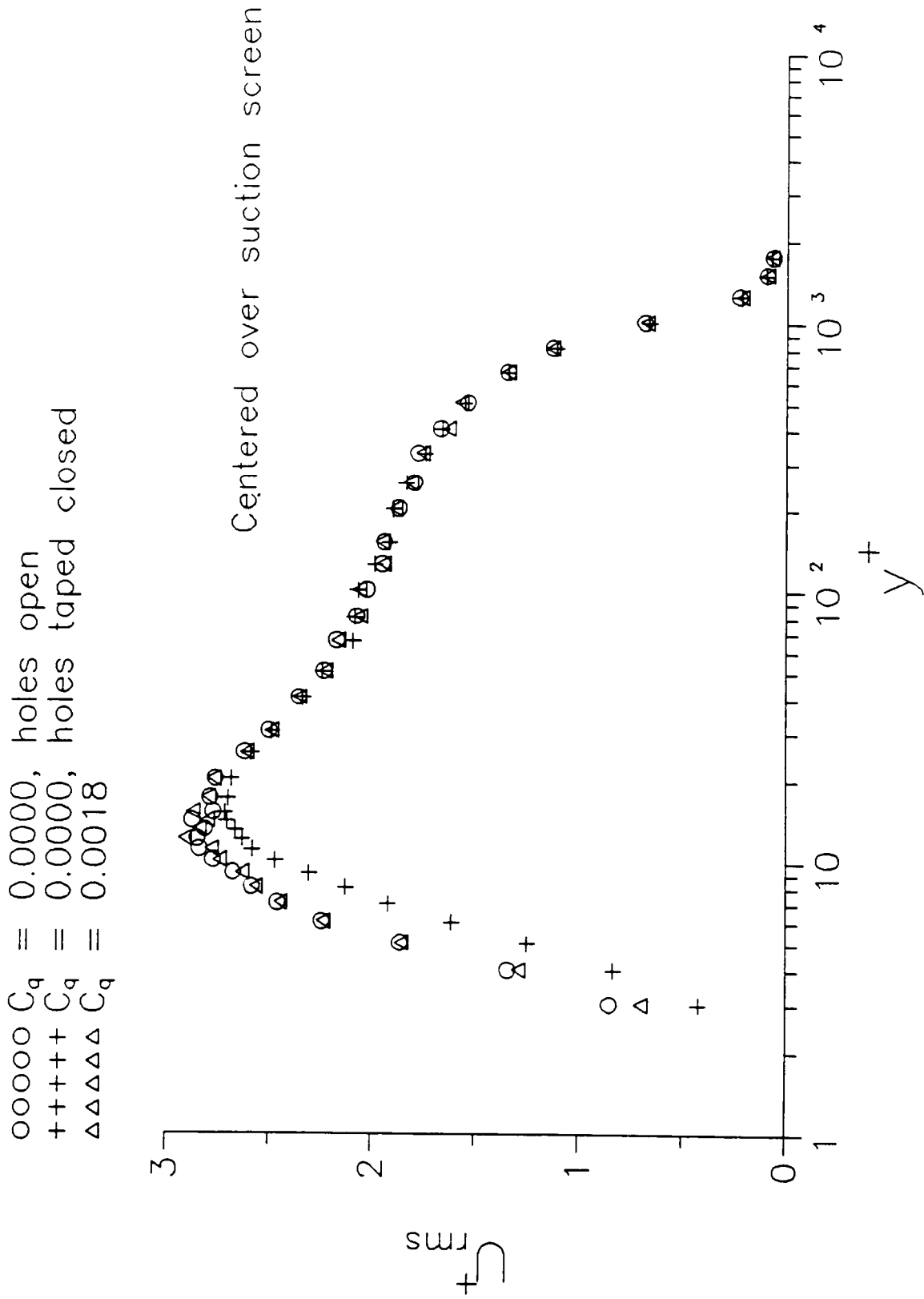


Figure 50. Normal Profiles of RMS Velocity.

$C_q = 0.0000$, holes open
 $C_q = 0.0000$, holes open
 $C_q = 0.0000$, holes taped closed
 $C_q = 0.0018$

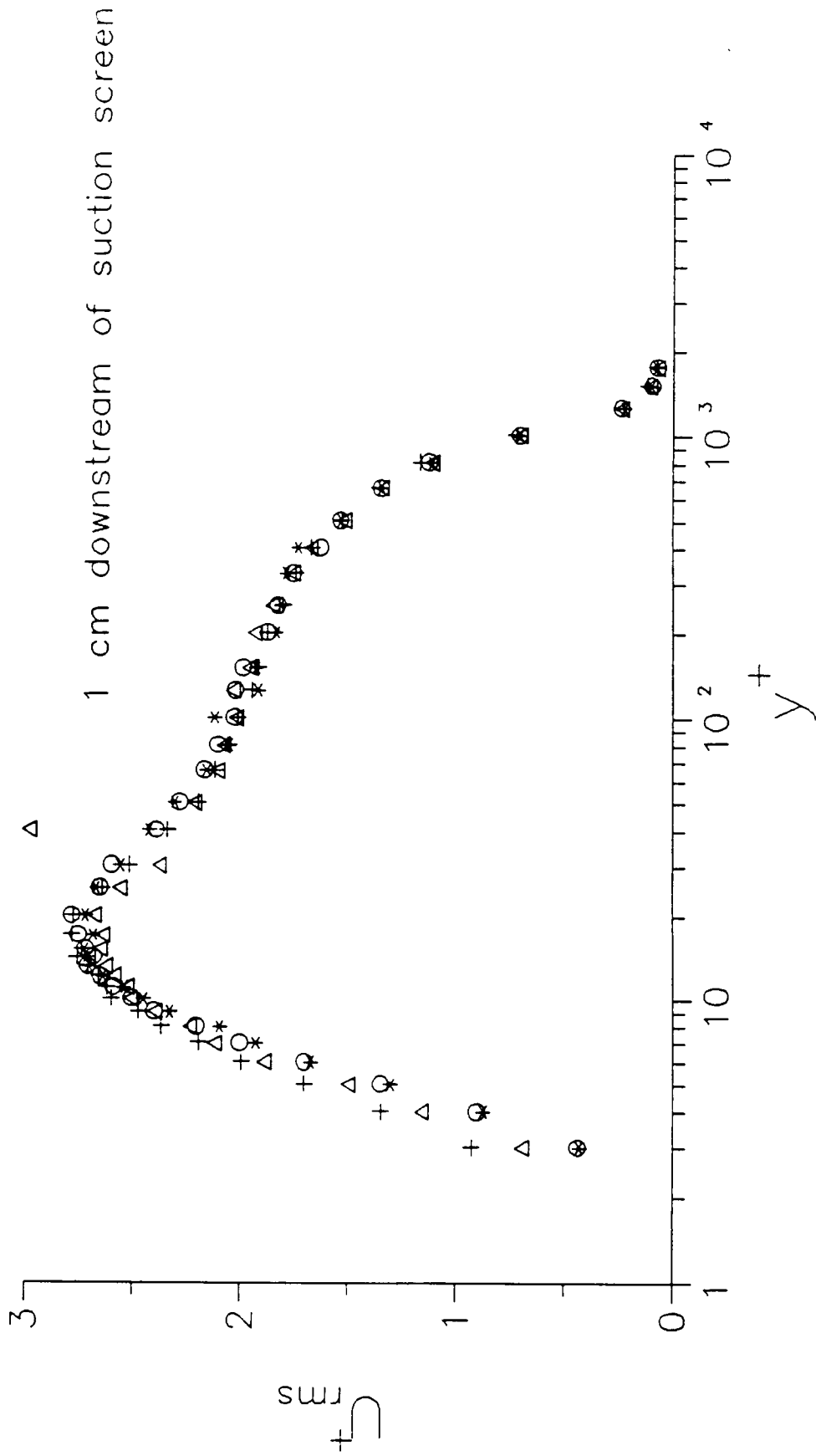


Figure 51. Normal Profiles of RMS Velocity.

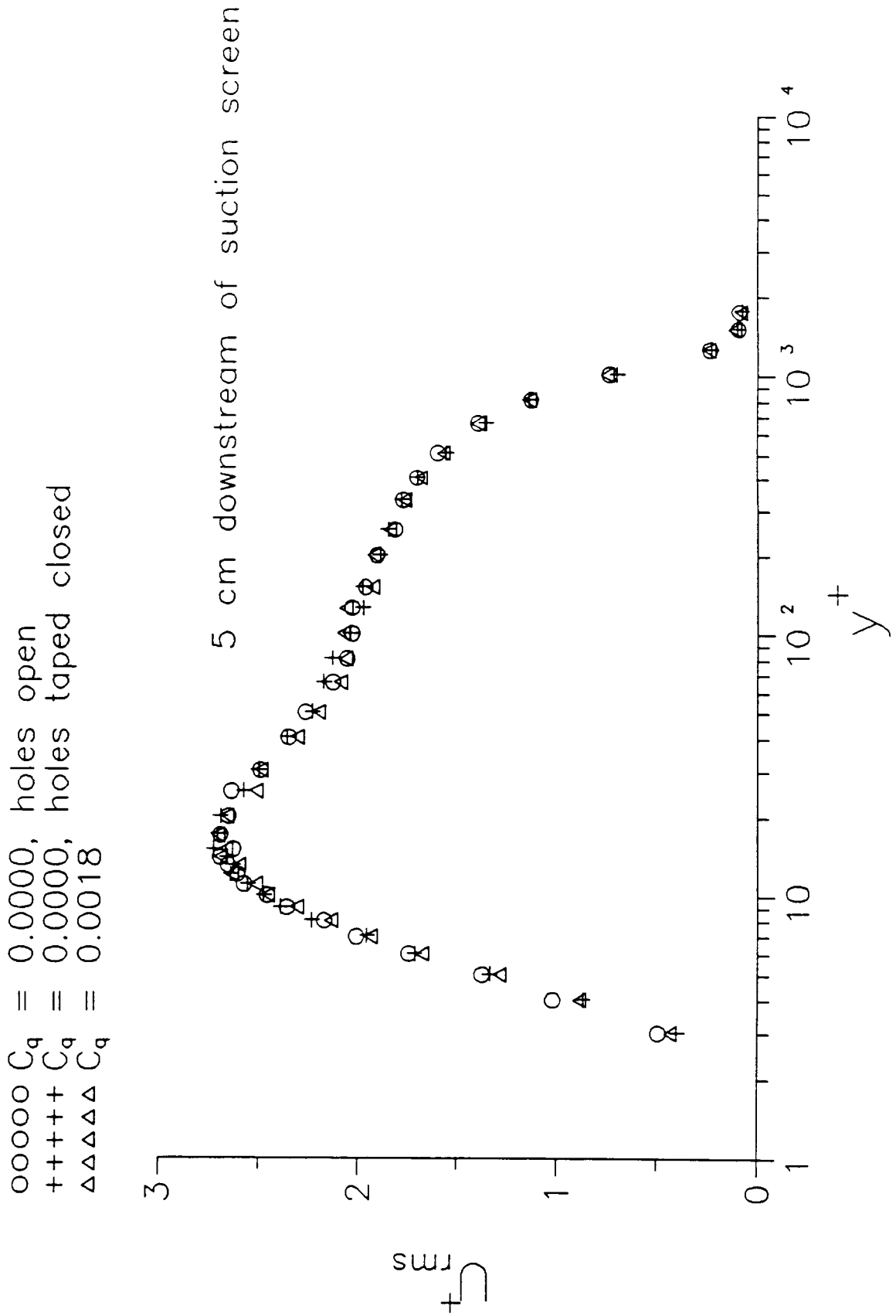


Figure 52. Normal Profiles of RMS Velocity.

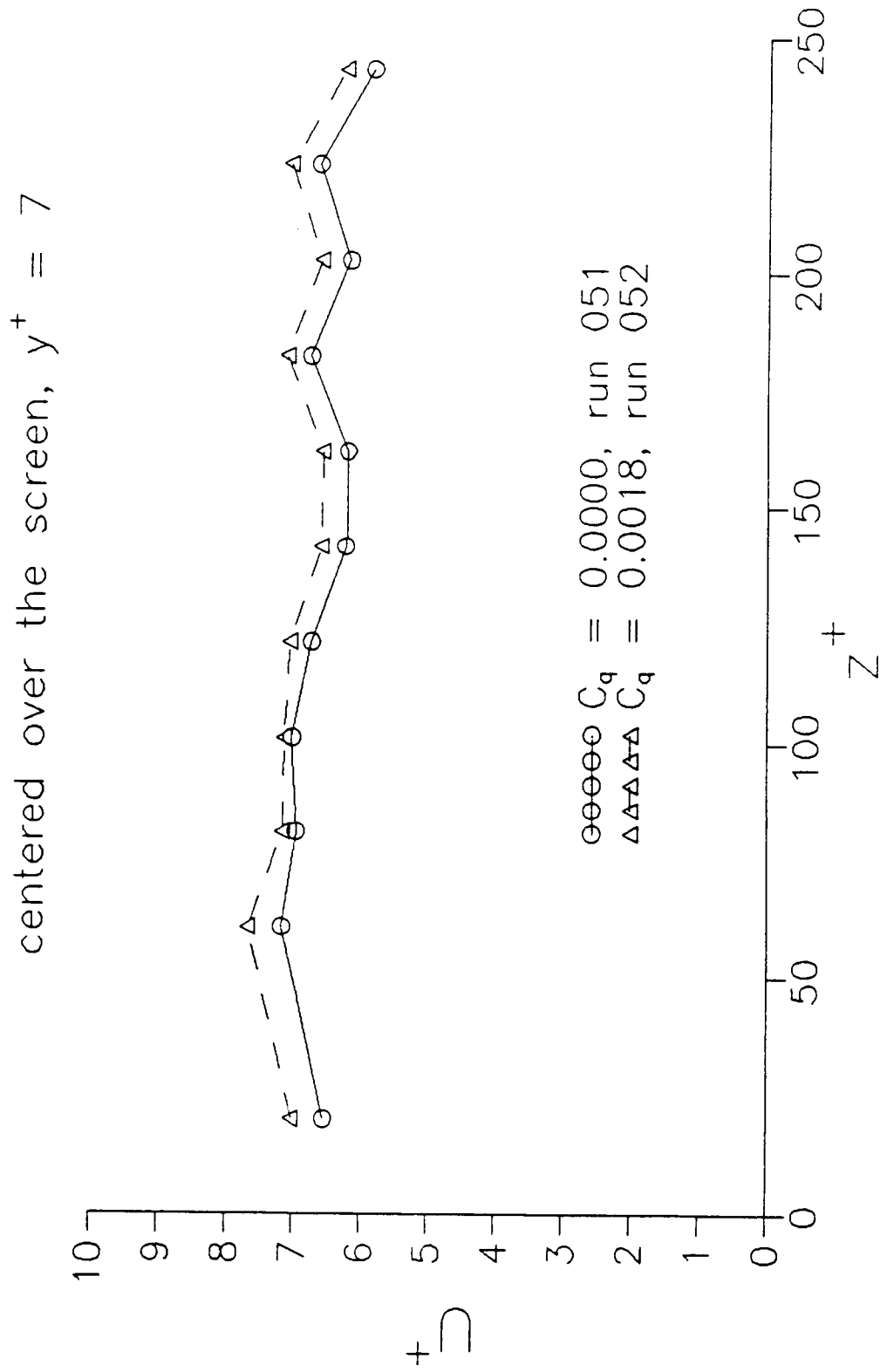


Figure 53. Spanwise Profiles of Mean Velocity.

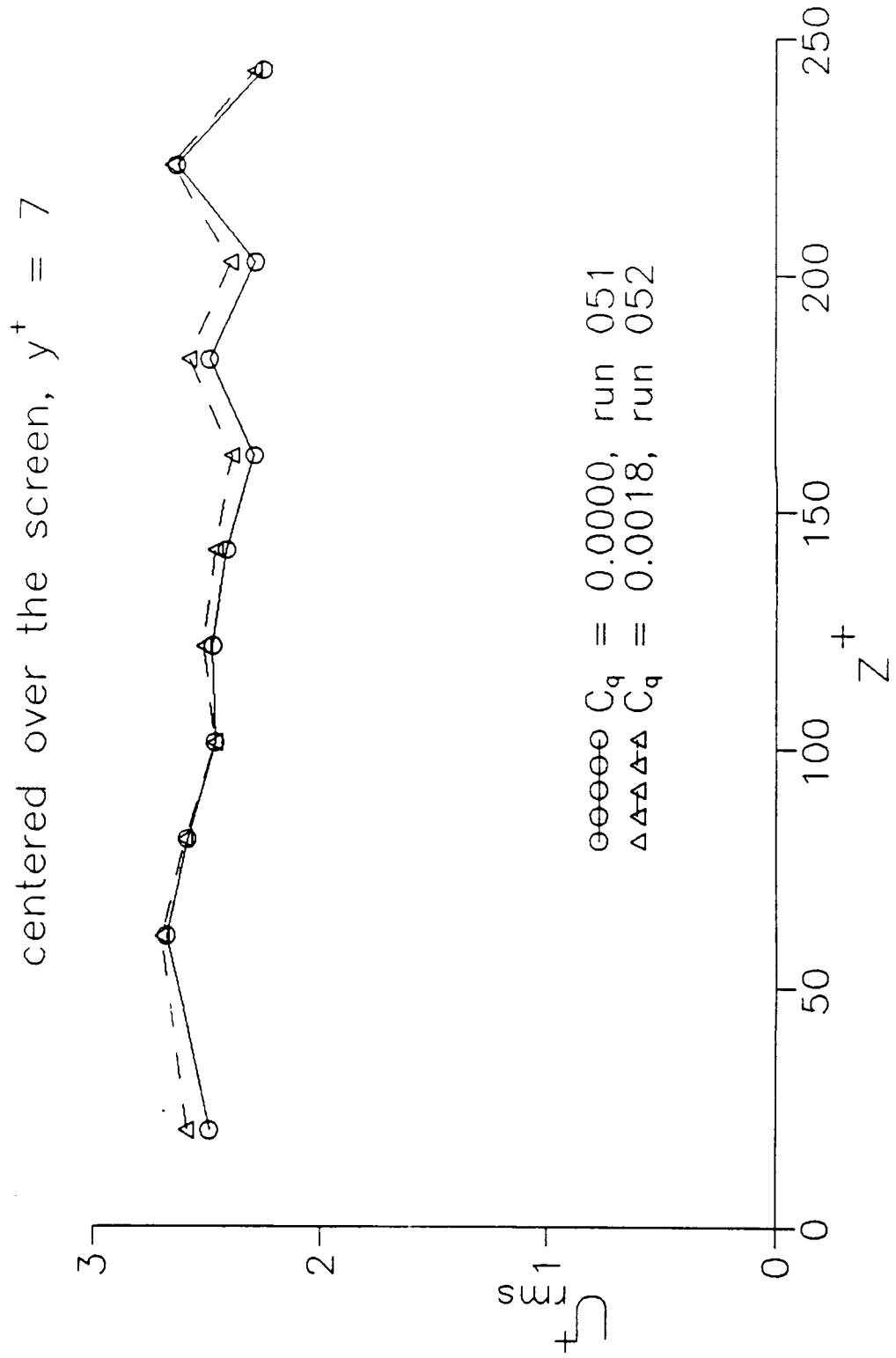


Figure 54. Spanwise Profiles of RMS Velocity.

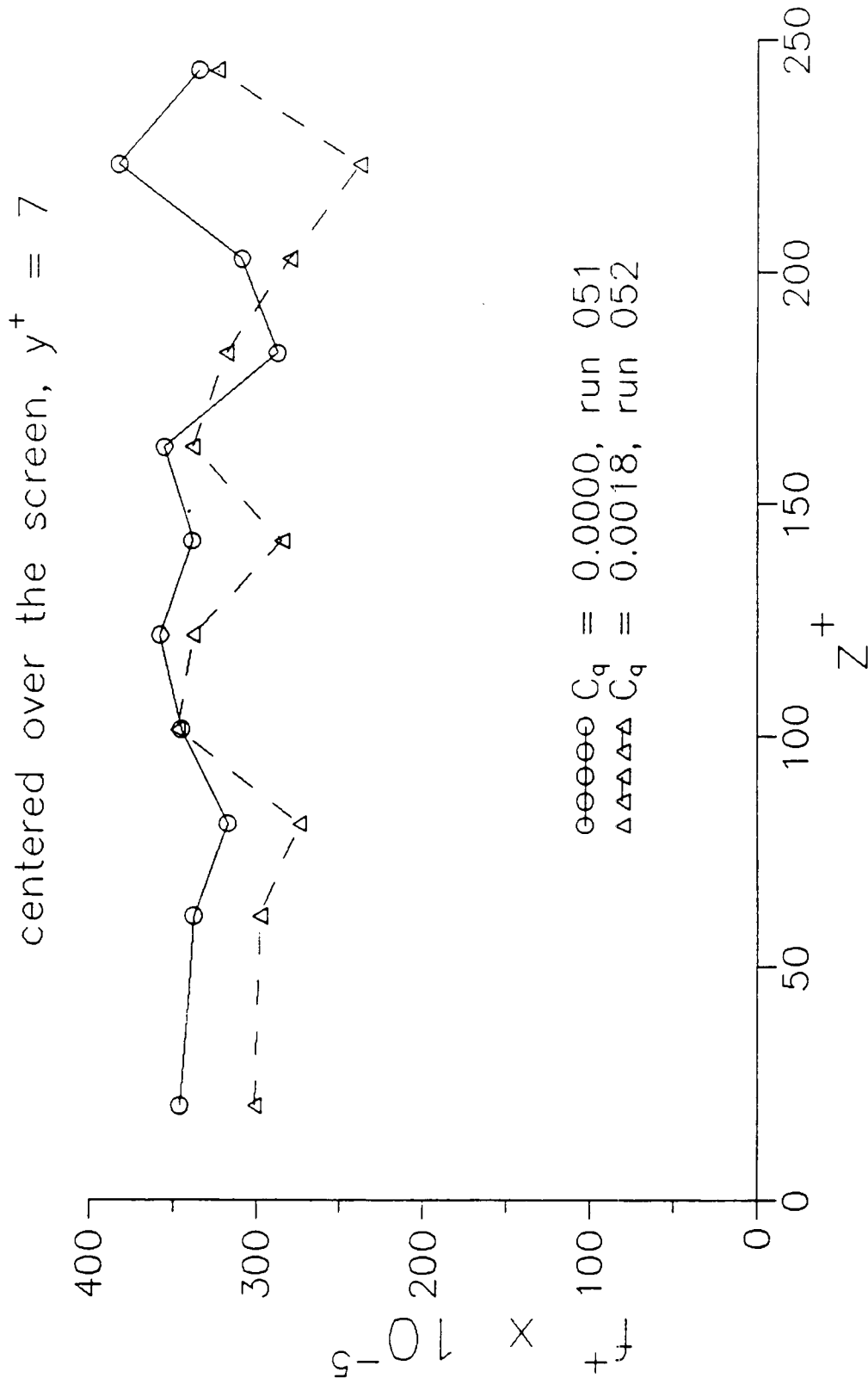


Figure 55. Spanwise Distribution of Bursting Frequency.

11. SUMMARY

The primary objective of the present research was to investigate experimentally the feasibility of substantially reducing the skin friction drag in a turbulent boundary layer using a novel technique. The innovation combines the beneficial effects of suction and a longitudinally ribbed surface. The selective suction technique requires minuscule energy expenditure and alleviates the need for using porous materials. During the first phase, artificial bursts were generated in laminar and turbulent boundary layers. Phase II research was divided into two tasks. In the first, conducted in a towing tank, suction from a single streamwise slot was used to eliminate artificially generated bursts. In the second task, conducted in a wind tunnel, the selective suction method was applied to eliminate natural bursts occurring in the presence of cylindrical longitudinal roughness elements. Velocity profiles and bursting statistics were measured.

During the first task of Phase II research, the feasibility of the innovation was determined by conducting a set of well-controlled experiments using a zero-pressure-gradient boundary layer that develops on a flat plate towed in an 18-meter water channel and a single streamwise suction slot to obliterate natural and artificial bursts. Selective suction from the slot was used to eliminate either a single burst-like event or a periodic train of artificially generated bursts in laminar and turbulent boundary layers that develop on a flat plate towed in a water channel. Flow visualization and hot-film probe measurements were used together with pattern recognition algorithms to demonstrate the feasibility of the concept. It is shown, under optimum conditions, that minute amount of fluid withdrawn continuously or impulsively from the streamwise suction slot is sufficient to eliminate natural and artificially generated bursts. Equivalent values of C_q as low as 0.0006 were sufficient to eliminate these bursts. As discussed in Sections 6.5 and 8.2, an even lower C_q is feasible if finite-length slots are used periodically in the streamwise direction. A factor of 2-3 reduction in the suction coefficient is perhaps attainable.

Introducing wall suction locally in a boundary layer is an extremely complex event even in a laminar flow and the present results shed some light on the accompanying phenomena. Weak impulsive suction from two spanwise holes results in the generation of a hairpin vortex. At high

suction rates, the vortex bursts, and at yet higher rates a turbulent spot is produced. Continuous suction from the two holes results in the generation of a periodic train of hairpin vortices but no bursting is observed. The frequency of detachment of these depends on the freestream speed to the power $3/2$.

Suction from the single streamwise slot results in the generation of two low-speed streaks. These streaks are stable for continuous suction or for weak impulsive suction. However, when the impulsive suction rate is increased, the two streaks converge and two new streaks are generated, eventually leading to the birth of a turbulent spot. The evolution of such a spot as determined from the present visualization results seems to confirm the vortex filaments model discussed by Perry et al. (1981).

The process of optimizing the suction from the streamwise slot to obliterate the bursts in a given boundary layer is quite tedious. Many parameters have to be varied simultaneously and large number of experiments are conducted. It seems to be worthwhile to develop a theoretical/numerical model of the present flow problem to conduct the necessary optimization using the numerical simulations before embarking on more experimental work.

The second task of Phase II research was conducted in a subsonic, low-turbulence, closed-return wind tunnel. The selective suction was applied to eliminate natural bursts occurring in the presence of cylindrical longitudinal roughness elements. Velocity profiles and bursting statistics were measured using hot-wire probes and the VITA and streak detection algorithms described in Section 6.8.

The visualization results of Johansen and Smith (1986) and the present work indicate that the LSS are focussed over the LREs for $y^+ < 10$. However the velocity measurements presented in figures 40 and 41 indicate that this result is due to the no-slip boundary condition over the LREs, and consequently one expects to see a lower velocity near the LREs.

The mean velocity profiles indicate that the average low speed fluid above the LREs extends outward to $y^+ \approx 15$, whereas the regions between the LREs showed very little effect on

the mean profile. The role of the spanwise velocity seems to be important in randomizing the LSS. That is, even though the LSS are associated with the LREs at $y^+ = H^+$, the lower speed fluid above the LRE is buffeted in the spanwise direction at slightly higher elevations as illustrated on the right hand side of Figure 42c. The data at $y^+ = 18$ (not shown) suggest that this process is so strong that the LSS appear to be completely random for $y^+ > 15$.

The bursting frequency and low-speed streaks detected across the span show a trend of relaxation back to flat plate boundary layer values between the strings. If the LSS were perfectly aligned over the LREs, then the bursting frequency and the number of streaks should tend to zero between the LREs. Since the data measured between the LREs is comparable with the flat plate values, the spatial randomness of the sublayer structure is only decreased in a region very close to the roughness elements.

One of the remaining questions is whether the small amount of order imposed by the LREs is sufficient to assist in turbulent modification schemes. If the turbulence modification depends only upon the structure at the wall, the LREs may impose sufficient order to be of assistance. However if the modification depends upon the structure being locked in space above $y^+ \approx 15$, it is doubtful that LREs will be useful.

In the laminar environment, our results favorably indicate the feasibility of the selective suction idea. The measured values of suction coefficient (0.0006) to eliminate artificially generated streaks could potentially indicate a drag reduction of the order of 50% (see the discussion in Section 5). Unfortunately, our experiments in the turbulent environment do not indicate such saving. We feel however that further optimization of the geometry may lead to more positive results. Moreover, the recent experiments of Wilkinson and Lazos (1987) and Wilkinson (1988) are indicating the soundness of our original concept. Streamwise vortices seem to form at the base of Wilkinson's thin-element riblets. Moreover, peak suction or valley blowing, although not yielding net drag reduction at least in the suction case, is far less damaging as far as skin friction is concerned than valley suction or peak blowing. Careful inspection of Figure 2 of the present report may help explain Wilkinson's observations. Peak suction or valley blowing reduces the

spanwise shear $\partial U/\partial z$, while valley suction or peak blowing increases the spanwise shear. Inflectional profiles are inviscidly unstable with growth rates proportional to the shear. Hence, in the first scenario the resulting instabilities are weakened by the suction/injection process, and the reverse is true in the second arrangement. Net drag reduction is not achieved in Wilkinson's experiments with selective suction because of the momentum penalty associated with withdrawing fluid at the wall (Section 5) and the increased surface area due to the non-planar geometry. The goal of future optimization is to ensure that the saving resulting from inhibiting the various boundary layer instabilities exceeds the penalty.

REFERENCES

- Antonia, R. A. (1981) "Conditional Sampling in Turbulence Measurements," Ann. Rev. Fluid Mech. **13**, p. 131.
- Antonia, R.A., Fulachier, L., Krishnamoorthy, L.V., Benabid, T., and Anselmet, F. (1988) "Influence of Wall Suction on the Organized Motion in a Turbulent Boundary Layer," J. Fluid Mech. **190**, p. 217.
- Arakeri, J., and Narasimha, R. (1983) "Effect of Pulsed Slot Suction on a Turbulent Boundary Layer," AIAA J. **21**, p. 306.
- Batchelor, G.K. (1967) An Introduction to Fluid Dynamics, Cambridge University Press, London.
- Bechert, D. W., Hoppe, G., and Reif, W.-E. (1985) "On the Drag Reduction of the Shark Skin," AIAA Paper No. 85-0546.
- Berman (1978) "Drag Reduction by Polymers," Ann. Rev. Fluid Mech. **10**, p. 47.
- Blackwelder, R. F. (1978) "The Bursting Process in Turbulent Boundary Layers," in Coherent Structures of Turbulent Boundary Layers, eds. C. R. Smith & D. E. Abbott, Dept. Mech. Eng., Lehigh University, Bethlehem, PA, p. 211.
- Blackwelder, R.F. (1979) "Boundary Layer Transition," Phys., Fluids **22**, p. 583.
- Blackwelder, R. F., and Haritonidis, J. H. (1983) "Scaling of the Bursting Frequency in Turbulent Boundary Layers," J. Fluid Mech. **132**, p. 87.
- Blackwelder, R.F., and Kaplan, R.E. (1976) "On the Wall Structure of the Turbulent Boundary Layer," J. Fluid Mech. **76**, p. 89.
- Brodkey, R. S., Wallace, J. M., and Eckelmann, H. (1974) "Some Properties of Truncated Turbulence Signals in Bounded Shear Flows," J. Fluid Mech. **63**, p. 209.
- Bushnell, D.M. (1983) "Turbulent Drag Reduction for External Flows," AIAA Paper No. 83-0227.
- Cantwell, B. J., Coles, D., and Dimotakis, P. E. (1978) "Structure and Entrainment in the Plane of Symmetry of a Turbulent Spot," J. Fluid Mech. **87**, p. 641.
- Clauser, F. H. (1956) "The Turbulent Boundary Layer," Adv. Appl. Mech. **4**, p. 1.
- Coles, D.E. (1968) "The Young Person's Guide to the Data," Proc. of the Computations of Turbulent Boundary Layers, AFOSR-IFP-Stanford Conference, Vol. 2, Stanford University, California.
- Corino, E. R., and Brodkey, R. S. (1969) "A Visual Investigation of the Wall Region in Turbulent Flow," J. Fluid Mech. **37**, p. 1.
- Eléna, M. (1975) "Etude des Champs Dynamiques et Thermiques d'un Ecoulement Turbulent en Conduit avec Aspiration à la Paroi," Thèse de Doctorat ès Sciences, Université d'Aix-Marseille, Marseille, France.

Falco, R. (1979) "Structural Aspects of Turbulence in Boundary Layer Flows," in Symp. on Turb., eds. G. K. Patterson & J. L. Zakins, U. of Missouri-Rolla, p. 1.

Falco, R. E. (1980) "The Production of Turbulence Near a Wall," AIAA Paper No. 80-1356.

Favre, A., Dumas, R., Verollet, E., and Coantic, M. (1966) "Couche Limite Turbulente sur Paroi Poreuse avec Aspiration," J. de Mecanique 5, p. 3.

Gad-el-Hak, M. (1986) "The Use of the Dye-Layer Technique for Unsteady Flow Visualization," J. Fluids Eng. 108, p. 34.

Gad-el-Hak, M. (1987) "The Water Towing Tank as an Experimental Facility: An Overview," Exp. Fluids 5, p. 289.

Gad-el-Hak, M. (1988a) "Review of Flow Visualization Techniques for Unsteady Flows," in Flow Visualization IV, ed. C. Véret, Hemisphere, Washington, D.C., p. 1.

Gad-el-Hak, M. (1988b) "Visualization Techniques for Unsteady Flows: An Overview," J. Fluids Eng. 110, No. 3.

Gad-el-Hak, M. (1989a) "The Art and Science of Flow Control," in Frontiers in Experimental Fluid Mechanics, ed. M. Gad-el-Hak, Springer-Verlag, New York.

Gad-el-Hak, M. (1989b) "Flow Control," Appl. Mech. Rev. (to be published).

Gad-el-Hak, M., Blackwelder, R. F., and Riley, J. J. (1981) "On the Growth of Turbulent Regions in Laminar Boundary Layers," J. Fluid Mech. 110, p. 73.

Gad-el-Hak, M., Blackwelder, R. F., and Riley, J. J. (1983) "Visualization Techniques for Studying Turbulent and Transitional Flows," in Flow Visualization 3, ed. W. J. Yang, Hemisphere, Washington, D.C., p. 568.

Gad-el-Hak, M., Blackwelder, R. F., and Riley, J. J. (1984a) "On the Interaction of Compliant Coatings with Boundary Layer Flows," J. Fluid Mech. 140, p. 257.

Gad-el-Hak, M., Davis, S. H., McMurray, J. T., and Orszag, S. A. (1984b) "On the Stability of the Decelerating Boundary Layer," J. Fluid Mech. 138, p. 297.

Gad-el-Hak, M., and Ho, C.-M. (1985a) "Three-Dimensional Effects on a Pitching Lifting Surface," AIAA Paper No. 85-0041.

Gad-el-Hak, M., and Ho, C.-M. (1985b) "The Pitching Delta Wing," AIAA Journal 23, p. 1660.

Gad-el-Hak, M., and Ho, C.-M. (1986) "Unsteady Vortical Flow Around Three-Dimensional Lifting Surfaces," AIAA J. 24, p. 713.

Gad-el-Hak, M., and Hussain, A. K. M. F. (1986) "Coherent Structures in a Turbulent Boundary Layer. Part 1: Generation of 'Artificial' bursts," Phys. Fluids 29, p. 2124.

Hinz, J.O. (1975) Turbulence, Second Edition, McGraw-Hill, New York.

Hussain, A. K. M. F. (1980) "Coherent Structures and Studies of Perturbed and Unperturbed Jets," in Lect. Notes Phys. 136, ed. J. Jimeuer, Springer, Berlin, p. 252.

- Hussain, A. K. M. F. (1983a) "Coherent Structures - Reality and Myth," Phys. Fluids **26**, p. 2816.
- Hussain, A. K. M. F. (1983b) "Coherent Structures," Proc. Second Asian Congress of Fluid Mechanics, Beijing, China, p. 14.
- Hussain, A. K. M. F. (1983c) "Coherent Structures and Incoherent Turbulence," in Turbulence and Chaotic Phenomena in Fluids, ed. T. Tatsumi, North Holland, p. 453.
- Hussain, A. K. M. F., and Reynolds, W. C. (1972) "The Mechanics of an Organized Wave in Turbulent Shear Flow. Part 2. Experimental Results," J. Fluid Mech. **54**, p. 241.
- Hussain, A. K. M. F., and Zaman, K. B. M. Q. (1980) "Vortex Pairing in a Circular Jet Under Controlled Excitation. Part 2. Coherent Structure Dynamics," J. Fluid Mech. **101**, p. 493.
- Johansen, J. B., and Smith, C. R. (1986) "The Effects of Cylindrical Surface Modifications on Turbulent Boundary Layers," AIAA J. **24**, p. 1081.
- Kays, W.M., and Crawford, M.E. (1980) Convective Heat and Mass Transfer, McGraw-Hill, New York.
- Klebanoff, P. S., Tidstrom, K. D., and Sargent, L. M. (1962) "The Three-Dimensional Nature of Boundary Layer Instability," J. Fluid Mech. **12**, p. 1.
- Kline, S. J., Reynolds, W. C., Shraub, F. A., and Runstadler, P. W. (1967) "The Structure of Turbulent Boundary Layers," J. Fluid Mech. **30**, p. 741.
- Kunen, J. M. G., Ooms, G., and Vink, P. J. J. (1983) "On Detection Methods for Coherent Structures in Turbulent Flows," in Symp. on Turb., Vol. 8, eds. X. B. Reed et al., U. of Missouri-Rolla, p. 37.
- Landau, L.D., and Lifshitz, E.M. (1963) Fluid Mechanics, translated from Russian, Pergamon Press, Oxford.
- Lu, S. S., and Willmarth, W. W. (1973) "Measurements of the Structure of the Reynolds Stress in a Turbulent Boundary Layer," J. Fluid Mech. **60**, p. 481.
- Lumley, J.L. (1983) "Turbulence Modeling," J. Applied Mechanics **105**, p. 1097.
- Lumley, J.L. (1987) "Turbulence Modeling," Proc. 10th U.S. National Cong. of Applied Mechanics, ed. J.P. Lamb, ASME, New York, p. 33.
- Moin, P., and Kim, J. (1982) "Numerical Investigation of Turbulent Channel Flow," J. Fluid Mech. **118**, p. 341.
- Nishioka, M., Asai, M., and Iida, S. (1981) "Wall Phenomena in the Final Stages of Transition to Turbulence," in Transition and Turbulence, ed. R. E. Meyer, Academic Press, New York, p. 113.
- Offen, G. R., and Kline, S. J. (1975) "A Proposed Model of the Bursting Process in Turbulent Boundary Layers," J. Fluid Mech. **70**, p. 209.
- Panton, R.L. (1984) Incompressible Flow, Wiley-Interscience, New York.

- Perry, A. E., Lin, T. T., and Teh, E. W. (1981) "A Visual Study of Turbulent Spots," J. Fluid Mech. **104**, p. 387.
- Praturi, A. K., and Brodkey, R. S. (1978) "A Stereoscopic Visual Study of Coherent Structures in Turbulent Shear Flow," J. Fluid Mech. **89**, p. 241.
- Reshotko, E. (1980) "Blowing and Suction," in Viscous Flow Drag Reduction, ed. G. R. Hough, Prog. in Astro. & Aero., Vol. 72, AIAA, New York, p. 185.
- Riley, J. J., and Gad-el-Hak, M. (1985) "The Dynamics of Turbulent Spots," in Frontiers in Fluid Mechanics, eds. S. H. Davis & J. L. Lumley, Springer, New York, p. 123.
- Rosenhead, L. (1963) Laminar Boundary Layers, Clarendon Press, Oxford.
- Rotta, J. C., (1970) "Control of Turbulent Boundary Layers by Uniform Injection and Suction of Fluid," in Seventh Congress of the International Council of the Aeronautical Sciences, ICAS Paper No. 70-10, Rome.
- Sato, H. (1983) "Cognition and Description of Patterns in Turbulent Flows," Proc. Second Asian Congress of Fluid Mechanics, Beijing, China, p. 7.
- Schlichting, H. (1979) Boundary-Layer Theory, Seventh Edition, McGraw-Hill, New York.
- Simpson, R. L. (1970) "Characteristics of Turbulent Boundary Layers at Low Reynolds Numbers with and without Transpiration," J. Fluid Mech. **42**, p. 769.
- Simpson, R. L., Moffat, R. J., and Kays, W. M. (1969) "The Turbulent Boundary Layer on a Porous Plate," Int. J. Heat & Mass Transfer **12**, p. 771.
- Smith, C. R. (1983) "A Synthesized Model of the Near-Wall Behavior in Turbulent Boundary Layers," in Symp. on Turb., U. of Missouri-Rolla, Vol. 8, eds. X. B. Reed et al., p. 299.
- Sokolov M., Hussain, A. K. M. F., Kleis, S. J., and Hussain, Z. D. (1980) "A 'Turbulent Spot' in an Axisymmetric Free Shear Layer. Part 1," J. Fluid Mech. **98**, p. 65.
- Swearingen, J. D., and Blackwelder, R. F. (1984) "Instantaneous Streamwise Velocity Gradients in the Wall Region," Bull. Am. Phys. Soc. **29**, p. 1528.
- Van Dyke, M. (1982) An Album of Fluid Motion, The Parabolic Press, Stanford, California.
- Verollet, E., Fulachier, L., Dumas, R., and Favre, A. (1972) "Turbulent Boundary Layer with Suction and Heating to the Wall," in Heat and Mass Transfer in Boundary Layers, Vol. 1, eds. N. Afgan et al., Pergamon Press, Oxford, p. 157.
- Walsh, M. J. (1980) "Drag Characteristics of V-Groove and Transverse Curvature Riblets," in Viscous Flow Drag Reduction, ed. G. R. Hough, Prog. in Astro. & Aero., Vol. 72, AIAA, New York, p. 168.
- Walsh, M. J., (1982) "Turbulent Boundary Layer Drag Reduction using Riblets," AIAA Paper No. 82-0169.
- Walsh, M. J. (1983) "Riblets as a Viscous Drag Reduction Technique," AIAA J. **21**, p. 485.

Walsh, M. J., and Lindemann, A. M. (1984) "Optimization and Application of Riblets for Turbulent Drag Reduction, AIAA Paper No. 84-0347.

Wilkinson, S.P. (1988) "Direct Drag Measurements on Thin-Element Riblets with Suction and Blowing," AIAA Paper No. 88-3670-CP.

Wilkinson, S. P., Ash, R. L., and Weinstein, L. M. (1980) "Hybrid Suction Surface for Turbulent Boundary Layer Flow," in Viscous Flow Drag Reduction, ed. G. R. Hough, Prog. in Astro. & Aero., Vol. 72, AIAA, New York, p. 233.

Wilkinson, S.P., and Lazos, B.S. (1987) "Direct Drag and Hot-Wire Measurements on Thin-Element Riblet Arrays," in Turbulence Management and Relaminarization, eds. H.W. Liepmann and R. Narasimha, pp. 121-131, Springer-Verlag, New York.

Willmarth, W. W. (1975) "Structure of Turbulence in Boundary Layers," Adv. Applied Mech. 15, p. 159.

Wyganski, I. J., Sokolov, M., and Friedman, D. (1976) "On a Turbulent 'Spot' in a Laminar Boundary Layer," J. Fluid Mech. 78, p. 785.

Zaman, K. B. M. Q., and Hussain, A. K. M. F. (1981) "Taylor Hypothesis and Large-Scale Coherent Structures," J. Fluid Mech. 112, p. 379.

Zilberman, M., Wyganski, I., and Kaplan, R.E. (1977) "Transitional Boundary Layer Spot in a Fully Turbulent Environment," Phys. Fluids 20, p. S258.

**APPENDIX: PUBLICATIONS RESULTING
FROM PRESENT RESEARCH**

The following publications resulted from the present research and are available in the open literature or directly from the author of this report:

1. Gad-el-Hak & Hussain (1985) "Generation of 'Artificial' Bursts in a Turbulent Boundary Layer," Bul. Am. Phys. Soc. **30**, p. 1751.
2. Gad-el-Hak & Hussain (1986) "Generation of 'Artificial' Bursts in a Turbulent Boundary Layer," AIAA Paper No. 86-0504.
3. Gad-el-Hak (1986) "Use of Water Towing Tanks for Aerodynamics and Hydrodynamics," AGARD Conference Proceedings No. 413, Paper No. 24.
4. Gad-el-Hak & Hussain (1986) "Coherent Structures in a Turbulent Boundary Layer. Part I: Generation of 'Artificial' Bursts," Phys. Fluids **29**, p. 2124.
5. Gad-el-Hak & Blackwelder (1986) "Selective Suction for Turbulent Skin Friction Reduction," Bul. Am. Phys. Soc. **31**, p. 1724.
6. Gad-el-Hak & Blackwelder (1987) "A Drag Reduction Method for Turbulent Boundary Layers," AIAA Paper No. 87-0358.
7. Gad-el-Hak (1987) "Review of Flow Visualization Techniques for Unsteady Flows," in Flow Visualization **4**, ed. C. V  ret, p. 3, Hemisphere, Washington, D.C.
8. Gad-el-Hak (1987) "The Water Towing Tank as an Experimental Facility: An Overview," Exp. Fluids **5**, p. 289.
9. Roon, Blackwelder & Gad-el-Hak (1987) "Modification of Turbulent Boundary Layers by Longitudinal Roughness Elements," Bul. Am. Phys. Soc. **32**, p. 2075.
10. Blackwelder & Roon (1988) "The Effects of Longitudinal Roughness Elements Upon the Turbulent Boundary Layers," AIAA Paper No. 88-0134.
11. Gad-el-Hak (1988) "Visualization Techniques for Unsteady Flows: An Overview," J. Fluids Eng. **110**, No. 3.
12. Gad-el-Hak (1988) "Common Features of Techniques for Boundary Layer Control," Bul. Am. Phys. Soc. **33**, p. 2227.
13. Gad-el-Hak & Blackwelder (1989) "Selective Suction for Controlling Bursting Events in a Boundary Layer," AIAA J. **27**, No. 2.
14. Gad-el-Hak (1989) "Flow Control," Appl. Mech. Rev. (to be published).
15. Roon & Blackwelder (1989) "The Effects of Longitudinal Roughness Elements Upon the Turbulent Boundary Layer," AIAA J. (to be published).
16. Gad-el-Hak (1989) "The Art and Science of Flow Control," in Frontiers in Experimental Fluid Mechanics, ed. M. Gad-el-Hak, Springer, New York.

17. Gad-el-Hak (1989) "Control of Low Reynolds Number Airfoils: A Review," Conference on Low Reynolds Number Aerodynamics, Notre Dame, IN, 5-7 June.
18. Gad-el-Hak (1989) "Turbulent Flow Control," Proc. 2nd IUTAM Symp. on Structure of Turbulence and Drag Reduction, Zurich, Switzerland, 25-28 July.
19. Gad-el-Hak (1989) "Drag Reduction: An Overview," Proceedings of Drag Reduction 89, Davos, Switzerland, 31 July - 3 August.
20. Gad-el-Hak (1989) "Wall Turbulence Ability to Maintain Large Gradients Despite Large Viscous Diffusion," ASME Symposium on Unanswered Questions in Fluid Mechanics, San Francisco, CA, 10 - 15 December.



Report Documentation Page

1. Report No. NASA CR-4221	2. Government Accession No.	3. Recipient's Catalog No.	
4. Title and Subtitle Feasibility of Generating an 'Artificial' Burst in a Turbulent Boundary Layer - Phase II SBIR		5. Report Date March 1989	
		6. Performing Organization Code	
7. Author(s) Mohamed Gad-el-Hak		8. Performing Organization Report No. Flow Report No. 462	
		10. Work Unit No. 505-60-21-09	
9. Performing Organization Name and Address Flow Industries, Inc. 2414-68th Avenue South Kent, WA 98032		11. Contract or Grant No. NAS1-18292	
		13. Type of Report and Period Covered Final Technical Report 12 May 1986 - 30 October 1988	
12. Sponsoring Agency Name and Address National Aeronautics and Space Administration Langley Research Center Hampton, VA 23665-5225		14. Sponsoring Agency Code	
15. Supplementary Notes Phase II SBIR Final Technical Report Professor Mohamed Gad-el-Hak is currently affiliated with: Department of Aerospace and Mechanical Engineering University of Notre Dame Notre Dame, IN 46556 Langley Technical Monitor: Stephen P. Wilkinson			
16. Abstract Viscous drag accounts for about half of the total drag on commercial aircraft at subsonic cruise conditions. Two avenues are available to achieve drag reduction: either laminar flow control or turbulence manipulation. The present research deals with the latter approach. The primary objective of Phase II research was to investigate experimentally the feasibility of substantially reducing the skin-friction drag in a turbulent boundary layer using a novel technique. The method combines the beneficial effects of suction and a longitudinally ribbed surface. At a sufficiently large spanwise separation, the streamwise grooves act as a nucleation site causing a focusing of low-speed streaks over the peaks. Suction is then applied intermittently through longitudinal slots located at selected locations along those peaks to obliterate the low-speed regions and to prevent bursting. Phase two research was divided into two tasks. In the first, selective suction from a single streamwise slot was used to eliminate either a single burst-like event or a periodic train of artificially generated bursts in laminar and turbulent boundary layers that develop on a flat plate towed in a water channel. Our results indicated that equivalent values of the suction coefficient as low as 0.0006 were sufficient to eliminate the artificially generated bursts in a laminar boundary layer. This rate is 5 times smaller than that reported in other experiments employing uniform transpiration as the rate necessary to yield zero growth of the boundary layer's momentum thickness. In the second task, conducted in a subsonic, low-turbulence, closed-return wind tunnel, the selective suction technique was applied to eliminate natural bursts occurring on a grooved surface. Velocity profiles and bursting statistics were measured in the presence of longitudinal roughness elements (LREs). The LREs seem simply to impose a no-slip boundary condition at an elevation equivalent to their diameter.			
17. Key Words (Suggested by Author(s)) Boundary Layer Control; Suction; Drag Reduction; Skin Friction; Artificial Burst; Bursting Events; Turbulent Boundary Layers		18. Distribution Statement Unclassified-Unlimited Subject Category 34	
19. Security Classif. (of this report) Unclassified	20. Security Classif. (of this page) Unclassified	21. No. of pages 132	22. Price A07